MONTHLY NOTICES

OF THE

ROYAL ASTRONOMICAL SOCIETY

Volume 121 No. 1 1960

Published and Sold by the

ROYAL ASTRONOMICAL SOCIETY
BURLINGTON HOUSE
LONDON, W.1

Price £1 4s. 0d.; *in U.S.A.* $3.50

Subscription for volume: £6 ; *in U.S.A.* $18

The Geophysical Journal

OF THE

ROYAL ASTRONOMICAL SOCIETY

Price £1 per number; in U.S.A. $3. Annual Subscription £3; in U.S.A. $9

Volume 3 No. 3 September 1960

CONTENTS INCLUDE :

Orders should be addressed to :

The Assistant Secretary

Royal Astronomical Society, Burlington House, London, W.1

NOTICE TO AUTHORS

Presentation of Papers at Meeting

At some meetings of the Society the background and conclusions of selected papers are presented and then discussed. In order to assist the Secretaries in the selection of papers for such meetings, authors are asked to let the Society know, when submitting papers, whether they would be willing to give an account of their paper, if requested.

The attention of authors resident abroad is drawn to the fact that the Society welcomes information about their work. The Secretaries would be happy to consider having such work described at a meeting, in accordance with the author's wishes, either by a Secretary or other Fellow.

Publication of Papers

1. *General.*—It is the aim of the Society to be of the greatest possible service in disseminating astronomical results and ideas to the scientific community with the utmost possible speed. Contributors are accordingly urged to give the most careful consideration to the presentation of their work, for attention to detail will assuredly result in a substantial saving of time.

It is the practice of the Society to seek a referee's opinion on nearly every paper submitted for publication in *Monthly Notices*; experience has shown that frequently the comments of referees have enabled authors to improve the presentation of their work and so increase its scientific value.

2. *Communication.*—Papers must be communicated to the Society by a Fellow. They should be accompanied by a summary at the *beginning* of the paper conveying briefly the content of the paper, and drawing attention to important new information and to the main conclusions. The summary should be intelligible in itself, without reference to the paper, to a reader with some knowledge of the subject; it should not normally exceed 200 words in length. **Authors are requested to submit MSS. in duplicate.** These should be typed using double spacing and leaving a margin of not less than one inch on the left-hand side. Corrections to the MSS. should be made in the text and not in the margin. By Council decision, MSS. of accepted papers are retained by the Society for one year after publication; unless their return is then requested by the author they are destroyed.

3. *Presentation.*—Authors are allowed considerable latitude, but they are requested to follow the general style and arrangement of *Monthly Notices*. References to literature should be given either in the traditional form of a numbered list at the end of the paper, or as prescribed in *Notes on the Preparation of Papers to be Communicated to the Royal Society*.

4. *Notation.*—For technical astronomical terms, authors should conform closely to the recommendations of Commission 3 of the International Astronomical Union (*Trans. I.A.U.*; Vol. VI, p. 345, 1938). Council has decided to adopt the I.A.U. 3-letter abbreviations for constellations where contraction is desirable (Vol. IV, p. 221, 1932). In general matters, authors should follow the recommendations in *Symbols, Signs and Abbreviations* (London: Royal Society, 1951) except where these conflict with I.A.U. practice.

5. *Diagrams.*—**These should be designed to appear upright on the page, drawn about twice the size required in print and prepared for direct photographic reproduction except for the lettering, which should be inserted in pencil.** Legends should be given in the manuscript indicating where in the text the figure should appear. Blocks are retained by the Society for 10 years; unless the author requires them before the end of this period they are then destroyed. **Rough copies or prints of the diagrams should accompany each manuscript.**

6. *Tables.*—These should be arranged so that they can be printed upright on the page.

7. *Proofs.*—Authors are liable for costs of alteration exceeding 5 per cent of composition. It is therefore in their own and the Society's interests to seek the maximum conciseness and simplification of symbols and equations consistent with clarity.

CONTENTS

Printed in London by Taylor & Francis, Ltd., 1960 August

MONTHLY NOTICES

OF THE

ROYAL ASTRONOMICAL SOCIETY

Vol. 121 No. 1

Bibliographical Note

With Vol. 121 *Monthly Notices* becomes a journal entirely devoted to the publication of original papers of astronomical research in the widest sense.

A new journal, the *Quarterly Journal of the Royal Astronomical Society*, will contain the formal reports of meetings, the George Darwin Lecture, and all the material hitherto published in the Annual Council Report number of *Monthly Notices* (reports of progress in astronomy, special news of the Society, etc.). The *Quarterly Journal* will, in addition, contain articles of the kind hitherto published in *Occasional Notes* and other material of general interest. The new *Journal* will be sent automatically to all subscribers to *Monthly Notices*.

CONT[illegible]

Printed in London by [illegible]

MONTHLY NOTICES

OF THE

ROYAL ASTRONOMICAL SOCIETY

Vol. 121 No. 1

Bibliographical Note

With Vol. 121 *Monthly Notices* becomes a journal entirely devoted to the publication of original papers of astronomical research in the widest sense.

A new journal, the *Quarterly Journal of the Royal Astronomical Society*, will contain the formal reports of meetings, the George Darwin Lecture, and all the material hitherto published in the Annual Council Report number of *Monthly Notices* (reports of progress in astronomy, special news of the Society, etc.). The *Quarterly Journal* will, in addition, contain articles of the kind hitherto published in *Occasional Notes* and other material of general interest. The new *Journal* will be sent automatically to all subscribers to *Monthly Notices*.

MONTHLY NOTICES
OF THE
ROYAL ASTRONOMICAL SOCIETY
Vol. 121 No. 1

ON MR KING-HELE'S THEORY OF THE EFFECT OF THE EARTH'S OBLATENESS ON THE ORBIT OF A CLOSE SATELLITE

P. J. Message

(Received 1960 February 8)

Summary

The relations are obtained between α and Ω, the parameters defining King-Hele's plane Π, and the osculating inclination and longitude of node. The secular motion of the node is thereby obtained in terms of mean osculating elements in a form comparable to that arising in Brouwer's treatment of the canonical equations. A modification is made to King-Hele's theory which removes the singularities in the Je terms of $d\Omega/d\psi$, and it is also found that there are no terms of order Je^2 in α or Ω.

In view of the intrinsic interest of Mr King-Hele's theory (1) of the motion of a close satellite, and since it has played an important part in the study of the Earth's external potential by means of artificial satellite observations, it might perhaps be of interest to consider the relations between some of the novel parameters that he uses and the more usual osculating orbital elements.

He defines a plane Π, of constant inclination α to the equator, rotating about the Earth's axis in such a way that the satellite moves in it always in the same sense about the Earth's centre. (We shall see that while this can be done exactly to the order J, where the second harmonic term in the Earth's potential is $(2\mu J)/3r^{-3}P_2$, a modification is required to order Je.) In the plane Π he uses ψ for longitude measured from the line of greatest slope which lies in the northern hemisphere, and r for the radius vector. If $Oxyz$ is a moving frame of reference such that O is the centre of the Earth, Oxy is always the plane Π, Ox its intersection with the plane of the equator, the positive direction being that of the satellite when crossing the equator from south to north, and Oy the line $\psi = 0$, then we have for the position vector of the satellite, referred to this plane,

$$\mathbf{r} = (-r\sin\psi,\ r\cos\psi,\ 0). \tag{1}$$

Then, $OXYZ$ being an inertial frame, such that OXY is the plane of the equator, King-Hele's quantity Ω is the longitude of Ox measured backwards (i.e. in the opposite sense to ψ) along the equator. The formulae relating coordinates in the two frames are

$$\begin{aligned} X &= \ \ x\cos\Omega + \sin\Omega(y\cos\alpha - z\sin\alpha), \\ Y &= -x\sin\Omega + \cos\Omega(y\cos\alpha - z\sin\alpha), \\ Z &= \ \ y\sin\alpha + z\cos\alpha. \end{aligned}$$

Therefore the position vector is, referred to $OXYZ$,

$$\mathbf{r} = (-r\sin\psi\cos\Omega + r\cos\psi\cos\alpha\sin\Omega,\; r\sin\psi\sin\Omega + r\cos\psi\cos\alpha\cos\Omega,\; r\cos\psi\sin\alpha). \tag{2}$$

The velocity of the satellite relative to the frame $Oxyz$ is

$$(\mathbf{v}) = (-\dot{r}\sin\psi - r\dot{\psi}\cos\psi,\; \dot{r}\cos\psi - r\dot{\psi}\sin\psi,\; 0), \tag{3}$$

and relative to a fixed frame it is

$$\mathbf{v} = (\mathbf{v}) + \boldsymbol{\Theta}\wedge\mathbf{r} + O(Je) \tag{4}$$

where $\boldsymbol{\Theta} = (0, 0, -\dot{\Omega})$ referred to $OXYZ$. (Note that α is constant to order J.)

Now the osculating orbit plane is the plane defined by the vectors $\mathbf{r}$ and $\mathbf{v}$, so its unit normal is given by $\mathbf{n} = \mathbf{N}/|\mathbf{N}|$, where

$$\mathbf{N} = \mathbf{r}\wedge\mathbf{v} = \mathbf{r}\wedge(\mathbf{v}) + r^2\boldsymbol{\Theta} - \mathbf{r}(\mathbf{r}\,.\,\boldsymbol{\Theta}) + O(Je, \boldsymbol{\Theta}^2) \tag{5}$$

so that

$$\mathbf{N}^2 = \{\mathbf{r}\wedge(\mathbf{v})\}^2 + 2r^2\{\mathbf{r}\wedge(\mathbf{v})\}\,.\,\boldsymbol{\Theta} + O(Je, \boldsymbol{\Theta}^2).$$

Now referred to $Oxyz$,

$$\mathbf{r}\wedge(\mathbf{v}) = (0, 0, r^2\dot{\psi}),$$

and referred to $OXYZ$,

$$\mathbf{r}\wedge(\mathbf{v}) = (-r^2\dot{\psi}\sin\alpha\sin\Omega,\; -r^2\dot{\psi}\sin\alpha\cos\Omega,\; r^2\dot{\psi}\cos\alpha),$$

and thus

$$\mathbf{N}^2 = r^4\dot{\psi}^2 - 2r^4\dot{\psi}\dot{\Omega}\cos\alpha + O(Je, \dot{\Omega}^2),$$

$$|\mathbf{N}| = r^2\dot{\psi}\left(1 - \frac{d\Omega}{d\psi}\cos\alpha\right) + O\left\{Je, \left(\frac{d\Omega}{d\psi}\right)^2\right\}, \tag{6}$$

so that

$$\begin{aligned}\mathbf{n} = \Bigg\{ &-\sin\alpha\sin\Omega\left(1 + \frac{d\Omega}{d\psi}\cos\alpha\right) - \cos\psi\sin\alpha\frac{d\Omega}{d\psi}(\sin\psi\cos\Omega - \cos\psi\cos\alpha\sin\Omega),\\ &-\sin\alpha\cos\Omega\left(1 + \frac{d\Omega}{d\psi}\cos\alpha\right) + \cos\psi\sin\alpha\frac{d\Omega}{d\psi}(\sin\psi\sin\Omega + \cos\psi\cos\alpha\cos\Omega),\\ &+\cos\alpha\left(1 + \frac{d\Omega}{d\psi}\cos\alpha\right) - \frac{d\Omega}{d\psi} + \cos^2\psi\sin^2\alpha\frac{d\Omega}{d\psi}\Bigg\} + O\left\{Je, \left(\frac{d\Omega}{d\psi}\right)^2\right\}. \end{aligned} \tag{7}$$

Thus in terms of i, the inclination of the osculating plane, and Ω, the longitude of the ascending node, measured from OX, we readily see that

$$\mathbf{n} = (\sin i\sin\Omega,\; -\sin i\cos\Omega,\; \cos i). \tag{8}$$

Comparing these two expressions for $\mathbf{n}$ we see that

$$\begin{aligned} i &= \alpha + \frac{d\Omega}{d\psi}\sin\alpha\sin^2\psi + O\left\{Je, \left(\frac{d\Omega}{d\psi}\right)^2\right\},\\ \Omega &= -\Omega - \frac{d\Omega}{d\psi}\cos\psi\sin\psi + O\left\{Je, \left(\frac{d\Omega}{d\psi}\right)^2\right\}, \end{aligned} \tag{9}$$

or, using King-Hele's result $d\Omega/d\psi = JL^2R^2\cos\alpha + O(Je)$,

$$\begin{aligned} i &= \alpha + \tfrac{1}{2}JL^2R^2\sin 2\alpha\sin^2\psi + O(Je),\\ \Omega &= -\Omega - \tfrac{1}{2}JL^2R^2\cos\alpha\sin 2\psi + O(Je). \end{aligned} \tag{10}$$

Now α and Ω have no periodic parts of order J, and so these expressions give us at once the periodic perturbations of this order in i and Ω, and also show that the mean value of i is given by

$$i_0 = \alpha + \tfrac{1}{4}JL^2R^2\sin 2\alpha + O(Je). \tag{11}$$

When the satellite crosses the equator from south to north, the two angles Ω and $-\Omega$ are each equal to the longitude of the satellite measured from OX, and therefore they are equal to each other. Thus the mean rates of change of these two angles are the same. Now from King-Hele's equations (88) and (71) I derive

$$\overline{\frac{d\Omega}{dt}} = \frac{2\pi}{T}\cos\alpha\left\{J\left(\frac{R}{\bar{r}}\right)^2 + J^2\left(\frac{R}{\bar{r}}\right)^4\left(\frac{10}{3}\sin^2\alpha - \frac{5}{2}\right) + \frac{3}{14}D\left(\frac{R}{\bar{r}}\right)^4(4-7\sin^2\alpha)\right\}, \tag{12}$$

T being the mean period between successive returns to the same node. Using this, together with the expression for i_0 above, we obtain for the secular motion of the node in terms of the mean inclination i_0 and the mean radius vector $\bar{r}$,

$$\overline{\frac{d\Omega}{dt}} = -\frac{2\pi}{T}\cos i_0\left\{J\left(\frac{R}{\bar{r}}\right)^2 + J^2\left(\frac{R}{\bar{r}}\right)^4\left(\frac{23}{6}\sin^2 i_0 - \frac{5}{2}\right) + \frac{3}{14}D\left(\frac{R}{\bar{r}}\right)^4(4-7\sin^2 i_0)\right\}, \tag{13}$$

the J and J^2 terms of which are in agreement with the result deduced from Brouwer's treatment of the canonical equations for the perturbations (2) (which does not include the terms in D).

The terms of order Je in $d\Omega/d\psi$ as given by King-Hele's equation (48), contain singularities at $\psi = 0$ and $\psi = \pi$. Either one of these, but for general values of β not both, may be removed by a suitable choice of the disposable constant arising in the solution of the equation (47). Now a change $d\alpha$ in the value of α must be accompanied, if the value of the colatitude θ is to be unaltered, by a change $\operatorname{cosec}\alpha\cot\psi\, d\alpha$ in Ω, which on differentiation with respect to ψ gives an expression with the factor $\operatorname{cosec}^2\psi$, which is therefore associated with a change in α. The irreducible singularity in $d\Omega/d\psi$, arising through a factor $\operatorname{cosec}^2\psi$, is a consequence of the fact that we cannot define a rotating plane of constant inclination α to the equator such that the satellite always lies in it and always moves in the same sense on it round O unless its maximum northerly and southerly latitudes are the same, which they are not if both the eccentricity of the orbit and the perturbations are taken into account. Consequently α must be allowed to vary to order Je. If we make this modification to King-Hele's theory, then, and at the same time allow for possible terms of order Je^2 in α and Ω, we must put

$$\begin{aligned}\frac{d\Omega}{d\psi} &= \epsilon(1 + e\lambda + e^2\mathscr{H} + J\Lambda)\\ \frac{d\alpha}{d\psi} &= \epsilon(e\gamma + e^2K + J\Gamma).\end{aligned} \tag{14}$$

If we follow King-Hele's procedure, and also put α_0 for the mean value of α, we find that the equations of motion require, to order Je,

$$\tan\psi\frac{d\lambda}{d\psi} + 2\lambda - \operatorname{cosec}\alpha_0\left(\frac{d\gamma}{d\psi} - 2\tan\psi\,.\,\gamma\right) = 2\cos(\psi+\beta), \tag{15}$$

a particular integral of which, having no singularities, is

$$\begin{aligned}\lambda &= \tfrac{4}{3}\cos(\psi+\beta),\\ \gamma &= \tfrac{2}{3}\sin\alpha_0\sin(\psi+\beta).\end{aligned} \tag{16}$$

The equation for the terms of order Je^2 is

$$2\mathscr{H} + \tan\psi \frac{d\mathscr{H}}{d\psi} + 2\tan\psi \operatorname{cosec}\alpha_0 . K - \operatorname{cosec}\alpha_0 \frac{dK}{d\psi} = 0, \tag{17}$$

which can be solved by $\mathscr{H} = K = 0$, showing that there are no terms of this order in α or Ω. To the order of J^2 and D the equation is

$$\begin{aligned}\tan\psi \frac{d\Lambda}{d\psi} + 2\Lambda - \operatorname{cosec}\alpha_0 \left(\frac{d\Gamma}{d\psi} - 2\tan\psi . \Gamma\right) \\ = 2R^2L^2\left(1 - \frac{7}{3}\sin^2\alpha_0 - \frac{1}{3}\sin^2\alpha_0 \sin^2\psi\right) - 3R^2L^2(2\sin^2\alpha_0 \sin^2\psi + \cos^2\alpha_0) \\ + \frac{4}{7}\frac{D}{J^2} R^2L^2(3 - 7\sin^2\alpha_0 \cos^2\psi),\end{aligned} \tag{18}$$

which has the solution $\Gamma = 0$, and Λ as given by King-Hele in his equation (64).

Thus we have

$$\alpha = \alpha_0 - \tfrac{2}{3}e\epsilon \sin\alpha_0 \cos(\psi + \beta), \tag{19}$$

and the only modification to King-Hele's formulae for Ω is in the periodic terms of order Je. The mean value of $d\Omega/dt$ is unchanged, and so this modification leads to no change in the estimates of the values of J and D that have been derived from observations of this quantity for artificial satellites.

Gonville and Caius College,
Cambridge:
1960 *February* 5.

References

(1) D. G. King-Hele, *Proc. Roy. Soc.* A, **247**, 49–72, 1958.
(2) D. Brouwer, *A.J.*, **64**, 378–96, 1959.

A SOUTHERN HEMISPHERE SURVEY OF THE RADIANTS OF SPORADIC METEORS

A. A. Weiss and J. W. Smith

(Communicated by E. G. Bowen)

(Received 1960 January 4)

Summary

A further survey of sporadic meteor activity, from December 1956 to August 1958, has been made with 67 mc/s narrow-beam equipment operated at a limiting line density close to 10^{11} electrons/cm. Analysis of the echo rates suggests that the sporadic radiant distribution may be sharply divided into two components. One component is concentrated towards the apex and corresponds to a distribution of orbits uniform in heliocentric co-ordinates except for a moderate preponderance of direct over retrograde orbits. The other component lies close to the plane of the ecliptic, with radiants strongly concentrated in two regions centred on longitudes $\pm 68°$ from the apex. No change is apparent in the radiant distribution as the limiting sensitivity is lowered from the 3rd to the 7th visual magnitude.

---

1. *Introduction.*—Radio echo surveys of the rate of occurrence of sporadic meteors over extended periods have been made at Adelaide (Weiss 1957) and at Jodrell Bank (Hawkins 1956a). In the former survey the resolving power of the aerial was inadequate for the determination of the extent of the concentration of sporadic radiants towards the plane of the ecliptic, but groups of radiants near the Sun, the anti-Sun and the apex of the Earth's way were inferred from supplementary measurements of the directions of reflection points. The equipment used in the Jodrell Bank Survey had much greater resolving power, but the large statistical fluctuations resulting from the low echo rate (rarely exceeding 15/hr) tended to obscure the form of the diurnal and seasonal variations, with the result that full use could not be made of the resolving power of the equipment. Hawkins, by treating the whole of the data on a statistical basis, deduced a strong concentration of radiant points in the plane of the ecliptic except in the vicinity of the antapex, and a large preponderance of direct over retrograde orbits.

A second survey has now been completed at Adelaide, using a high-resolution equipment of the same type as that used by Hawkins, but with a much higher echo rate (up to 100/hr). Although this work is to some extent a repetition, in the southern hemisphere, of Hawkins's survey in the northern hemisphere, an important new feature is that the statistical fluctuations in the echo rate are now sufficiently small for the diurnal and seasonal variations to be easily recognized. The detailed study of these temporal variations leads to a sporadic radiant distribution which differs in some respects from that obtained by Hawkins.

2. *Collecting area and sensitivity of the equipment.*—The equipment, which also serves in the detection and measurement of meteor shower radiants, has already been described (Weiss 1955, 1960).

By virtue of the property of specular reflection, whereby an echo can be obtained from the ionized meteor trail only if the normal to the trail at the reflection

point passes through the observing station, the collecting areas for the two narrow-beam, low-elevation aerials are narrow strips on the celestial sphere, lying along great circles which intersect near the zenith. Contours of constant sensitivity for each aerial are drawn in Fig. 1. These contours have been prepared from the

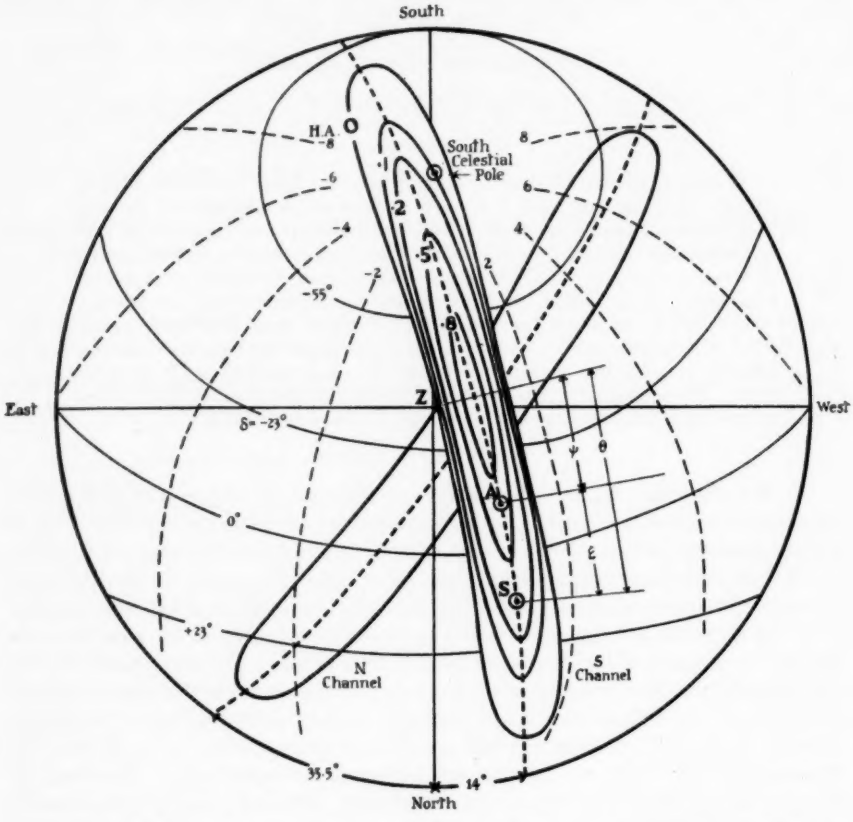

FIG. 1.—*Contours of constant sensitivity for the Adelaide survey equipment, drawn on the celestial sphere. Contours for the* N *and* S *channels are identical; only the zero contour is drawn for the* N *channel. Point A represents an arbitrary position of the apex of the Earth's way, and S an arbitrary point source, to illustrate the* ψ, θ, ϵ *system of co-ordinates.*

echo rates received from the concentrated Sun and anti-Sun sources, as a function of source zenith angle, in conjunction with the variation of the echo rates from several showers as their radiants move across the collecting areas. They apply to collection in the major lobe only; minor lobes in elevation are excluded by range selection of echoes and the minor lobes in azimuth have power gains less than 4 per cent of the maximum.

It will be seen from Fig. 1 that the times of appearance of echoes from a discrete source in the two channels are a unique function of its declination and right ascension; this fact forms the basis of measurement of radiant coordinates with this type of equipment. With the exception of radiants close to the south celestial pole, a radiant crosses the S collecting area in a direction roughly normal to its

axis, a situation never encountered with the N collecting area. The S collecting area alone contains the south celestial pole, consequently radiants with declinations less than $-65°$ do not appear at all in the N channel.

The line density of the faintest meteor segment detected is approximately 10^{11} electrons/cm, corresponding to a visual magnitude $M_V \sim +7$. This limit has been determined by two methods which give concordant results (Weiss 1960): (*a*) the dependence of the sporadic echo rate on equipment sensitivity; (*b*) a comparison of the echo rates of the Geminid stream, as detected by the present equipment and by the 27 mc/s Adelaide wind equipment, which has been calibrated absolutely. The sensitivity was not held constant over the period of the survey, both because of severe electrical interference, and of equipment modifications. The corrections to the echo rate to take account of these changes in operating conditions did not exceed 50 per cent and were usually much less.

Hawkins (1956a) has given a similar limit of 10^{11} electrons/cm for the Jodrell Bank survey, which seems inconsistent with the relative echo rates. However, he has subsequently (Hawkins 1956b) revised the Jodrell Bank limiting sensitivity to $M_V = +4{\cdot}2$.

3. *The observations.*—With the exception of a few short breaks, the observations were continuous from December 1956 to December 1957, and again from April 1958 to August 1958. No records were obtained from January to March 1958. Some 3 per cent of the operating time included echoes from accepted showers; records for these periods were rejected from the analysis.

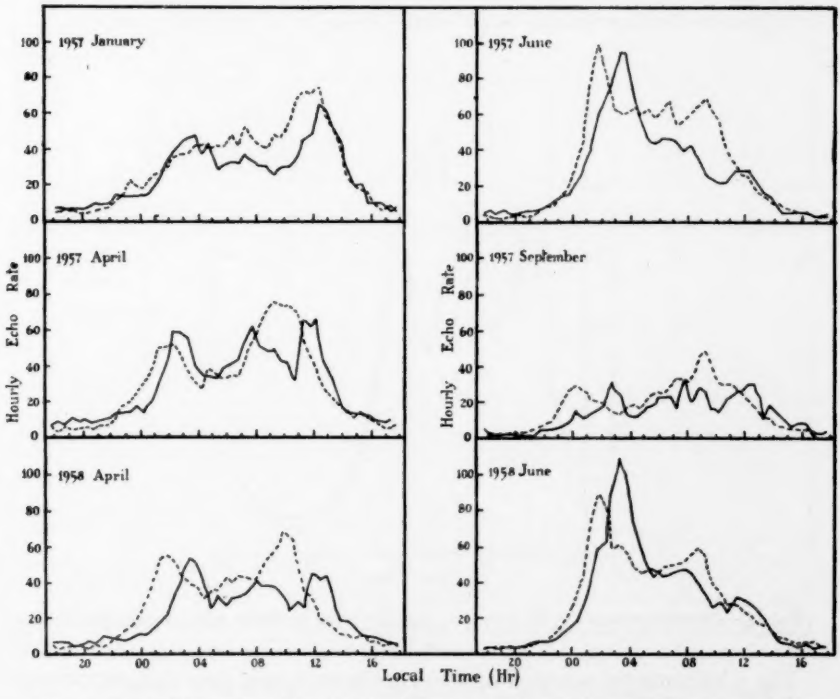

FIG. 2.—*Typical diurnal variations in the echo rate. Each curve is averaged over a calendar month.* – – – – N *aerial channel;* ——— S *aerial channel.*

Mean hourly rates, estimated by averaging the echo rate per ½-hr over a period of a month, are the basic material used in the following analysis. A first impression of the diurnal and seasonal variations in the echo rate may be obtained from the diurnal variations shown in Fig. 2 for the four seasons of the year; curves for two of the corresponding months in 1958 illustrate the repetition of the main features from year to year.

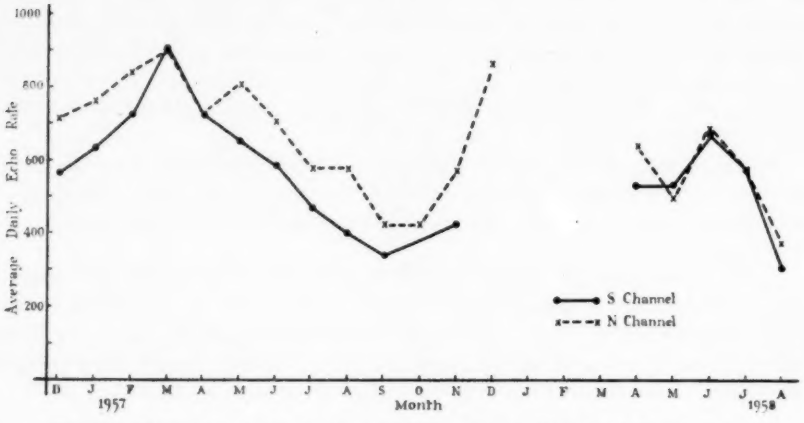

FIG. 3.—*Seasonal variation in the monthly average of the total daily echo rate.*

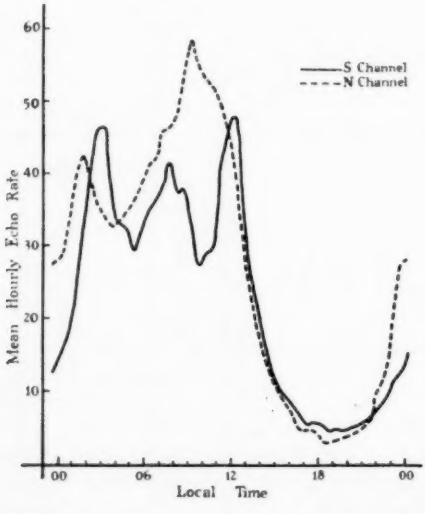

FIG. 4.—*Diurnal variation in the echo rate, averaged from December 1956 to November 1957.*

Fig. 3 indicates the seasonal variation in the total daily echo rate, corrected for equipment sensitivity. The average diurnal variation throughout the year, as found for the period December 1956 to November 1957, is sketched in Fig. 4.

4. *Analysis of the echo rates*

(*a*) *S aerial channel.*—In this channel the diurnal echo rate exhibits three peaks, each with different seasonal behaviour. The peaks near midnight and midday reach maxima in June and December respectively; the peak near 06 hr L.T. is a maximum in March and a minimum in September. The echo rate is a minimum near 19 hr in all months. On the supposition that this seasonal behaviour may be attributed to a sharp division of the sporadic radiant distribution into two components, contours of constant hourly echo rate have been prepared from the monthly diurnal variations. These are mapped in Fig. 5. Because it was known that the equipment sensitivity did not remain constant, the observed echo rates for some months have been corrected by small factors (from 0·76 to 1·50) needed for a reasonable compromise between regularity in the diurnal and in the seasonal variations.

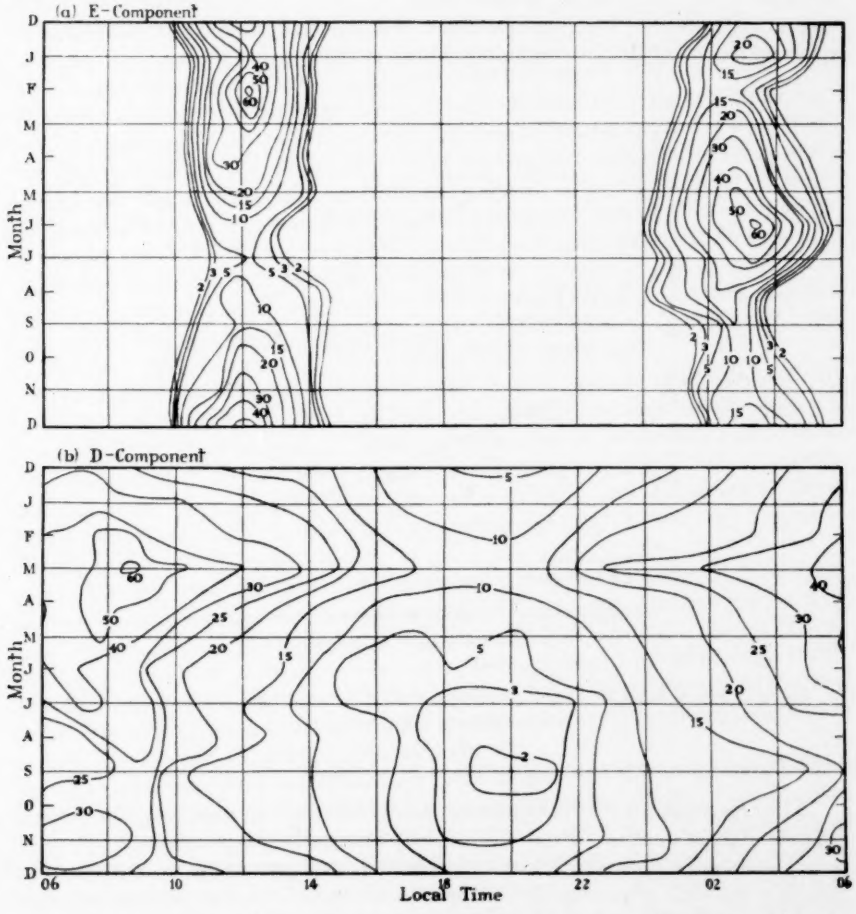

FIG. 5.—*Contours of constant echo rate from December 1956 to November 1957. Numbers against the contours are hourly echo rates. Contours have been prepared from diurnal variations similar to those in Fig. 2, on the assumption that the radiant distribution may be sharply differentiated into two components.*

The symmetry of these contours, and also of the average echo rates of Fig. 4, about 07 hr (or 19 hr) L.T. is what would be expected if the perihelia of the orbits are uniformly distributed in solar longitude, and if at the same time the ionosphere exerts no influence on the detection rate. This confirms the similar conclusion reached by Hawkins in his northern hemisphere survey.

The peak in the echo rate near 07 hr L.T. is due to antapex–apex streaming imposed by the motion of the Earth on a component of the sporadic radiant distribution which covers the whole of the celestial sphere. We will call this the *D*-component, and for convenience will refer to the apparent concentration round the apex as the apex source. The midday and midnight peaks originate in a second component, whose radiants are located in two regions with centres on the ecliptic at longitudes $\pm 68^\circ$ from the apex (Section 5). This is the *E*-component, with Sun and anti-Sun sources. The seasonal behaviour of the maximum echo rate from these two components is illustrated in Fig. 6. The inference from this diagram is that the *E*-component (Sun and anti-Sun) sources are more highly concentrated than the *D*-component (apex) source.

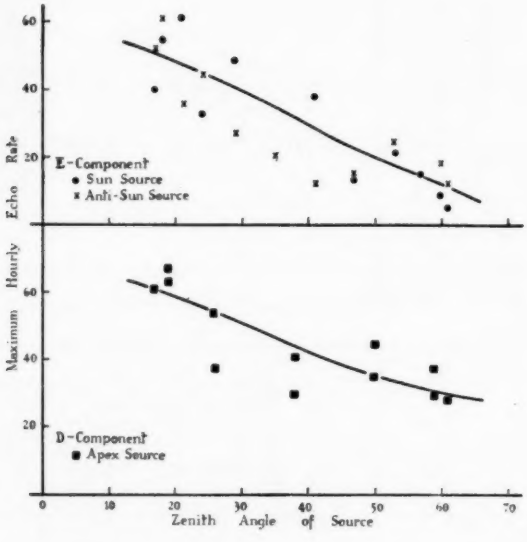

FIG. 6.—*The dependence of the echo rate from the Sun, anti-Sun and apex sources upon the zenith angle of the source.*

The echo rates for the S channel contain no information regarding the width in latitude of these sources. From Fig. 1 it is apparent that the axis of the S collecting area almost coincides with a line of constant hour angle (approximately + 1 hr), and that the time of passage of a point radiant across the collecting area increases slowly from 1 hr for $\delta = +25^\circ$ to 2 hr for $\delta = -55^\circ$. The time of appearance of echoes in the S channel (relative to transit time) and their duration is thus insensitive to the declination of any point source which is not too close to the south

celestial pole. Consequently the time of passage of a diffuse source centred on the ecliptic is determined almost completely by the width of the source in longitude. Hence the only influence of the gyrations of the ecliptic on the S channel rate is to alter the apparent strengths of the sources from month to month; the general form of the diurnal variation is unchanged and the three sources are clearly resolved at all times of the year.

(*b*) *N aerial channel.*—On the other hand, the peculiar form of the diurnal variation on the N channel, in which the anti-Sun source is always resolved but the apex and Sun sources are blended over most of the year, can only be understood if the *D*-component has considerable width in latitude whilst the diameters of the *E*-component sources are comparatively small. Lines of constant hour angle intersect the N collecting area at angles up to 90°, and the length of time over which echoes are detected from a diffuse source is now determined by the width in latitude as well as in longitude.

This is most clearly illustrated by the situation at the March equinox. If we postulate, for example, a high density of radiants in the *D*-component at elongations from the apex as small as 30°, this component in March will continue to give a high echo rate for some 6 hr after the apex itself has passed out of the N collecting area. Consequently echoes will be received from the *D*-component for some time after the centre of the Sun source (at $\delta = 0$) has passed through the collecting area, and the apex and the Sun sources cannot be resolved. The abrupt fall in the echo rate after midday, and the complete resolution of the apex and anti-Sun sources in all seasons, point to a close concentration of the *E*-component to its two centres.

At the September equinox the zenith angle of the apex source at transit is a maximum. The time of passage of the apex source is not so protracted and the echo rate is low, and one would expect the N channel rates to be dominated by the *E*-component sources. This also agrees with observation.

The diffuseness of the *D*-component also affords a natural explanation of the observation by Hawkins in his Jodrell Bank Survey that the echo rate in his sector 1 increases from 20 to 08 hr L.T., whilst the echo rate in his sector 2 decreases. Hawkins's sector 1 is equivalent to our N collecting area but is not so greatly inclined to the N–S meridian (25° compared with our 35°·5); his sector 2 is also inclined to this meridian at an angle of 25°, which is larger than the 14° for our S collecting area.

5. *The E-component.*—From the contours of Fig. 5 the width in R.A. (and hence in longitude) of each of the two sources of this component is approximately 5 hr. This agrees with the width of 75° found by Hawkins and Prentice (1957) for meteors brighter than $M_V \sim +3$. It is not possible to determine the width in latitude from the echo rates, but evidence from both channels suggests that the axes of the sources are comparatively short. Hawkins and Prentice give approximately equal widths in latitude and longitude.

The radiants of the two sources have been determined month by month from the times of appearance of echoes in the two channels. Radiant positions in ecliptical co-ordinates are illustrated in Fig. 7. The accuracy of the radiants does not warrant corrections for zenith attraction and diurnal aberration, even if the velocity were known, and they have not been applied. Although an analysis based on probability ellipses shows that the distribution of the radiant positions about the mean is approximately Gaussian, there is some suggestion of an annual variation in all four co-ordinates. It is not known whether this is a real effect or

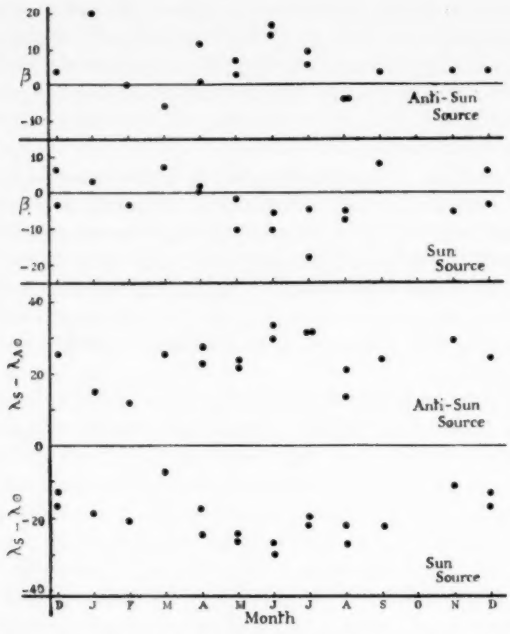

FIG. 7.—*Latitude and longitude of the Sun and anti-Sun sources from December 1956 to August 1958.*

due to errors introduced by the blending of the apex and Sun sources on the N aerial channel. The mean radiant positions are:

Sun source	$\lambda-\lambda_{\odot} = -20{\cdot}8 \pm 6{\cdot}1^{\circ}$	$\beta = -2{\cdot}7 \pm 6{\cdot}7^{\circ}$
Anti-Sun source	$\lambda-\lambda_{A\odot} = +24{\cdot}1 \pm 6{\cdot}4^{\circ}$	$\beta = +5{\cdot}5 \pm 7{\cdot}6^{\circ}$

The centres of the two sources most probably lie on the ecliptic at elongations $\pm 68^{\circ}$ from the apex. This is in excellent agreement with the elongations of $\pm 66^{\circ}$ found by Hawkins (1956a).

The orbits of the meteors constituting the *E*-component have been described by Hawkins. They are probably direct, elliptical with high eccentricity, and with semi-major axes comparable with those of the short period meteor streams.

6. *The D-component.*—Because the apex source is not resolved on the N channel, it is not possible to determine the centre of the radiant area at the time of maximum activity in the same way as for the *E*-component; the identification of this point with the apex rests on the results of previous surveys. In confirmation of Hawkins's result, from 15–21 hrs L.T. there is no time displacement between N and S channels, which suggests an avoidance of the ecliptic over this period. This is consistent with antapex–apex streaming in the *D*-component, but the following qualification is necessary. The seasonal variation in the echo rate near the time of passage of the antapex is indicated in Fig. 8, in which is plotted the hourly echo rate averaged over the period 18–20 hr L.T. Since the celestial pole lies inside the S collecting area, this suggests that high declination radiants exist in unusual numbers in the early part of the year. This has already been noted (Weiss 1957) as a time of relatively low density of meteors in the Earth's orbit.

There are in Section 4 two lines of evidence that the *D*-component is only weakly concentrated to the apex. Although the present survey affords no evidence, it is reasonable to suppose that for this component the radiant density is a function of the apparent elongation ϵ from the apex; the visual results of Hawkins and Prentice (1957) lend weight to this supposition. This radiant density law includes the special cases in which the heliocentric velocities of all meteors are the same and the meteor orbits are distributed uniformly in heliocentric co-ordinates. These are the models *U* already introduced in interpreting the results of the previous Adelaide survey. Although neither of these assumptions is justified, these models *U* form a convenient starting point for the interpretation of the contours of Fig. 5 (*b*).

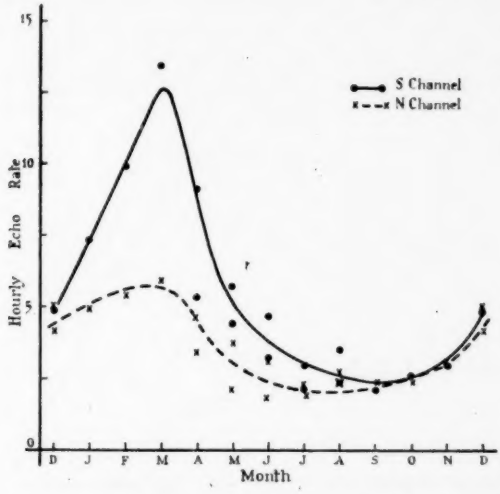

FIG. 8.—*The seasonal variation in the echo rate on the two aerial channels from* 18–20 *hr L.T., around the time of passage of the antapex.*

Computation of complete theoretical contours for comparison with Fig. 5 is not justified. The extent to which models *U* fail to account for the observations can be judged adequately by confining attention to the echo rates at those times when the apex or antapex lies on the axis of the S collecting area (approximately 07 and 19 hrs L.T.). Echo rates at these times are plotted in Fig. 9 as a function of angular distance ψ, where $90-\psi$ is the elevation of the apex along the great circle representing the axis of the S collecting area (see Fig. 1). Additional information is available at 13 hr L.T. in June and December, when the apex–antapex axis is approximately perpendicular to the S collecting area; the echo rate is then 16/hr.

The S collecting area (Fig. 1) is a strip of almost constant angular width centred on the great circle perpendicular to the direction of maximum echo sensitivity, which is at elevation 10°, azimuth 14°N of E. The behaviour of the echo rate across a traverse of this strip is (from shower data) independent of the elevation of the traverse. It is then reasonable to approximate this collecting area by a strip of constant angular width, with uniform sensitivity along any traverse, and sensitivity as a function of elevation $90-\theta$ as deduced from Fig. 6. Denote this sensitivity by $W(\theta)$. Let us now consider the times when the apex falls on the axis of this collecting area, and denote by $D(\epsilon)$ the apparent radiant density along

any great circle joining the apex and antapex. $D(\epsilon)$ so defined is independent of season. Provided the collecting strip is not too wide, the solid angle subtended at the centre of the celestial sphere by a small element ϵ to $\epsilon + d\epsilon$ or the collecting strip is independent of ϵ except in the vicinity of the apex or antapex where, for given $d\epsilon$, the solid angle first increases and then decreases to zero as $\epsilon \to 0$ or 180°.

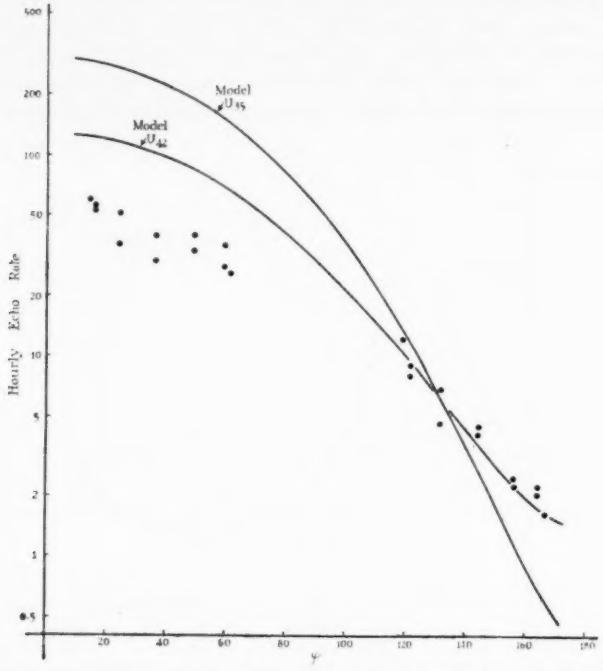

FIG. 9.—*Comparison of observed and predicted echo rates as a function of elevation, 90–ψ, of the apex along the axis of the S collecting area. Predicted rates are normalized to the echo rate of 16/hr observed when the apex–antapex axis is perpendicular to the S collecting area.*

To a sufficient approximation, the echo rate when the apex lies on the axis of the S collecting area is

$$N(\psi) = \int_{-\pi/2}^{\pi/2} W(\theta)\, D(\theta - \psi)\, d\theta$$

where ψ is a function of season. The apparent radiant density $D(\epsilon)$ is given by

$$D(\epsilon) = \frac{V'}{V} \frac{\sin \epsilon_0}{\sin \epsilon} \frac{d\epsilon_0}{d\epsilon}.$$

ϵ_0 is the true elongation of the radiant whose apparent elongation is ϵ, V is the heliocentric velocity and V' the geocentric velocity of the meteor. We have

$$\epsilon_0 = \epsilon + \arcsin\left(\frac{V_E}{V} \sin \epsilon\right)$$

$$\frac{d\epsilon_0}{d\epsilon} = 1 + \left(1 - \frac{V_E^2}{V^2} \sin^2 \epsilon\right)^{-1/2} \frac{V_E}{V} \cos \epsilon$$

$$V'^2 = V^2 + V_E^2 + 2V_E V \cos \epsilon_0.$$

V_E is the velocity of the Earth.

Computed echo rates for $V = 42$, 35 km/sec are shown in Fig. 9. These have been normalized to an echo rate of 16/hr when the apex–antapex axis is perpendicular to the axis of the collecting strip; the computed echo rate is then

$$N_{\epsilon=90} = D(\epsilon = 90^\circ) \int_{-\pi/2}^{+\pi/2} W(\theta)\, d\theta.$$

It is evident that the observed echo rates for the D-component may be satisfied *formally* by a uniform heliocentric radiant distribution with hyperbolic velocities; further calculation indicates $V \sim 50$ km/sec. This is reminiscent of the hyperbolic orbits inferred from visual counts under an identical set of assumptions. Since the hyperbolic velocities are no longer acceptable, the observations imply an excess of direct over retrograde orbits. The actual ratios of direct to retrograde orbits are found to be 2·5 for $V = 42$, 4·0 for $V = 40$, 15 for $V = 35$ km/sec. These ratios are much smaller than that found by Hawkins (1956 a), who gives a ratio of 30 for $V = 40$ km/sec; Hawkins and Prentice (1957) find a still larger ratio (~ 50) from their visual observations.

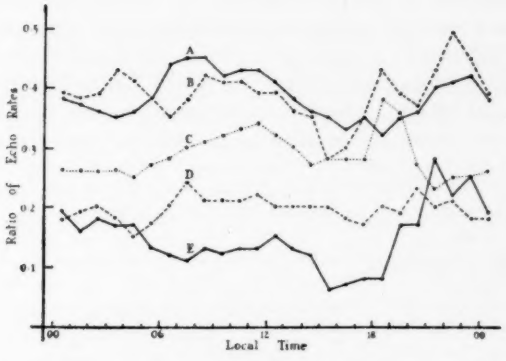

FIG. 10.—*Diurnal variation of echo rate as a function of equipment sensitivity, 1957. Each curve is a ratio of the echo rates measured with a common receiver and two video outputs, one held at constant high sensitivity whilst the other varies between medium and low sensitivity* A—*Oct. 26 to Nov. 12*; B—*Nov. 21 to Nov. 27*; C—*Dec. 2 to Dec. 25*; D—*Nov. 27 to Dec. 2*; E—*Nov. 12 to Nov. 16.*

That this discrepancy in the ratio of direct to retrograde orbits is not an effect of different limiting sensitivities between the three surveys is established by Fig. 10. In this diagram are plotted the ratios (smoothed in a running group of 3) of echo counts made on the N channel with a common receiver and two video output stages, one held at constant high sensitivity whilst the other was varied between medium and low sensitivity. At lowest sensitivity the maximum echo rate was 8/hr, and at highest sensitivity, 75/hr. There is a tendency for the echo rate at low sensitivity to be comparatively lower near 18 hrs L.T. than near 06 hr, which would imply an increase in the proportion of direct orbits amongst the fainter meteors.

7. *Comparison with the 27 mc/s survey.*—The 27 mc/s survey, extending from 1952 to 1956, was made with a broad-beam aerial system directed towards the zenith. The resolving power was so low that, on the basis of the echo rates alone, it was not possible to distinguish between a distribution of radiants confined

to the plane of the ecliptic with an apparent apex–antapex ratio of 4 : 1 (model *E*), and a distribution uniform in heliocentric co-ordinates, except for a moderate preponderance of direct over retrograde orbits. Supplementary measurements of the directions of reflection points of trails indicated a concentration of sporadic radiants to the apex, with additional strong concentrations near the helion and antihelion positions.

The model E, with radiants closely confined to the plane of the ecliptic, is ruled out by the present survey. We then see that the two surveys agree as to the main features of the sporadic radiant distribution. In particular, neither survey supports a very great preponderance of direct over retrograde orbits in the *D*-component.

In the present survey the equipment sensitivity was not sufficiently well controlled for any firm conclusions to be possible regarding the variation of density of meteors round the Earth's orbit. It is however apparent that there is no evidence for annual variations much larger than the ± 20 per cent found in the earlier Adelaide survey.

We have already had occasion to refer more than once to the excellent agreement between the present results and the northern hemisphere radio and visual surveys. Although some discrepancy remains as to the extent, but not the existence, of the excess of direct over retrograde orbits, there is little doubt that the discrepancy is not an astronomical effect. There is no major change in the sporadic radiant distribution as the threshold brightness is lowered from the 3rd to the 7th magnitude.

Division of Radiophysics, C.S.I.R.O.,
Department of Physics,
University of Adelaide:
1959 *December* 31.

References

Hawkins, G. S., 1956a, *M.N.*, **116**, 92.
Hawkins, G. S., 1956b, *Astron. J.*, **61**, 386.
Hawkins, G. S., and Prentice, J. P. M., 1957, *Astron. J.*, **62**, 234.
Weiss, A. A., 1955, *Aust. J. Phys.*, **8**, 148.
Weiss, A. A., 1957, *Aust. J. Phys.*, **10**, 77.
Weiss, A. A., 1960, *M.N.*, **120**, 387.

ABSOLUTE MEASURES OF STELLAR RADIATION

R. V. Willstrop

(Communicated by the Director of the Cambridge Observatories)

(Received 1960 February 10)

Summary

Observations at the Cambridge Observatories showed that the broad-band V and B photometric systems may be reproduced by observations in narrow bands about 200 A broad centred at 5410 A and at 4390 A respectively. At the Royal Observatory, Cape of Good Hope, measurements were made of the radiation flux outside the Earth's atmosphere in four narrow ($\sim$ 200 A) wave-length bands from stars of known magnitude and colour index, by comparing bright stars with an artificial star, composed of a calibrated lamp and blue filter. A 4-inch refractor was used, with interference filters and a d.c. photometer. The results are given in Table I. They are in good agreement with some other recent measurements. Systematic errors are discussed in detail.

Narrow-band visual magnitudes were measured for 221 stars, and compared with broad-band visual magnitudes determined by Johnson, by Hogg and by Eggen, and with early and recent Cape results. When linear colour equations are removed the standard deviations of the residuals are between $\pm 0^{m}{\cdot}014$ and $\pm 0^{m}{\cdot}036$. The internal random errors of the best individual series are believed to be $\pm 0^{m}{\cdot}010$ (narrow-band) $\pm 0^{m}{\cdot}007$ (Johnson) and $\pm 0^{m}{\cdot}007$ (Cape). It follows that the large differences usually found between similar broad-band visual magnitudes cannot be explained by differences of band-width and equivalent wave-length combined with differences of stellar spectra.

There is good agreement between the present narrow-band colour indices and gradients on the Greenwich system measured at Mt Stromlo. The relation between absolute and Greenwich gradients was found to be $\phi = G_G + 1{\cdot}11$, in excellent agreement with the best previous results.

---

1. *Introduction.*—The total radiation of a star cannot be measured, for the Earth's atmosphere absorbs large parts of the ultra-violet and infra-red radiation, and no receiver is perfectly absorbing at all wave-lengths. "Monochromatic" measures in regions only 1 A wide, say, are also impracticable, for the sensitivity would be inconveniently low, and the measures would not represent the brightness of the star as this is normally understood because stellar spectra do not have a smooth black-body energy distribution but are affected by absorption or emission lines or bands. Narrow-band measures are an acceptable compromise, for, as Woolley (1) has shown, if measures of spectra are restricted to a band-width of less than 200 A in the visual region the average intensity in the band will be proportional to the intensity at its centre, within 0·1 per cent. Only the most intense stellar spectral features would seriously affect measures made in a region 200 A wide.

There are now accurate broad-band photometric measures of several hundred bright stars, and less accurate measures of many thousands more. It would, therefore, be of considerable value to theoretical astrophysicists to determine the flux of radiation of certain wave-lengths received, outside the Earth's atmosphere, from stars of apparent magnitude $V = 0{\cdot}00$ and of various colour

indices. The present problem is to select suitable narrow-band regions of the spectrum, to measure the intensity of stellar radiation in them, and to find with what accuracy narrow-band measures may imitate broad-band measures. The observations required were made at the Cambridge Observatories and at the Royal Observatory, Cape of Good Hope, and are described below.

In all absolute determinations of stellar radiation it is necessary to measure and to allow for the atmospheric absorption. An important practical advantage of narrow-band measurements is that the effective wave-length is defined almost entirely by the equipment; it is scarcely affected by the spectral distribution of the stars observed. Therefore the atmospheric absorption is not sensibly dependent on the colours of these stars. The spectral sensitivity of the detector used cannot always be measured with the greatest precision, but if, as here, narrow-band measures are made, it can have but little effect on the equivalent wave-length of the equipment. Sources with widely different colour temperatures may then be compared more reliably.

2. *The selection of suitable narrow-band regions.*—If narrow-band measures are made at the equivalent wave-length of the broad-band V system, say, the relative brightnesses of stars of various colour indices will be changed very little. There will be a quadratic term in the relative colour equation of the two systems, due to the band-width of the V system, but this may be smaller than observational errors. On the other hand, if the narrow-band measures are made at too short a wave-length, red stars will appear relatively faint, blue stars relatively brighter, than in the V system. This then provides an observational method of selecting suitable narrow-band regions. Ideally, many stars covering a wide range of colour index should be observed.

Observations were made with the 36-inch reflector of the Cambridge Observatories to find the required regions of the spectrum. Two monochromators were used, the first using quartz lenses and prisms, the second a grating and mirror in the Ebert–Fastie arrangement (**2**). Slits were placed in the spectrum to transmit the desired wave-length regions. The "blurring" of the edges of the regions transmitted caused by the seeing tremor disk or by maladjustment of the star image in the focal plane diaphragm was small compared with the width of the regions—about 200 A.

Using the first photometer, narrow-band observations were made of stars in certain of the Kapteyn Areas at $+15^{\circ}$ which had been measured on the International System (**3**), and in the galactic clusters IC 4665 and M39 measured on the U, B, V system (**4, 5**). The second photometer was used to make narrow-band observations of stars in the two clusters NGC 752 and Praesepe, also measured on the U, B, V system (**6, 7**).

The centres of regions 200 A wide which gave the best fit to the International System were at 4365 A and at 5435 A. The first of these does not agree well with the value of the effective wave-length of the I_{pg} region, 4270 A, determined by Seares and Joyner (**8**). Their value was the weighted mean wave-length to which Seed 27 plates were sensitive, the plates being exposed in a small spectrograph to "northern skylight". This method gives too much weight to the shorter wave-lengths, for even in a milky sky far more blue light will be scattered from the atmosphere into the spectrograph than yellow. The better agreement for the I_{pv} region between the present result, 5435 A, and the result of Seares and Joyner, 5430 A, is readily explained by the much smaller band-width

of that region, making their result less sensitive to the spectral distribution of the skylight used. The regions giving the best agreement with observations on the U, B, V system were centred at 4390 A and 5410 A. The ultra-violet region cannot be matched by a narrow-band region, except very roughly, because of the presence of more intense and more numerous spectral lines and other features there.

The atmosphere at Cambridge is rarely suitable for the most precise photometry, particularly if it is desired to compare a calibrated lamp with the stars. The observations were therefore continued at the Royal Observatory at the Cape of Good Hope.

3. *The measurement of stellar radiation in narrow-band regions.*—At the Royal Cape Observatory an artificial star, composed of a calibrated lamp and a colour temperature conversion filter, was compared with bright stars. A 4-inch refractor was used, and a d.c. photometer with an E.M.I. photomultiplier and four interference filters, y, b_1, b_2, and b_3, which were chosen using the Cambridge results as a guide. y had its peak transmission at 5410 A. b_2 had its maximum transmission at 4390 A, but was relatively transparent at 4340 A and it was feared therefore that Hγ would affect measures of A-type stars. The two other filters,

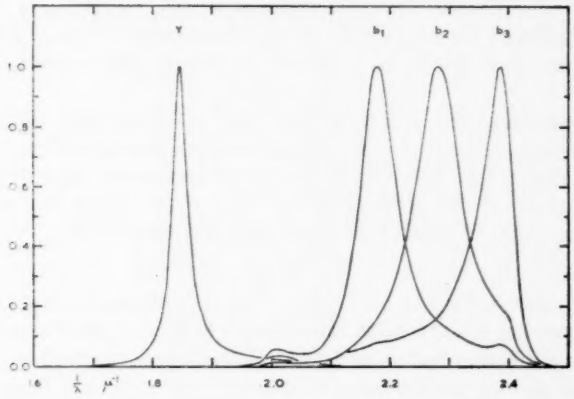

FIG. 1.—*The response of the photometer used at the Cape. Secondary maxima in the transmissions of the 'b' filters were removed with a dichroic filter, which is responsible for the cut-off at 4150A and the dip and rise at 4900A to 5000A common to all three. Secondary maxima in the 'y' filter transmission were avoided by using a photomultiplier insensitive at 7000A, and incorporating yellow glass in the filter.*

b_1, with maximum transmission at 4600 A, and b_3 at 4220 A. were chosen to avoid Hβ, Hγ and Hδ. The transmissions of these filters were measured at the Cape with a double monochromator and d.c. photometer, the light falling on the filters just as when they were in use in the telescope. The relative sensitivity of the photomultiplier was obtained from an E.M.I. publication; it is sufficiently precise to use typical manufacturers' data, for the filters alone define the equivalent wave-lengths of the photometer rather accurately. Although the sensitivity of the photomultiplier falls rapidly near 5400 A the equivalent wave-length of the y filter is changed only 25 A if the change of sensitivity is neglected. The response of the photometer is shown in Fig. 1. Each of the b filters was used with a dichroic filter to remove secondary maxima.

Observations were made to determine the magnitudes and colours of 16 "standard stars". Each of these was compared with the next at nearly equal altitudes on at least 20, and in some cases on 25 nights, in the order *a–b–a–b*. The average standard error for a comparison based on 20 nights was $\pm 0^{m}\cdot 003$; the closing error in the magnitudes was $0^{m}\cdot 014 \pm 0^{m}\cdot 012$. This closing error was removed by arbitrarily applying corrections of $0^{m}\cdot 001$ to all but two of the comparisons. Magnitudes were then adopted for the standard stars, in agreement with these comparisons, and adjusting the origin of the scale to agree with that of other visual magnitude systems. The colour indices were adjusted to be equal to each other and to $(B-V)$ at $(B-V)=+0\cdot 5$.

The standard stars were also compared at unequal altitudes to determine the extinction. When each standard star was at about 30° altitude in the East it was compared with the standard star approaching the meridian, in the order *a–x–a–x–a*. The values of sec z for the times of the individual observations were obtained from graphs drawn for this purpose, and the zenith extinction was computed. Average values for the zenith extinction were:

y: $0^{m}\cdot 197$, b_1-y: $0^{m}\cdot 093$, b_2-y: $0^{m}\cdot 122$, b_3-y: $0^{m}\cdot 139$

but these must be corrected (Section 4.4) for systematic errors, less than $0^{m}\cdot 01$ in each case. On the total of 55 nights, fewer than 15 per cent of the means for the night differed by more than $0^{m}\cdot 025$ from these values. This includes intrinsic scatter, and errors of observation, which were mainly caused by scintillation.

The extra-atmospheric deflection for each standard star when near the meridian was then calculated, and compared with the deflection obtained on pointing the telescope to the artificial star, to determine the apparent magnitude and colour indices of the artificial star. The mean values for these, before applying corrections for systematic errors (all less than $0^{m}\cdot 01$), were

y: $-1^{m}\cdot 563$, b_1-y: $+0^{m}\cdot 618$, b_2-y: $+0^{m}\cdot 599$, b_3-y: $+0^{m}\cdot 691$.

The standard error of each is $\pm 0^{m}\cdot 003$. The observations of the artificial star were usually but not always made immediately before or after a determination of the extinction, for they had to be fitted into the programme without interfering with the equal altitude comparisons of standard stars. In the intervals left by these observations 1005 measurements were made of 205 other stars to try to discover how accurately narrow-band measures may reproduce broad-band measures, and to find the relations between the narrow-band y magnitudes and $b-y$ colour indices and broad-band V, $B-V$ measures.

The flux of radiation of certain wave-lengths received outside the Earth's atmosphere from a star of apparent magnitude $V=0\cdot 00$ was then determined from the following measurements:

(i) the colour temperature and luminous intensity of the lamp,

(ii) the transmission of the colour temperature conversion filter (see Section 4.2, below),

(iii) the distance of the objective of the telescope from the lamp,

(iv) the apparent magnitude and colour indices of the artificial star on the natural system of the photometer, after corrections for systematic errors had been applied, and

(v) the relations between this natural system and the standard U, B, V system of Johnson (**9**), defined by the narrow- and broad-band magnitudes and colour indices of the stars observed.

The results are shown in Table I. The relative values in most of this table are believed to have a standard error of ±1 per cent, the absolute values ±2 per cent, but the errors may be as large as ±3 per cent for stars of colour index $B-V$ greater than +1·2. It will be seen in Fig. 5 below that only four very red stars were measured both on the narrow-band system and by Johnson on the U, B, V system. These are not sufficient to define the relations between these two systems more precisely.

TABLE I

The flux of radiation received outside the Earth's atmosphere from a star of magnitude $V=0{\cdot}00$

(Unit = 10^{-7} ergs cm^{-2} sec^{-1} (100A)$^{-1}$)

$(B-V)$	5390A	4571A	4401A	4311A
−0·3	4·01	7·06	8·02	8·57
0·2	3·99	6·73	7·45	8·05
−0·1	3·98	6·41	6·91	7·52
0·0	3·96	6·12	6·40	6·96
+0·1	3·94	5·82	5·91	6·36
0·2	3·92	5·48	5·46	5·74
0·3	3·90	5·06	5·03	5·14
0·4	3·89	4·68	4·59	4·58
0·5	3·87	4·37	4·18	4·10
0·6	3·85	4·12	3·80	3·69
0·7	3·83	3·89	3·47	3·31
0·8	3·82	3·67	3·18	2·96
0·9	3·80	3·45	2·92	2·62
1·0	3·78	3·23	2·66	2·32
1·1	3·76	3·02	2·41	2·05
1·2	3·75	2·81	2·17	1·81
1·3	3·73	2·60	1·96	1·59
1·4	3·71	2·41	1·76	1·40
1·5	3·70	2·23	1·57	1·23
+1·6	3·68	2·06	1·41	1·08

4. *Systematic errors*

4.1. *Calibration of the lamp.*—The lamp compared with the stars, known as lamp A, was calibrated in 1957 August at the National Physical Laboratory, Teddington (N.P.L.), in 1958 May at the Council for Scientific and Industrial Research Laboratories, Pretoria, South Africa (C.S.I.R.), in 1959 January by comparison with other lamps calibrated at the N.P.L., and in 1959 March by comparison with a ribbon filament lamp calibrated at Professor Kienle's laboratory at Heidelberg. At the C.S.I.R. Laboratories the luminous intensity alone was measured; in every other case both the colour temperature and the luminous intensity were measured. The current in the lamp was adjusted by measuring the potential drop in a well-aged series resistor of about 0·12 ohms. The same series resistance, potentiometer, and calibrating standard cell were used at all calibrations and when the lamp was compared with the stars.

At the N.P.L., lamp A was aged and the current in it was then adjusted so that its colour matched a tertiary sub-standard lamp of colour temperature 2360 °K. The potential drop in the series resistance, 0·0937 volts, was then measured with the potentiometer and standard cell. The luminous intensity

was also measured, and was found to be 1·88 candelas. 1 candela is defined as the luminous intensity of 1/60 cm^2 projected area of a black-body at the temperature of melting platinum, 2042 °K. At the C.S.I.R. Laboratories the lamp was run as before, and the luminous intensity was found to be 1·90 candelas. By comparison with other lamps from the N.P.L. in 1959 January, when the stellar observations had been completed, the luminous intensity was found to be 1·917 candelas. The stellar comparisons do not confirm the small brightening of the lamp indicated by these laboratory calibrations. This does not necessarily prove an inconsistency, however, for the small difference in question could just about be accounted for by possible small secular changes in the behaviour of this type of lamp, going beyond the normal tolerances on the laboratory calibrations. Comparisons with the ribbon filament lamp yielded an intensity 3·2 per cent greater than the final N.P.L. result, illustrating the greater difficulty of absolute calibrations. It may be noted that the N.P.L. lamps were referred to a black-body at the platinum point, and the ribbon filament lamp to a black-body at the gold point.

As noted above, three determinations of the colour temperature of the lamp were made, at different times, in different regions of the spectrum, and by comparison with lamps calibrated with different black-bodies. The two N.P.L. calibrations, made at the beginning and at the end of the stellar observations, gave colour temperatures 2360 °K and 2380 °K respectively. This apparent rise in colour temperature may be due to ageing of the lamp, but is not confirmed by all the stellar comparisons. The emissivity of tungsten is not constant, but in the visible spectrum rises from long wave-lengths to short, more rapidly from 7000 A to 5500 A than from 5500 A to 4000 A. The colour temperature of a tungsten filament therefore depends on the wave-length at which it is measured. The N.P.L. results given above refer to the visible spectrum as a whole, but here we are interested only in the region from 5500 A to 4000 A. Measures of the emissivity of tungsten may be used to show that the colour temperature in the blue and green region of the spectrum is approximately 15 °K lower than in the whole of the visible spectrum (**10, 11**). The N.P.L. results given above are therefore equivalent to results of 2345 °K and 2365 °K in the blue and green region. The comparison with the ribbon filament lamp, after the stellar observations, gave the result 2375 °K in the blue and green region. The difference of 10 °K from the second N.P.L. result is a measure of the difficulty and uncertainty of absolute calibrations based on comparisons with different black-bodies. The mean of the N.P.L. results for the blue and green region was 2355 °K; the adopted colour temperature including the ribbon filament comparison was 5 °K higher, viz. 2360 °K in the blue and green region of the spectrum. These discordances in the calibration of the lamp, though small, are larger than the uncertainty in the comparison of the lamp with the stars. In any repetition of this work it would be advisable to make frequent photoelectric monochromatic comparisons of the lamp with a black-body source at a known temperature, and so avoid many of the present uncertainties.

The weighted mean luminous intensity of lamp A, at the mean epoch of the stellar comparisons, was, for the N.P.L. and C.S.I.R. calibrations alone,

$$1/4(1{\cdot}88)+1/4(1{\cdot}90)+1/2(1{\cdot}917)=1{\cdot}903 \text{ candelas.}$$

Because a tungsten filament is brighter in the green part of the spectrum than a

black-body matched for brightness, as at the N.P.L., over the whole of the visible spectrum, this is to be increased by 0·3 per cent when determining the intensity at 5390 A. Comparisons with the ribbon filament lamp indicated a result 3·2 per cent higher. Equal weight was given to the two measures by increasing the N.P.L. result by a further 1·6 per cent. The final value adopted for the luminous intensity of lamp A was 1·939 candelas.

The emission of a black-body at 2360 °K was obtained from tables (**12**) based on the following values of the radiation constants:

$$c_1 = 2hc^2 = 1{\cdot}1909 \times 10^{-5} \text{ erg cm}^2 \text{ sec}^{-1} \text{ radian}^{-2},$$

$$c_2 = hc/k = 1{\cdot}4380 \text{ cm } ^\circ\text{K},$$

where

$$B(\lambda) = \frac{c_1 \lambda^{-5}}{(e^{c_2/\lambda T} - 1)} \text{ erg cm}^{-3} \text{ sec}^{-1} \text{ radian}^{-2}.$$

These relative values were then normalized to make the luminous intensity of lamp A equal to 1·939 candelas, using the Relative Visibility Factor, or the sensitivity of the standard human eye, which is tabulated in various handbooks, and the relation between candelas and watts: 680·2 candelas of light of maximum visibility (5550 A) are equivalent to 1 watt radian^{-2}. These relations are consistent with each other and with the definition of the candela as the luminous intensity of 1/60 cm^2 of a black-body at the temperature of freezing platinum, 2042 °K.

4.2. *Calibration of the filter.*—The transmission of the blue colour temperature conversion filter was measured at the N.P.L., and at the Royal Cape Observatory, by the writer. An ideal colour temperature conversion filter should do nothing but change the spectrophotometric gradient of the lamp, a quantity which is almost independent of the wave-length at practicable temperatures. The logarithm of the transmission of the filter should therefore be a linear function of reciprocal wave-length. The best relation of this form which fitted the measures was

$$\log_{10} \tau = -1{\cdot}54(2{\cdot}490 - 1/\lambda).$$

In Fig. 2 the residuals

$$\log_{10} \tau + 1{\cdot}54(2{\cdot}490 - 1/\lambda)$$

are plotted against $1/\lambda$ to show the deviations of the filter from the ideal, either more transparent ($+ve$) or less ($-ve$). It will be noted that although the agreement between the N.P.L. and Cape measures is excellent from 5300 A to 6000 A there is an apparently systematic difference between the two sets of measures from 4200 A to 5200 A. However, the greatest difference, at 4800 A, is only 0·3 per cent of the light incident on the filter.

The measurements of the transmission of this filter made at the Cape were obtained with a double monochromator and the photoelectric photometer from the 4-inch telescope. A Hilger 4-prism spectrograph formed one half of the monochromator, with the plateholder replaced by an electric lamp with a small filament. Its dispersion ranged from 4 A/mm at 4000 A to 20 A/mm at 6000 A. The band pass varied between 4 and 20 A. The position of the lamp was measured carefully, and the wave-length transmitted was found within ±0·4 to ±2·0 A.

A Hilger Constant Deviation Spectrometer was the other half of the double monochromator. The photometer was removed bodily from the 4-inch telescope and its focal plane diaphragm served as the final slit.

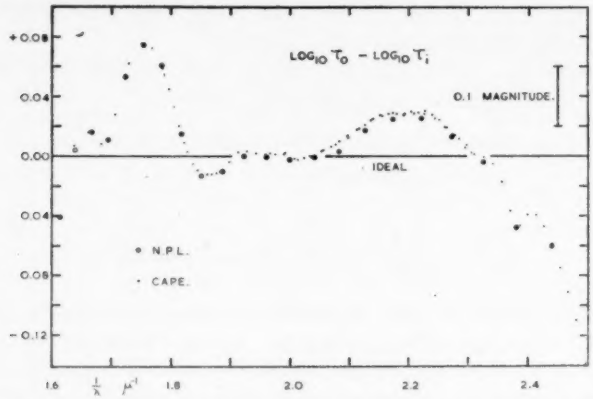

FIG. 2.—*The transmission of the colour temperature conversion filter relative to the "ideal" transmission,* $\log_{10} \tau = -1{\cdot}54\,(2{\cdot}490 - 1/\lambda)$.

The difference between the N.P.L. and Cape results might be explained by a systematic error of not more than 5 A in the measurement of the wave-lengths. The Cape measures were made in two runs, overlapping between 4335 A and 5142 A, the "camera" of the 4-prism spectrograph being readjusted between the two runs. An error in the Cape measures of the wave-lengths would show as a scatter between 4335 A and 5142 A. There is a slight scatter, but this is not as great as the difference between the Cape and N.P.L. results. A scale error in the photometer used would be expected to be greatest when measuring low transmissions, at long wave-lengths, but here the agreement is excellent. Tests showed that scattered light was negligible; the apparent transmission of one of the interference filters was found at one wave-length to be less than 2 parts in 10^6, while the maximum transmission was about 20 per cent. The colour temperature conversion filter was uniform, and the measurement of different areas, both central on the filter, could make no difference.

In the determination of a smoothed transmission equal weight was therefore given to each measurement. As the Cape measures were not made at wave-lengths for which the Planck Function is tabulated, the N.P.L. values were used at first in the calculation of the energy from the lamp incident on the telescope objective as a function of wave-length. These results were plotted against reciprocal wave-length, and a smooth curve was then drawn which bore the same relation to these points as did the smoothed transmission function to the N.P.L. values of the transmission. The intensity of the energy reaching the telescope was read from this graph at intervals of 25 A, and these values were weighted according to the relative sensitivity of the photometer with each filter in use.

4.3. *The distance of the lamp from the objective of the telescope.*—This was determined from a survey of the Royal Observatory grounds (**13**), and checked by direct measurement. The mean of the two results was 111·20 m and the difference between them 6 cm.

4.4. *The apparent stellar magnitude and colour indices of the artificial star.*—The artificial star was compared with a standard star near the zenith once every two or three hours. The atmospheric absorption was determined by comparing two stars, one near the zenith and the other at an altitude of about 30° in the East. Lower observations would give greater "leverage", but to be reliable would require the atmosphere to be uniform over a much larger distance, and the traces obtained on the Brown Recorder would have shown greater scintillation. The extinction was determined from the observations assuming that it was dependent linearly on $\sec z$, and independent of the azimuth and the colour indices of the stars observed. These assumptions are justified respectively if the air mass is equal to $\sec z$, as it very nearly is up to $\sec z = 2{\cdot}0$, if the atmosphere is well mixed, as it usually is by the south-easterly wind at the Cape, and if, as here, narrow-band measurements are made, making the effective wave-length of the star–atmosphere–telescope–filter–receiver combination very nearly independent of the colours of the stars.

Four very small corrections have to be made to the apparent magnitude and colour indices of the artificial star found in this way, because:

(i) the zenith distance at which the extinction star was observed was changing rapidly;

(ii) flexure and magnetic effects may alter the sensitivity of the photometer in different directions;

(iii) the air in the path of the light from the artificial star absorbed and scattered it; and

(iv) the artificial star faded slowly when unattended.

(i) The sidereal time of the middle of each observation was recorded to 0·1 min, and the value of $\sec z$ for the star was found from graphs drawn for this purpose. The zenith distance of one standard star of each pair compared was small and changed slowly, but the other, the "extinction star", was rising rapidly; on the average $\sec z$ decreased by 0·012 per minute. Each colour, y, b_1, b_2, b_3, was observed for about 50 seconds in that order. The y observations were accordingly made 75 seconds before the time of mid-observation, b_1 25 seconds before, b_2 25 seconds after, and b_3 75 seconds after.

The correction to the y magnitude of the artificial star is small, so it is sufficiently accurate to assume that the extinction star was at an altitude of 30°, $\sec z = 2{\cdot}0$, at the time of the y observation. The value of $\sec z$ for the standard star was, on the average, 1·08. The true difference of $\sec z$ would then be $2{\cdot}00 - 1{\cdot}08 = 0{\cdot}92$, but the observed difference, that for the time of mid-observation, $1{\cdot}985 - 1{\cdot}08 = 0{\cdot}905$. The y zenith extinction was therefore not, on the average, $0^{m}{\cdot}197$ but

$$0^{m}{\cdot}197 \times \frac{0{\cdot}905}{0{\cdot}920} = 0^{m}{\cdot}1938.$$

The difference between the corrected and uncorrected values of the y zenith extinction is $-0^{m}{\cdot}0032$, and the correction to the y magnitude of the artificial star, which was compared with standard stars observed through an average air mass of 1·08, is therefore

$$1{\cdot}08 \times -0^{m}{\cdot}0032 = -0^{m}{\cdot}0035.$$

Similarly it may be shown that the corrections to the blue magnitudes of the artificial star are

$$b_1: \ -0^{m}\cdot0017, \qquad b_2: \ +0^{m}\cdot0018, \qquad b_3: \ +0^{m}\cdot0059,$$

and the corrections to the colour indices are

$$b_1-y: \ +0^{m}\cdot0018, \qquad b_2-y: \ +0^{m}\cdot0053, \qquad b_3-y: \ +0^{m}\cdot0094.$$

(ii) Flexure following movement of the telescope and photometer may change the optical path or the illuminated area of the photomultiplier cathode, and will also change the orientation of the photomultiplier in the Earth's magnetic field. These effects may alter the sensitivity of the photometer and were therefore investigated.

The photometer was attached to the telescope by a welded angle iron frame. Flexure was certainly slight, and movement of the Fabry image small compared with its own diameter of 3 mm. The average sensitivity of the cathode over an area of this size may be assumed to vary almost linearly if the movement is small. The photomultiplier and its housing were rotated through 120° after each night on which 50 or more observations were made, or after a similar number of observations on two nights or more. In this way a comparable number of observations was made in each orientation, and the effect of flexure is virtually eliminated.

If the E.M.I. photomultiplier used were perfectly symmetrical about its longitudinal axis, rotation about that axis would not alter the effect of the Earth's magnetic field on its sensitivity, but rotation about any other axis might. The cell was tested by mounting a radium spot firmly a short distance from the photocathode. It was found that the sensitivity varied as the telescope was moved to point in turn to the artificial star, the average standard star position and the average extinction star position, but the variations were different for the three different orientations of the photomultiplier and its housing relative to the telescope. The peak-to-peak variation in any orientation of the photomultiplier was of the order of $0^{m}\cdot01$, but when the average in all three orientations was calculated it was found that the sensitivity when pointing to the standard star position was only about $0^{m}\cdot0007$ greater than the average of the sensitivities when pointing to the artificial star and to the average extinction star position. Because the artificial, standard and extinction stars were observed through air masses of approximately 0, 1, and 2 units, the correction to the magnitude of the artificial star is $-0^{m}\cdot0014$. No correction is required for the colour indices.

This effect may be explained if the stream of electrons liberated from the cathode is not symmetrically placed in the dynode assembly; more electrons may be "spilled" off the edges of the dynodes in some orientations than in others. The cathode of this photomultiplier is displaced about 2 mm from the mechanical centre of the glass envelope.

(iii) The artificial star was about 111 metres from the telescope. It is reasonable to suppose that the absorption and scattering of light by the air in this path is the same as that by a similar thickness elsewhere, for the observations carrying greatest weight were made in windy, turbulent conditions. At 15 °C the scale height of the atmosphere is about 8·5 kilometres and the extinction of the artificial star was approximately 111/8500 of the zenith extinction. The corrections are

y	b_1-y	b_2-y	b_3-y
$-0^{m}\cdot0026$	$-0^{m}\cdot0012$	$-0^{m}\cdot0016$	$-0^{m}\cdot0018$.

Ozone contributes about $0^m.03$ to the zenith extinction at 5400 A and is absent at ground level, but the corrections are not appreciably affected by this refinement.

The observations of Stebbins and Kron at the Lick Observatory (**14**) over an air path five times as long as that used here showed that this simple approach is justified by its accuracy.

(iv) More than an hour after switching on the lamp, when the accumulator had reached an almost constant potential and the controlling resistors had reached a steady temperature, the current in the lamp fell very slowly as the accumulator discharged. The lamp then faded at a rate between $0^m.02$ and $0^m.03$ per hour if the current was not readjusted. The artificial star was therefore observed as soon as possible, about four minutes, after readjusting the current. In this interval it would fade by about $0^m.0017$.

The systematic corrections to the magnitude and colour indices of the artificial star are summarized in Table II.

TABLE II

Summary of corrections to the magnitude and colour indices of the artificial star

	y	b_1-y	b_2-y	b_3-y
Observed, uncorrected:	−1·563	+0·618	+0·599	+0·691
Changing zenith distance:	−0·0035	+0·0017	+0·0053	+0·0094
Magnetic effect:	−0·0014	...	...	...
Absorption of light from the artificial star:	−0·0026	−0·0012	−0·0016	−0·0018
Fading of the artificial star when unattended:	−0·0017	−0·0003	−0·0003	−0·0003
Observed, corrected:	−1·572	+0·618	+0·602	+0·698

5. *Comparison with other workers' results*

5.1. *Absolute measures.*—The result given in Table I for the radiation flux received from a star of apparent magnitude $V=0.00$ and colour index $(B-V)=0.60$ is

$$(3.85\pm0.08)\times10^{-7}\ \text{ergs cm}^{-2}\,\text{sec}^{-1}\,(100\,\text{A})^{-1}\ \text{at 5390 A.}$$

This may be compared with the result of Woolley and Stibbs (**15**) for a star of magnitude $I_{pv}=0.00$ and of solar type,

$$(3.37\pm0.13)\times10^{-7}\ \text{ergs cm}^{-2}\,\text{sec}^{-1}\,(100\,\text{A})^{-1}\ \text{at 5430 A.}$$

Woolley and Stibbs used Kuiper's (**16**) value of the apparent magnitude of the Sun, $I_{pv}=-26.84\pm0.04$. If the more recent value of Stebbins and Kron (**14**) is used, $I_{pv}=-26.73\pm0.03$, and if allowance is made for the difference of zero point between the I_{pv} and V scales (**9, 17**), $0^m.017$, the result of Woolley and Stibbs for a star of $V=0.00$ becomes

$$(3.67\pm0.11)\times10^{-7}\ \text{ergs cm}^{-2}\,\text{sec}^{-1}\,(100\,\text{A})^{-1}\ \text{at 5430 A.}$$

The remaining difference of 4·8 per cent cannot fully be explained as the result of differences of line absorption in the solar spectrum between 5380 A and 5480 A and in stellar spectra of solar type near 5390 A; such differences are not likely to be more than 1 per cent. If the colour temperature of the Sun is 6500 °K at 5400 A the difference to be expected from the change of intensity of its continuous spectrum alone is only 0·7 per cent.

Dunkelman and Skolnik (**18**) have measured the solar radiation flux, and found

$$19.7\ \text{microwatts cm}^{-2}\,\text{A}^{-1}\ \text{at 5390 A.}$$

If this is combined with the writer's value, the apparent magnitude of the Sun is found to be $V = -26{\cdot}772$ or $I_{pv} = -26{\cdot}755$, in good agreement with Stebbins and Kron's value, $I_{pv} = -26{\cdot}73$.

5.2. *Magnitudes and colour indices.*—Narrow-band magnitudes and colour indices of 221 stars are given in Table III. The internal agreement of measures of stars other than standards shows that the standard error of one observation is $\pm 0^{m}{\cdot}020$ in the magnitudes, and about $\pm 0^{m}{\cdot}025$ in the colour indices.

TABLE III

Magnitudes and colour indices of 221 stars

The stars are identified by their numbers in the Revised Harvard Photometry (H.A.**50**), and by their names. The narrow-band magnitude, y, and colour indices, $b-y$, are given, and the number, N, of observations. Standard stars are indicated by S. In the last column, Notes, stars observed recently at the Cape (**20**), by Johnson (**9**), Hogg (**21**), or by Eggen (**22**) for magnitudes and colour indices, or by S. C. B. Gascoigne at Canberra (**24**) for relative gradients, are indicated by C, J, H, E and G respectively.

HR	Name	y	b_1-y	b_2-y	b_3-y	N	Notes
15	α And	2·09	+0·105	−0·03	−0·105	5	H
39	γ Peg	2·835	+0·06	−0·105	−0·175	6	JHEG
45	χ Peg	4·845	+1·28	+1·605	+1·915	5	J
98	β Hyi	2·855	+0·57	+0·595	+0·655	5	C HEG
99	α Phe	2·46	+0·89	+1·065	+1·23	5	C HE
188	β Cet	2·105	+0·84	+0·97	+1·15	S	C HE
437	η Psc	3·68	+0·815	+0·945	+1·07	5	JHE
472	α Eri	0·49	+0·095	−0·085	−0·145	6	H G
493	107 Psc	5·295	+0·695	+0·80	+0·945	5	J E
509	τ Cet	3·555	+0·645	+0·72	+0·78	S	CJHEG
531	χ Cet	4·68	+0·385	+0·35	+0·315	6	C
553	β Ari	2·65	+0·25	+0·18	+0·135	5	JHEG
591	α Hyi	2·885	+0·355	+0·285	+0·265	5	C HEG
617	α Ari	2·08	+0·92	+1·115	+1·305	5	JHE
674	ϕ Eri	3·565	+0·10	−0·06	−0·12	5	C H G
718	ξ^2 Cet	4·29	+0·15	+0·01	−0·07	4	CJHE
779	δ Cet	4·07	+0·05	−0·125	−0·165	4	C HEG
804	γ Cet	3·485	+0·21	+0·11	+0·05	5	C E
813	μ Cet	4·315	+0·37	+0·325	+0·30	4	CJHE
875	...	5·165	+0·24	+0·145	+0·07	5	CJH
897/8	θ Eri	2·935	+0·235	+0·135	+0·08	5	C G
911	ν Cet	2·595	+1·325	+1·66	+1·93	6	C E
996	κ Cet	4·905	+0·605	+0·645	+0·71	5	CJHE
1030	o Tau	3·67	+0·77	+0·845	+0·945	5	CJ
1084	ϵ Eri	3·80	+0·72	+0·85	+0·97	S	CJHE
1101	10 Tau	4·335	+0·555	+0·555	+0·595	5	C E
1136	δ Eri	3·58	+0·775	+0·90	+1·025	5	C E
1208	γ Hyi	3·32	+1·30	+1·615	+1·885	6	C HE
1231	γ Eri	3·035	+1·25	+1·595	+1·875	6	C
1346	γ Tau	3·715	+0·805	+0·94	+1·10	6	JH
1347	41 Eri	3·575	+0·095	−0·055	−0·135	6	C H G
1373	δ Tau	3·835	+0·805	+0·94	+1·10	9	J
1409	ϵ Tau	3·595	+0·825	+0·955	+1·125	5	JH
1412	θ^2 Tau	3·425	+0·26	+0·205	+0·14	5	J
1457	α Tau	0·965	+1·205	+1·54	+1·81	5	J E

TABLE III—*continued*

HR	Name	y	b_1-y	b_2-y	b_3-y	N	Notes
1465	α Dor	3·265	+0·115	−0·04	−0·11	6	C G
1520	μ Eri	4·04	+0·10	−0·055	−0·15	6	C
1543	π^3 Ori	3·23	+0·475	+0·445	+0·445	6	CJHEG
1552	π^4 Ori	3·68	+0·10	−0·06	−0·155	5	CJHEG
1666	β Eri	2·815	+0·25	+0·155	+0·075	6	CJHEG
1713	β Ori	0·20	+0·185	+0·025	−0·03	S	JH G
1829	β Lep	2·87	+0·72	+0·785	+0·855	5	C
1865	α Lep	2·625	+0·315	+0·235	+0·18	6	C EG
1899	ι Ori	2·79	+0·045	−0·14	−0·23	4	CJ G
1903	ϵ Ori	1·71	+0·10	−0·095	−0·16	5	CJH G
1998	ζ Lep	3·57	+0·21	+0·135	+0·04	6	CJH G
2004	κ Ori	2·095	+0·11	−0·07	−0·135	6	CJH G
2085	η Lep	3·775	+0·385	+0·315	+0·285	5	C
2282	ζ CMa	3·025	+0·06	−0·12	−0·195	5	C H G
2294	β CMa	1·99	+0·055	−0·135	−0·215	5	C HEG
2326	α Car	−0·70	+0·275	+0·175	+0·135	5	H G
2429	ν^2 CMa	4·045	+0·84	+1·00	+1·19	6	C
2443	ν^3 CMa	4·515	+0·905	+1·11	+1·275	4	C
2491	α CMa	−1·40	+0·14	+0·025	−0·065	S	JH G
2550	α Pic	3·285	+0·315	+0·23	+0·19	5	C HEG
2596	ι CMa	4·41	+0·18	+0·01	−0·05	4	C
2618	ϵ CMa	1·505	+0·065	−0·115	−0·195	5	C G
2653	o^2 CMa	3·055	+0·16	−0·015	−0·07	6	C H G
2693	δ CMa	1·895	+0·625	+0·645	+0·695	5	C HEG
2763	λ Gem	3·59	+0·205	+0·12	+0·055	5	J
2773	π Pup	2·79	+1·32	+1·61	+1·835	5	C
2827	η CMa	2·485	+0·165	−0·01	−0·06	5	C HEG
2943	α CMi	0·395	+0·445	+0·405	+0·41	7	CJHEG
2985	κ Gem	3·62	+0·77	+0·895	+1·03	5	J
3131	...	4·635	+0·21	+0·10	+0·045	6	C
3165	ζ Pup	2·255	+0·03	−0·17	−0·23	6	C HEG
3206/7	γ Vel	1·755	−0·11	−0·18	−0·22	S	C H G
3249	β Cnc	3·605	+1·16	+1·455	+1·725	5	CJH
3307	ϵ Car	1·95	+1·125	+1·32	+1·42	5	C H
3314	c Hya	3·92	+0·14	+0·025	−0·085	5	CJH
3447	o Vel	3·60	+0·08	−0·105	−0·18	5	C H G
3454	η Hya	4·305	+0·06	−0·115	−0·195	5	CJHEG
3468	α Pyx	3·68	+0·09	−0·09	−0·155	7	C H G
3485	δ Vel	1·96	+0·175	+0·055	−0·025	5	C HEG
3547	ζ Hya	3·17	+0·835	+0·96	+1·13	5	E
3659	a Car	3·44	+0·07	−0·115	−0·19	6	C H G
3665	θ Hya	3·895	+0·13	−0·01	−0·10	8	CJ G
3685	β Car	1·685	+0·17	+0·035	−0·03	5	C HEG
3699	ι Car	2·27	+0·285	+0·195	+0·155	5	C HE
3748	α Hya	2·07	+1·135	+1·415	+1·69	S	C HE

TABLE III—*continued*

HR	Name	y	b_1-y	b_2-y	b_3-y	N	Notes
3849	κ Hya	5·075	+0·09	−0·06	−0·165	7	C E
3873	ϵ Leo	3·02	+0·74	+0·78	+0·84	3	
3982	α Leo	1·37	+0·115	−0·05	−0·13	9	JH G
4031	ζ Leo	3·47	+0·38	+0·305	+0·30	4	E
4037	ω Car	3·325	+0·135	−0·035	−0·08	6	C H G
4054	40 Leo	4·82	+0·495	+0·45	+0·465	6	JHE
4133	ρ Leo	3·855	+0·12	−0·05	−0·12	4	CJ EG
4199	θ Car	2·755	+0·045	−0·15	−0·215	6	C G
4216	μ Vel	2·745	+0·76	+0·85	+0·975	6	C
4232	ν Hya	3·19	+0·99	+1·205	+1·425	5	C E
4357	δ Leo	2·565	+0·24	+0·165	+0·085	6	E
4456	90 Leo	5·925	+0·11	−0·065	−0·17	6	JH
4467	λ Cen	3·145	+0·14	−0·01	−0·08	6	C H G
4517	ν Vir	4·095	+1·185	+1·53	+1·845	6	
4534	β Leo	2·145	+0·215	+0·12	+0·045	9	J EG
4540	β Vir	3·63	+0·545	+0·535	+0·57	8	CJHE
4630	ϵ Crv	3·09	+1·05	+1·285	+1·535	7	C
4662	γ Crv	2·60	+0·11	−0·05	−0·125	S	CJHEG
4729/30/31	α Cru	0·76	+0·02	−0·165	−0·22	5	H G
4757	δ Crv	2·965	+0·15	+0·015	−0·07	7	C HEG
4786	β Crv	2·71	+0·77	+0·85	+0·96	5	C H
4819	γ Cen	2·175	+0·14	+0·025	−0·05	7	C HEG
4825/6	γ Vir	2·78	+0·41	+0·34	+0·34	7	C EG
4844	β Mus	3·06	+0·055	−0·125	−0·19	5	C H G
4853	β Cru	1·26	+0·04	−0·165	−0·225	5	C H G
4932	ϵ Vir	2·885	+0·785	+0·90	+1·045	5	E
5011	59 Vir	5·25	+0·555	+0·555	+0·63	5	E
5019	61 Vir	4·78	+0·64	+0·71	+0·75	6	CJHE
5020	γ Hya	3·05	+0·77	+0·86	+1·01	6	C EG
5028	ι Cen	2·77	+0·17	+0·06	−0·02	5	C EG
5056	α Vir	0·98	+0·05	−0·14	−0·215	S	CJH G
5072	70 Vir	4·985	+0·67	+0·70	+0·76	6	J E
5107	ζ Vir	3·40	+0·23	+0·14	+0·07	6	C E
5132	ϵ Cen	2·28	+0·06	−0·14	−0·205	4	C H G
5190	ν Cen	3·405	+0·045	−0·14	−0·225	3	C H G
5231	ζ Cen	2·535	+0·04	−0·16	−0·235	4	C G
5235	η Boo	2·71	+0·575	+0·575	+0·61	7	J EG
5264	τ Vir	4·265	+0·23	+0·14	+0·095	5	C H
5267	β Cen	0·625	+0·055	−0·145	−0·21	3	H G
5288	θ Cen	2·14	+0·845	+0·97	+1·15	5	C HE
5338	ι Vir	4·13	+0·51	+0·49	+0·505	4	C E
5340	α Boo	0·00	+0·99	+1·21	+1·405	6	JHE
5459/60	α Cen	−0·23	+0·64	+0·675	+0·76	3	G
5463	α Cir	3·205	+0·31	+0·235	+0·22	7	C EG
5469	α Lup	2·31	+0·065	−0·125	−0·185	4	C G

TABLE III—*continued*

HR	Name	y	b_1-y	b_2-y	b_3-y	N	Notes
5477/8	ζ Boo	3·775	+0·195	+0·10	+0·02	5	E
5511	109 Vir	3·76	+0·155	+0·02	−0·055	6	CJH
5531	α^2 Lib	2·775	+0·245	+0·16	+0·105	S	CJHEG
5576	κ Cen	3·16	+0·055	−0·135	−0·195	3	G
5685	β Lib	2·62	+0 115	−0·035	−0·11	5	CJHEG
5694	5 Ser	5·07	+0·51	+0·515	+0·59	6	CJHE
5793	α CrB	2·245	+0·135	+0·03	−0·04	5	J E
5812	τ Lib	3·66	+0·08	−0·095	−0·17	4	C G
5842	ι Ser	4·50	+0·205	+0·10	+0·035	3	J
5854	α Ser	2·695	+0·94	+1·13	+1·355	5	CJHE
5867	β Ser	3·68	+0·195	+0·10	+0·045	5	JHE
5868	λ Ser	4·48	+0·57	+0·575	+0·61	4	CJHE
5881	μ Ser	3·55	+0·175	+0·05	−0·04	3	C
5897	β TrA	2·86	+0·38	+0·305	+0·29	6	C G
5933	γ Ser	3·88	+0·505	+0·47	+0·505	6	JHE
5977/8	ξ Sco	4·20	+0·48	+0·44	+0·46	3	C E
5984/5	β Sco	2·51	+0·165	+0·01	−0·055	S	CJHEG
6056	δ Oph	2·79	+1·275	+1·60	+1·935	3	C E
6075	ϵ Oph	3·295	+0·81	+0·92	+1·065	3	C E
6095	γ Her	3·765	+0·35	+0·285	+0·26	5	J E
6148	β Her	2·835	+0·785	+0·90	+1·025	3	E
6165	τ Sco	2·83	+0·045	−0·15	−0·225	2	C H G
6175	ζ Oph	2·585	+0·24	+0·095	+0·04	5	CJ EG
6217	α TrA	2·01	+1·10	+1·425	+1·68	3	C H
6241	ϵ Sco	2·36	+0·925	+1·105	+1·335	3	C HEG
6252	μ^2 Sco	3·57	+0·055	−0·14	−0·21	3	C G
6378	η Oph	2·435	+0·195	+0·10	+0·03	S	C EG
6380	η Sco	3·36	+0·445	+0·385	+0·395	5	C EG
6486	44 Oph	4·205	+0·32	+0·25	+0·25	3	C
6553	θ Sco	1·88	+0·435	+0·375	+0·39	5	C EG
6556	α Oph	2·105	+0·27	+0·20	+0·15	4	HEG
6561	ξ Ser	3·57	+0·33	+0·265	+0·245	5	C
6580	κ Sco	2·42	+0·04	−0·14	−0·18	2	C HEG
6603	β Oph	2·83	+0·945	+1·12	+1·35	5	CJ E
6615	ι^1 Sco	3·07	+0·54	+0·51	+0·515	4	C HEG
6629	γ Oph	3·755	+0·225	+0·125	+0·005	3	CJHE
6698	ν Oph	3·40	+0·835	+0·95	+1·135	2	C E
6710	ζ Ser	4·665	+0·42	+0·36	+0·36	4	CJ E
6752	70 Oph	4·055	+0·70	+0·83	+0·96	3	C E
6832	η Sgr	3·115	+1·315	+1·59	+1·90	5	C
6859	δ Sgr	2·79	+1·08	+1·345	+1·64	4	C
6869	η Ser	3·325	+0·78	+0·885	+1·025	4	CJHE
6879	ϵ Sgr	1·84	+0·155	+0·02	−0·035	4	C HEG
6913	λ Sgr	2·90	+0·85	+1·01	+1·175	4	C E
6973	α Sct	3·93	+1·04	+1·29	+1·57	5	C

TABLE III—*continued*

HR	Name	y	b_1-y	b_2-y	b_3-y	N	Notes
7061	110 Her	4·24	+0·475	+0·455	+0·48	5	J E
7121	σ Sgr	2·085	+0·065	−0·11	−0·17	3	C H G
7141/2	θ Ser	4·035	+0·27	+0·22	+0·17	2	CJ
7194	ζ Sgr	2·615	+0·195	+0·105	+0·04	S	C EG
7235	ζ Aql	3·00	+0·17	+0·04	−0·02	4	J EG
7236	λ Aql	3·455	+0·10	−0·04	−0·105	3	C HEG
7264	π Sgr	2·935	+0·415	+0·35	+0·34	3	C G
7340	ρ^1 Sgr	3·95	+0·28	+0·24	+0·225	3	C E
7377	δ Aql	3·40	+0·37	+0·33	+0·295	3	E
7525	γ Aql	2·815	+1·18	+1·49	+1·775	3	E
7536	δ Sge	3·815	+1·265	+1·465	+1·63	3	
7557	α Aql	0·805	+0·28	+0·22	+0·18	5	CJHEG
7602	β Aql	3·785	+0·725	+0·825	+0·925	7	CJHE
7710	θ Aql	3·25	+0·11	−0·02	−0·105	3	C G
7754	α^2 Cap	3·635	+0·78	+0·905	+1·08	4	C G
7776	β Cap	3·135	+0·71	+0·765	+0·85	S	C E
7869	α Ind	3·18	+0·815	+0·95	+1·115	5	C
7913	β Pav	3·43	+0·27	+0·185	+0·15	4	C HEG
7950	ϵ Aqr	3·785	+0·155	+0·035	−0·04	5	CJH
8131	α Equ	3·975	+0·49	+0·51	+0·54	4	E
8173	1 Peg	4·165	+0·875	+1·05	+1·245	3	J
8204	ζ Cap	3·82	+0·82	+0·975	+1·115	3	C G
8232	β Aqr	2·95	+0·72	+0·795	+0·88	S	C G
8308	ϵ Peg	2·47	+1·235	+1·53	+1·785	5	HE
8313	9 Peg	4·42	+0·96	+1·125	+1·325	3	E
8353	γ Gru	3·02	+0·095	−0·05	−0·12	5	C G
8414	α Aqr	3·01	+0·82	+0·93	+1·06	5	HEG
8430	ι Peg	3·805	+0·475	+0·425	+0·46	5	J E
8450	θ Peg	3·55	+0·195	+0·105	+0·03	6	C E
8502	α Tuc	2·955	+1·09	+1·35	+1·62	5	C
8518	γ Aqr	3·88	+0·115	−0·01	−0·09	5	C E
8558/9	ζ Aqr	3·70	+0·46	+0·405	+0·405	2	CJ E
8597	η Aqr	4·05	+0·11	−0·02	−0·10	4	C H
8665	ξ Peg	4·255	+0·50	+0·505	+0·51	5	JHE
8673	69 Aqr	5·69	+0·16	+0·05	−0·05	5	
8675	ϵ Gru	3·515	+0·195	+0·09	+0·04	5	C G
8704	74 Aqr	5·79	+0·145	−0·005	−0·08	7	CJ
8709	δ Aqr	3·29	+0·195	+0·105	+0·025	S	C G
8717	ρ Peg	4·91	+0·18	+0·07	−0·02	5	CJHE
8728	α PsA	1·18	+0·19	+0·11	+0·04	6	C HEG
8729	51 Peg	5·505	+0·595	+0·64	+0·705	4	J E
8773	β Psc	4·545	+0·095	−0·04	−0·115	4	C
8781	α Peg	2·52	+0·155	+0·025	−0·045	5	JHEG
8795	55 Peg	4·595	+1·25	+1·585	+1·88	5	CJHE
8852	γ Psc	3·755	+0·775	+0·91	+1·025	5	C E

TABLE III—*continued*

HR	Name	y	b_1-y	b_2-y	b_3-y	N	Notes
8911	κ Psc	4·95	+0·175	+0·08	+0·02	5	C E
8969	ι Psc	4·18	+0·53	+0·51	+0·52	5	JHE
8984	λ Psc	4·515	+0·295	+0·22	+0·165	6	C
8988	ω^2 Aqr	4·49	+0·145	+0·025	−0·045	4	C
9098	2 Cet	4·55	+0·145	+0·01	−0·065	5	C
9103	3 Cet	5·045	+1·285	+1·63	+1·93	5	

The standard errors of the tabulated magnitudes and colours are believed to be $\pm 0^{m}\cdot 010$ and $\pm 0^{m}\cdot 013$ respectively. They are rounded off to the nearest $0^{m}\cdot 005$. Colour indices may usually be measured more accurately than magnitudes, but in this case because of the small aperture of the telescope the principal source of random errors was scintillation, and the colours, depending on comparisons of ratios of deflections, cannot be measured as accurately as the magnitudes, which depend on comparisons of single deflections.

These magnitudes and colour indices have been compared with broad-band measures made at the Cape (**19, 20**), and by Johnson (**9**), Hogg (**21**) and Eggen (**22**). The relations between broad- and narrow-band visual magnitudes are sensibly linear, but those between colour indices or blue magnitudes are non-linear and in some cases have inflections, because of the greater band-width of the region measured for B magnitudes and because spectral lines are stronger there and more numerous than in the visual region.

The comparisons of the narrow-band magnitudes and colours with two series of measurements made at the Cape, and with Johnson's measures, are shown in Figs. 3 to 7. The V and $B-V$ measures in the first Cape series (**19**) (Fig. 3) were determined from the B_{pg} and C_{pe} measures of Cape Mimeogram No. 1, using the relations (**20**)

$$V = B_{pg} - 1\cdot 31 C_{pe} - 0\cdot 035 + (0\cdot 012 - 0\cdot 0437(C_{pe} - 0\cdot 52)^2) + E$$

and

$$B - V = 1\cdot 037 C_{pe} + 0\cdot 195$$

where E is an empirical term for stars with $B-V$ less than $-0\cdot 1$. These magnitudes were determined photographically by the Fabry method; the colours, measured photoelectrically in 1949, 1950 and 1951, required corrections for non-linearity in the galvanometer, lamp, and scale combination. These measures are not regarded at the Cape as a first-class series, and have been superseded by magnitudes and colour indices measured photoelectrically with the 18-inch reflector at the Royal Cape Observatory (**20**). This series, known in this paper as the second Cape series, is now almost completed. Clearly the agreement with the second Cape series (Fig. 4) is much better than with the first. In Fig. 4 the circle represents γ Vel, a star with a Wolf–Rayet spectrum. The only other star showing a residual greater than $0^{m}\cdot 04$ from the mean colour equation, η Sgr, has not yet been fully observed at the Cape. There appears to be no scale error (Fig. 6) and the residuals do not appear to increase significantly for the faint stars. There are some variations of the residuals with right ascension (Fig. 7) but a comparison made eight months ago, when the y magnitudes were completed and the Cape magnitudes more than half complete, showed no variation with right ascension except that which is now shown between 2^{h} and 8^{h}.

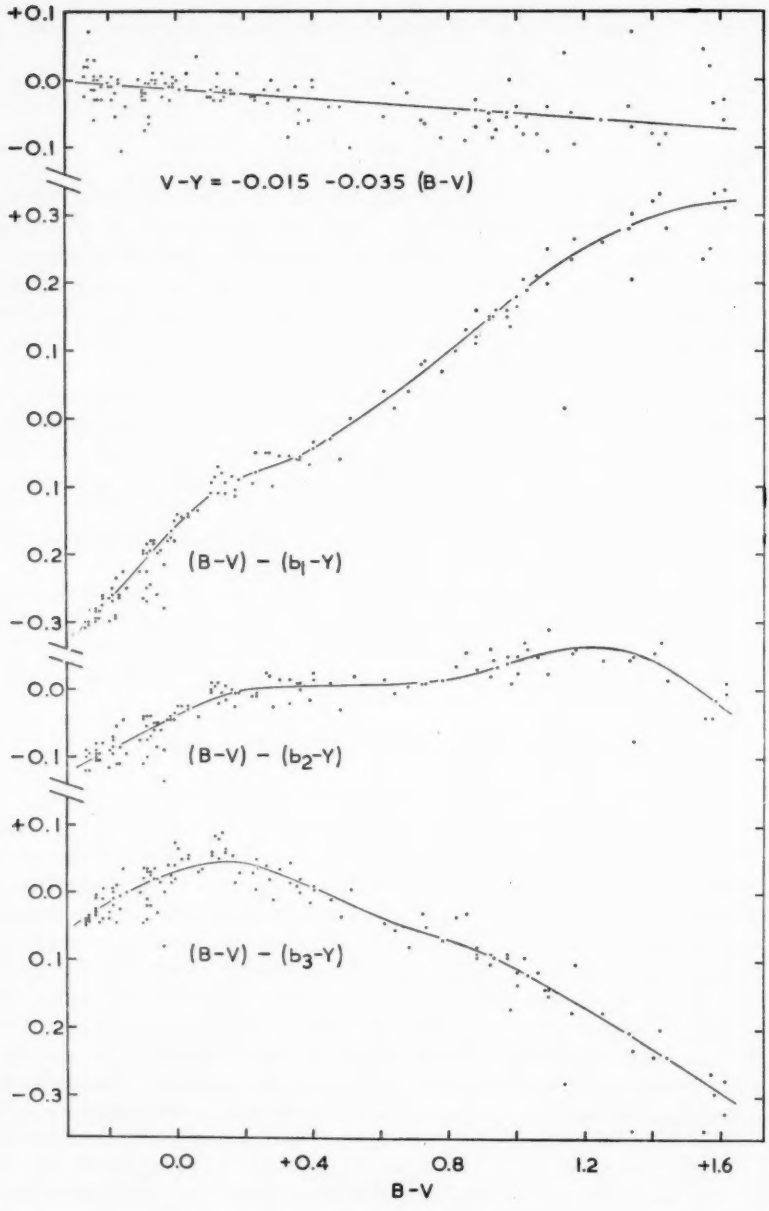

FIG. 3.—*Comparison of narrow-band measures with V and B—V measures derived from Cape Mimeogram No. 1.*

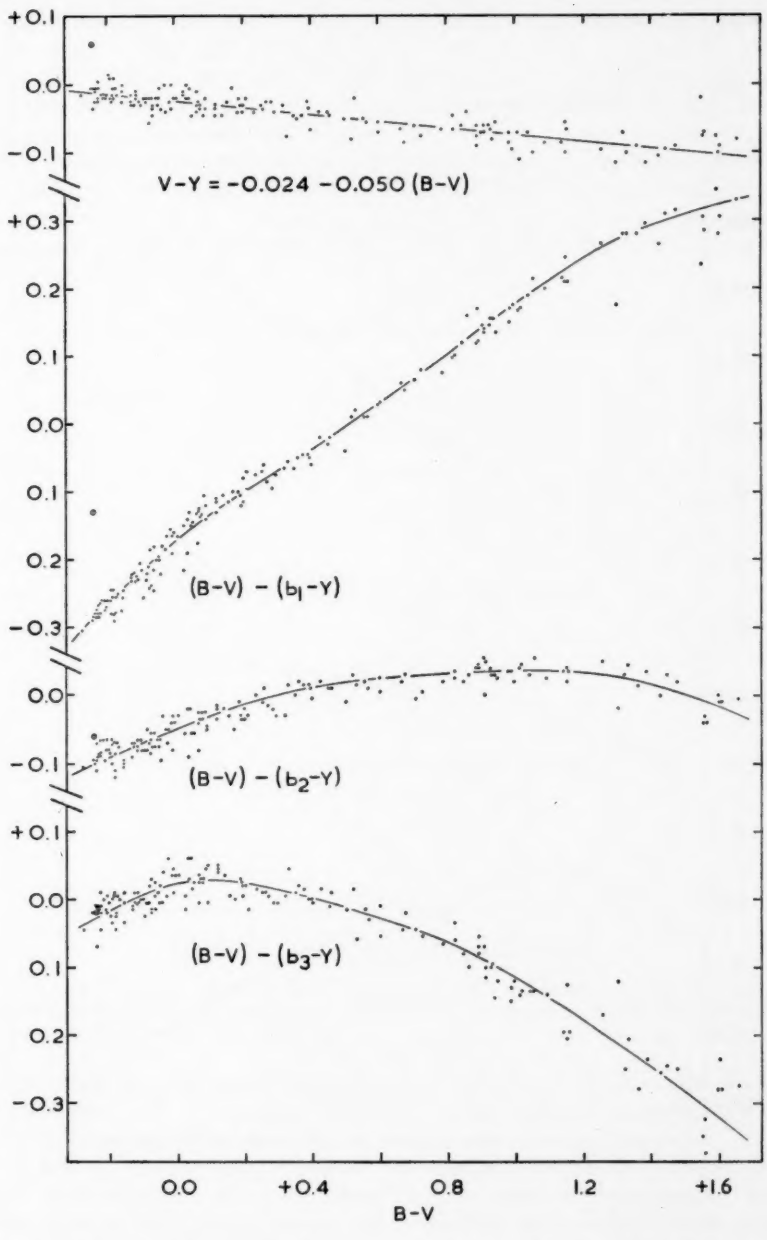

FIG. 4.—*Comparison of narrow-band measures with the latest Cape V and B−V measures. γ Vel, a star with a Wolf–Rayet spectrum, is shown as a circle.*

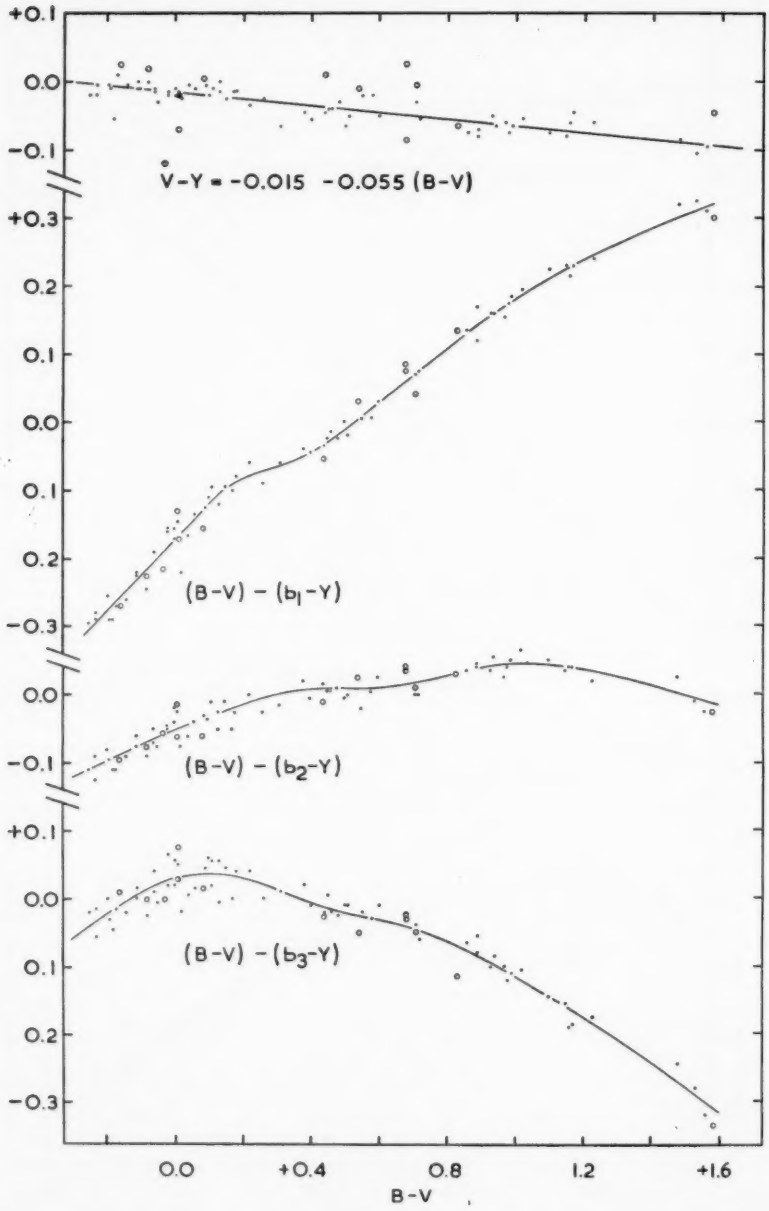

FIG. 5.—*Comparison of narrow-band measures with V and B−V measures of Johnson. The stars shown as circles are α CMa, β Ori, and eleven stars fainter than V=4·8.*

A preliminary comparison with magnitudes measured by Johnson (**9**) (Fig. 5) was less satisfactory, but a large part of this disagreement was traced to eleven stars fainter than $V = 4{\cdot}8$, which presumably had not been measured accurately by the writer with the 4-inch telescope and narrow-band filters, and two very bright stars, α CMa and β Ori, shown as circles in Figs. 5, 6 and 7. The agreement between the narrow-band and Johnson's magnitudes for the remaining 65 stars is as good as between the narrow-band and second Cape series of magnitudes; the differences between the results appear to be independent of the magnitudes of the stars and very nearly independent of their right ascensions. The scatter of the residuals appears to be a little larger between 2^h and 8^h; as this is also shown in the comparison with the second Cape series the writer's magnitudes are almost certainly at fault. The errors in the first Cape series obscure these small variations.

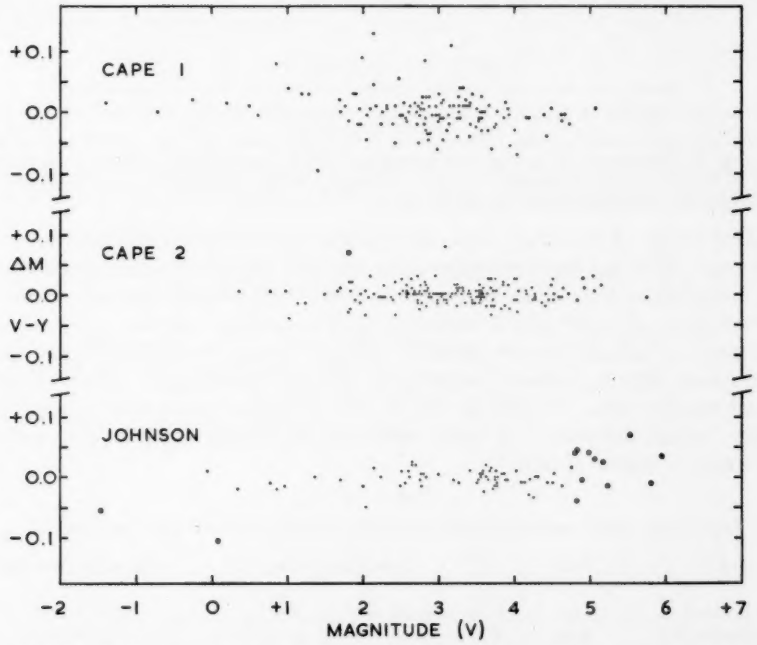

FIG. 6.—*Comparison of narrow-band y magnitudes with V magnitudes measured at the Cape and by Johnson versus magnitude after corrections for colours are applied. The stars shown as circles are described in the legends to Figs. 4 and 5.*

Comparisons of the narrow-band measures with the V, $B-V$ results of Hogg (**21**) and the V, $P-V$ results of Eggen (**22**) show differences similar to those found in the comparison with the first Cape series.

The best linear colour equations between the broad- and narrow-band visual magnitudes are given in Table IV. The standard deviations are those of the residuals between the narrow-band and other magnitudes after the colour equation is removed. It includes all errors of measurement, and the small random differences to be expected as a result of the different band-widths and equivalent wave-lengths measured and the peculiarities of stellar spectra. The internal

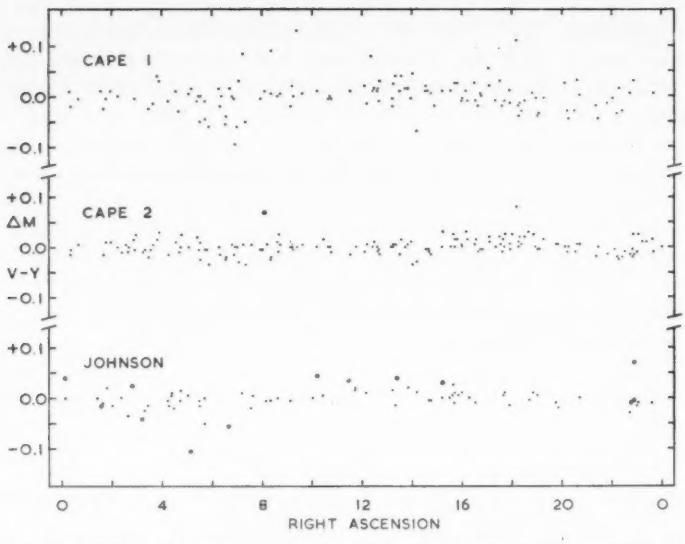

FIG. 7.—*Comparison of narrow-band y magnitudes with V magnitudes measured at the Cape and by Johnson versus right ascension after corrections for colours are applied. The stars shown as circles are described in the legends to Figs. 4 and 5.*

standard errors of the latest Cape magnitudes and Johnson's are believed to be $\pm 0^{m}.007$. The residuals between these and the narrow-band magnitudes are very little larger than is to be expected from their internal errors; a further external error of $\pm 0^{m}.007$ is sufficient fully to account for the residuals. If such good agreement may be obtained between broad- and narrow-band visual magnitudes, slightly different broad-band systems should agree with each other at least equally well. In general they do not, but this cannot now be explained by the "slight differences of band-width and equivalent wave-length, and the properties of stellar spectra".

TABLE IV

Best linear colour equations relating broad- and narrow-band visual magnitudes

Source of V	Ref.	Colour equation	Standard deviation
Cape Series I	(19)	$V=y-0.015-0.035\,(B-V)$	$\pm 0^{m}.032$
Cape Series II	(20)	$V=y-0.024-0.050\,(B-V)$	$\pm 0^{m}.014$
Johnson	(9)	$V=y-0.015-0.055\,(B-V)$	$\pm 0^{m}.023$
Johnson		(rejecting 13 stars)	$\pm 0^{m}.014$
Hogg	(21)	$V=y-0.015-0.015\,(B-V)$	$\pm 0^{m}.028$
Eggen	(22)	$V=y-0.020-0.070\,(P-V)$	$\pm 0^{m}.036$

A comparison of the b_1 magnitudes, at equivalent wave-length 4571 A, and the narrow-band magnitudes m_{4550} of Hogg and Hall (**23**) shows a colour equation of the expected sign and magnitude:

$$m_{4550}-b_1=-0.262+0.023(B-V).$$

The zero difference is large because Hogg and Hall adjusted their magnitudes to be equal to B or V magnitudes at $(B-V)=0.0$, while the b_1-y colour indices were made equal to $(B-V)$ at $+0.5$. The residuals, $\pm 0^{m}.023$, are rather larger

than would be expected from the stated internal errors of the two series, $\pm 0^{m}\cdot 008$ in the m_{4550} measures, $\pm 0^{m}\cdot 010$ in the y magnitudes and $\pm 0^{m}\cdot 013$ in the b_1-y colour indices from which the b_1 magnitudes were found.

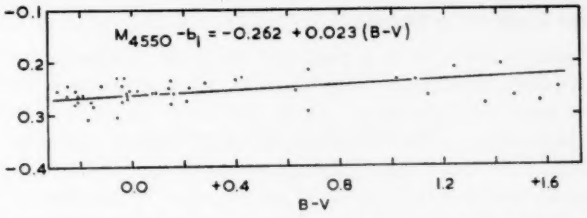

FIG. 8.—*Comparison of narrow-band b_1 and m_{4550} magnitudes of Hogg and Hall.*

5.3. *Gradients.*—The $b-y$ colour indices are compared with gradients on the Greenwich system determined at Mt Stromlo (**24**) in Fig. 9. The straight lines have the theoretical slope

$$\Delta C/\Delta G = \frac{1}{\lambda_1} - \frac{1}{\lambda_2} \Big/ 0\cdot 921$$

and are drawn through the mean positions of the groups of points representing the hotter stars. Cooler stars deviate systematically from these relations, for the effects of spectral lines are greater at short wave-lengths and lower temperatures. It will be noticed, for instance, that their effect is much greater in the colour index b_3-y than in b_1-y.

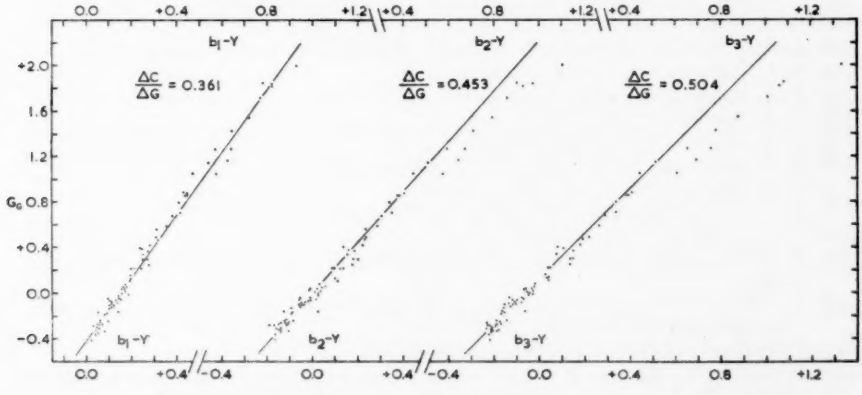

FIG. 9.—*Comparison of narrow-band colour indices $b-y$ and relative gradients G of Gascoigne.*

The relation between Greenwich gradients and spectrophotometric gradients was determined from the colour temperature of the lamp and the transmission of the colour temperature conversion filter, the colour indices of the artificial star formed by the lamp and filter, and the Greenwich gradients corresponding to these colour indices, obtained from the straight line relations in Fig. 9. Greenwich gradient zero corresponds to the following absolute gradients:

$$b_1-y: \ +1\cdot 10, \qquad b_2-y: \ +1\cdot 16, \qquad b_3-y: \ +1\cdot 12.$$

The second of these results must be rejected, for the b_2 filter transmits very readily at 4340 A and the b_2-y colour indices are affected by Hγ. The mean

of the other two results is in excellent agreement with the best previous results, $\phi = G_0 + 1{\cdot}11$ (**25**), but the agreement is partly fortuitous, for there is no guarantee that the effects of line absorption should be identical at 5390 A, 4571 A and 4311 A, in the spectra of hot stars, though these do have but few lines and the differences are likely to be small.

6. *Acknowledgments.*—It is a pleasure to thank Professor R. O. Redman and Dr R. H. Stoy, under whose supervision this research was carried out, for providing the necessary facilities. They, and other members of the staffs of the Cambridge and Cape Observatories, provided much valuable advice and encouragement. Dr A. W. J. Cousins provided the results of observations with the 18-inch reflector in advance of publication. Some lamps and the blue filter were calibrated in the Light Division, National Physical Laboratory, and the writer was able to discuss the problems involved in this research with several members of the staff. The ribbon filament lamp was calibrated through the courtesy of Professor Kienle. The writer also wishes gratefully to acknowledge a D.S.I.R. maintenance allowance held from 1955 to 1957, and a Goldsmiths' Company's postgraduate travelling scholarship from 1957 to 1959.

The Observatories,
Cambridge:
1960 *February* 8.

References

(1) R. v. d. R. Woolley, *Vistas in Astronomy, Vol. II*, p. 1095, 1956.
(2) W. G. Fastie, *J.O.S.A.*, **42**, 641, 1952.
(3) A. Beer, R. O. Redman, and G. G. Yates, *Mem. R.A.S.*, **67**, Pt. 1, 1954.
(4) H. L. Johnson, *Ap. J.*, **119**, 181, 1954.
(5) H. L. Johnson, *Ap. J.*, **117**, 353, 1953.
(6) H. L. Johnson, *Ap. J.*, **117**, 356, 1953.
(7) H. L. Johnson, *Ap. J.*, **116**, 640, 1952.
(8) F. H. Seares and M. C. Joyner, *Ap. J.*, **98**, 302, 1943.
(9) H. L. Johnson, *Ann. d'Ast.*, **18**, 292, 1955.
(10) J. C. deVos, *Physica*, **20**, 690, 1954.
(11) R. C. Larrabee, *J.O.S.A.*, **49**, 619, 1959.
(12) H. Aiken, Progress Report No. AF-51, Computation Laboratory, Harvard University, 1958.
(13) D. Gill, *A History and Description of the Royal Observatory, Cape of Good Hope*, London, H.M.S.O., 1913.
(14) J. Stebbins and G. E. Kron, *Ap. J.*, **126**, 266, 1957.
(15) R. v. d. R. Woolley and D. W. N. Stibbs, *The Outer Layers of a Star*, p. 273, Oxford, 1953.
(16) G. P. Kuiper, *Ap. J.*, **88**, 429, 1938.
(17) F. H. Seares, *Trans. I.A.U.*, **1**, 69, 1922.
(18) L. Dunkelman and R. Skolnik, *J.O.S.A.*, **49**, 356, 1959.
(19) Cape Mimeogram No. 1, 1953.
(20) A. W. J. Cousins, unpublished.
(21) A. R. Hogg, *Photometric Measurements of 244 Bright Stars.* Mount Stromlo, 1958.
(22) O. J. Eggen, Lick Obs. Bull., No. 532, *A. J.*, **60**, 65, 1955.
(23) A. R. Hogg and Beryl Hall, *M.N.*, **111**, 325, 1951.
(24) S. C. B. Gascoigne, *M.N.*, **110**, 15, 1950.
(25) C. W. Allen, *Astrophysical Quantities*, p. 180, London, 1955.

THE PHOTO-DETACHMENT OF H^-

T. L. John

(Communicated by M. J. Seaton)

(Received 1960 January 28)

Summary

The photo-detachment cross section of H^- is calculated numerically using exchange free waves. The improvement got by using exchange wave functions is shown by making a comparison with experimental results.

The process

$$H^- + h\nu \rightarrow H + e^-$$

is of interest because of the rôle it plays in determining absorption in stellar atmospheres.

The physical situation is that, initially, the ion is in its ground state, the electrons having spins in opposite directions, and, after the transition has taken place, the hydrogen atom is in its ground state, the electron spins remaining the same.

This is a problem in quantum theory which can be treated using first order time-dependent perturbation theory. This leads to the usual dipole formulae* for the absorption coefficient,

$$\kappa_\nu = \frac{8\pi^3 e^2 \nu}{c}\left|\int \Psi^*_{\mathrm{A}}(\mathbf{r}_1, \mathbf{r}_2)(z_1+z_2)\Psi_{\mathrm{B}}(\mathbf{r}_1, \mathbf{r}_2)d\tau_1 d\tau_2\right|^2$$

dipole length

$$= \frac{e^2h^2}{2\pi m^2 c\nu}\left|\int \Psi^*_{\mathrm{A}}(\mathbf{r}_1, \mathbf{r}_2)\left(\frac{\partial}{\partial z_1}+\frac{\partial}{\partial z_2}\right)\Psi_{\mathrm{B}}(\mathbf{r}_1, \mathbf{r}_2)d\tau_1 d\tau_2\right|^2 \qquad (1)$$

dipole velocity

$$= \frac{e^6}{2\pi m^2 c\nu^3}\left|\int \Psi^*_{\mathrm{A}}(\mathbf{r}_1, \mathbf{r}_2)\left(\frac{z_1}{r_1^3}+\frac{z_2}{r_2^3}\right)\Psi_{\mathrm{B}}(\mathbf{r}_1, \mathbf{r}_2)d\tau_1 d\tau_2\right|^2$$

dipole acceleration

where $h\nu = E_{\mathrm{B}} - E_{\mathrm{A}}$, E_{A}, E_{B} being the energies of the system.

The functions Ψ are solutions of the Schrödinger equation

$$\left\{-\tfrac{1}{2}\nabla_1^2 - \tfrac{1}{2}\nabla_2^2 - \frac{1}{r_1} - \frac{1}{r_2} + \frac{1}{r_{12}} - E\right\}\Psi(\mathbf{r}_1, \mathbf{r}_2) = 0 \qquad (2)$$

in atomic units ($m = e = \hbar = 1$). Here the coordinates $\mathbf{r}_1$ and $\mathbf{r}_2$ refer to the positions of the electrons and the proton is treated as having an infinite mass.

* These formulae differ from those quoted by Chandrasekhar due to differences in the normalization of Ψ_{B} (see equation (3*b*) below).

Since the electron spins are anti-parallel, the functions Ψ must be symmetrical, i.e. $\Psi(\mathbf{r}_1, \mathbf{r}_2) = +\Psi(\mathbf{r}_2, \mathbf{r}_1)$. Also the orthonormality relations,

$$\int \Psi^*_{\mathrm{A}}(\mathbf{r}_1, \mathbf{r}_2)\Psi_{\mathrm{A}'}(\mathbf{r}_1, \mathbf{r}_2)d\tau_1, d\tau_2 = \delta_{\mathrm{A},\mathrm{A}'} \tag{3a}$$

for bound states and

$$\int \Psi^*_{\mathrm{B}}(\mathbf{r}_1, \mathbf{r}_2)\Psi_{\mathrm{B}'}(\mathbf{r}_1, \mathbf{r}_2)d\tau_1 d\tau_2 = \delta(E_{\mathrm{B}} - E_{\mathrm{B}'}) \tag{3b}$$

for continuous states must hold.

The function Ψ_{A} corresponds to the initial bound state of the system. The final states of the system Ψ_{B} are positive energy solutions of (2) and correspond to the system of a hydrogen atom in its ground state plus a free electron. The same functions have to be considered in calculating the cross section for elastic scattering of electrons by H atoms.

As yet, it has not been possible to solve the Schrödinger equation (2) exactly; in order to get any solutions certain approximations are necessary. The dipole formulae (1) give identical results only for exact solutions. The work done so far in this problem shows that the absorption coefficient is sensitive both to the functions Ψ and to the particular dipole formula used.

Solutions for the H^- ion are got by the usual bound-state variational method. The accuracy of the wave function is dependent on the number of parameters used and it is most reliable for values of $\mathbf{r}_1$ and $\mathbf{r}_2$ giving the largest contributions to the energy integral

$$\int \Psi^*_{\mathrm{A}}(\mathbf{r}_1, \mathbf{r}_2)\left\{-\tfrac{1}{2}\nabla_1^2 - \tfrac{1}{2}\nabla_2^2 - \frac{1}{r_1} - \frac{1}{r_2} + \frac{1}{r_{12}}\right\}\Psi_{\mathrm{A}}(\mathbf{r}_1, \mathbf{r}_2)d\tau_1 d\tau_2.$$

The usual collision theory treatment of scattering of electrons by hydrogen atoms consists in making a partial wave analysis of the wave function as follows:

$$\Psi(\mathbf{r}_1, \mathbf{r}_2) = \sum_{l=0}^{\infty} \Psi_l(\mathbf{r}_1, \mathbf{r}_2)$$

where

$$\Psi_l(\mathbf{r}_1, \mathbf{r}_2) = \frac{1}{\sqrt{2}}\left\{\Psi(\mathbf{r}_1)F_l(\mathbf{r}_2) + \Psi(\mathbf{r}_2)F_l(\mathbf{r}_1)\right\}$$

and $\Psi(\mathbf{r})$ corresponds to the normalized ground state wave function of the hydrogen atom,

$$\Psi(\mathbf{r}) = (\pi)^{-1/2}e^{-r}.$$

The functions $F_l(\mathbf{r})$ may be written

$$F_l(\mathbf{r}) = Y_{l,0}(\hat{\mathbf{r}})\frac{1}{r}f_l(r)$$

where $Y_{l,0}(\hat{\mathbf{r}})$ is the normalized spherical harmonic,

$$Y_{l,0}(\hat{\mathbf{r}}) = \left(\frac{2l+1}{4\pi}\right)^{1/2}P_l(\cos\theta).$$

It can be shown that in the exchange approximation, a full account of which is to be found in an earlier paper (1), the functions $f_l(r)$ satisfy the equation

$$\left\{\frac{d^2}{dr^2} - \frac{l(l+1)}{r^2} + V(r) + k^2\right\}f_l(r) = K(r)f_l(r), \tag{4}$$

where the potential $V(r)$ is given by

$$V(r)=2\left(1+\frac{1}{r}\right)e^{-2r}$$

and the exchange operator $K(r)$ by

$$K(r)f_l(r)=4re^{-r}\left[-(1+k^2)\int_0^\infty xe^{-x}f_l(x)dx+\frac{2}{2l+1}\left(r^{-l-1}\int_0^r e^{-x}x^{l+1}f_l(x)dx\right.\right.$$
$$\left.\left.+r^l\int_r^\infty e^{-x}x^{-l}f_l(x)dx\right)\right].$$

The functions $f_l(r)$ are normalized to have the asymptotic form

$$f_l(r)\underset{r\to\infty}{\sim}\left(\frac{2}{\pi k}\right)^{1/2}\sin(kr-\tfrac{1}{2}l\pi+\eta_l).$$

Using atomic units this gives positive energy functions satisfying the normalization condition (3*b*); k^2 is numerically equal to the kinetic energy of the ejected electron in Rydbergs (13·60 eV).

If $K(r)\equiv 0$ and $V(r)\equiv 0$ then the solutions $f_l(r)$ would be spherical Bessel functions and in this case $\eta_l=0$. This approximation corresponds to using plane waves for the final state. The phases obtained when $K(r)$ and $V(r)$ are non-zero may be used to determine the elastic scattering cross section.

The central field equation is got by putting $K(r)\equiv 0$. Numerical solutions of this equation for $l=0, 1$, for the energy range $0\leqslant k^2\leqslant 1{\cdot}75$, have been obtained by Chandrasekhar and Breen (**2**). Solutions of the exchange equations for $l=0$, 1 and 2 have been calculated numerically for the range $0\leqslant k^2\leqslant 1$ on the English Electric Computor DEUCE by the present author. A full account of this work will be given elsewhere. The equations solved include those for the antisymmetric function, obtained from (4) by replacing $K(r)$ by $-K(r)$. These antisymmetric solutions have the property

$$\Psi_l(\mathbf{r}_1,\mathbf{r}_2)=-\Psi_l(\mathbf{r}_2,\mathbf{r}_1).$$

The solutions of the exchange equations will be used in the investigation of the free–free transitions of H^- which will be undertaken shortly. The photo-detachment and free–free processes are both of importance for absorption in stellar atmospheres.

The exchange approximation, whilst it allows for the possibility of exchange of electrons, otherwise neglects the distortion of the atom by the scattered electron. This distortion can be shown to introduce an extra potential, the polarization potential, which has the asymptotic form

$$-\frac{\alpha}{2r^4}$$

where α is the polarizability of the atom. At small energies and large distances this effect could be important.

Because of selection rules the only solutions of (4) which contribute to (1) are those for $l=1$. Chandrasekhar (**3**) has shown that the integrals involved in (1) can be simplified to the form

$$\int_0^\infty W(r)f_1(r)dr \qquad (5)$$

TABLE I

Photo detachment cross sections of H^- (in units 10^{-17} cm^2)

	With central field free wave functions			With exchange free wave functions		
	11-parameter H^- function	20-parameter H^- function		11-parameter H^- function	20-parameter H^- function	
k^2 (in units of 13·60 eV)	Dipole velocity* formula	Dipole velocity† formula	Dipole length formula	Dipole velocity formula	Dipole velocity formula	Dipole length formula
1·75	0·0657	0·0656	...	...	...	...
1·0	...	...	0·20	0·22	0·22	0·29
·8	0·333	0·342	0·30	0·32	0·32	0·40
·5	0·740	0·751	0·65	0·64	0·65	0·73
·4	...	...	0·88	0·88	0·88	0·95
·35	1·231	1·226	...	...	...	...
·3	...	...	1·31	1·26	1·24	1·34
·25	1·84	1·83	1·66	1·55	1·53	1·67
·2	2·32	2·30	2·20	1·95	1·94	2·16
·175	2·62	2·61	...	...	...	...
·15	2·97	2·98	2·97	2·53	2·54	2·88
·125	3·39	3·41	...	...	...	...
·1	3·87	3·90	3·84	3·37	3·40	3·68
·09	4·06	4·09	...	...	...	...
·08	...	...	4·02	3·74	3·77	3·85
·07	4·41	4·41	...	...	...	...
·06	...	...	3·87	4·02	4·01	3·72
·055	4·52	4·49	...	...	...	...
·05	4·50	4·45	3·61	4·05	4·01	3·47
·045	4·44	4·37	...	...	...	...
·04	...	...	3·16	3·92	3·85	3·05
·035	4·13	4·03	...	...	...	...
·03	...	...	2·52	3·53	3·42	2·43
·02	2·96	2·83	1·67	2·75	2·62	1·63
·015	...	...	1·20	2·16	2·04	1·17
·010	1·50	...	0·72	1·44	1·35	0·70
·005	...	...	0·28	0·63	0·58	0·27
0	...	...	$8·58 \times 10^2 k^3$	$2·21 \times 10^3 k^3$	$2·03 \times 10^3 k^3$	$8·44 \times 10^2 k^3$

* Calculated by Chandrasekhar. † Calculated by Chandrasekhar and Elbert.

where $W(r)$ is a simple function and in the dipole length and velocity formulae consists of polynomials and exponentials.

Chandrasekhar (**4**) in his most recent work used a 20-parameter H^- wave function due to Hart and Herzberg together with plane waves. He found that, in the dipole velocity formula, there was no appreciable change from his earlier work with an 11-parameter function.

Chandrasekhar and Elbert (**5**) used this 20-parameter function and solutions in the central field approximation for the dipole velocity formula and came to the same conclusion. In this work they gave an indication that exchange might be important.

The main part of the present work concerns itself with the use of exchange functions in (5) and their effect on the absorption coefficient. The integrations were done numerically on DEUCE and the particular cases covered were:

(1) The dipole velocity formula with 11- and 20-parameter H^- functions.

(2) The dipole length formula with the 20-parameter function and both exchange and central field free functions.

In Table I the absorption coefficient is given for the particular cases cited above including the results of Chandrasekhar and Elbert. The wave length is given by the formula

$$\lambda = \frac{911{\cdot}2671}{k^2 + I} \text{ A}$$

I being the electron affinity of the ion in Rydbergs; I takes on the values 0·05512 and 0·055289 for the 11 and 20-parameter functions respectively.

Recently Smith and Burch (**6**) have been able to measure the frequency dependence of the photo detachment reaction. Their results were given in arbitrary units relative to the value at 5,280 A. They estimate that their measurements are correct to about 2 per cent. Branscomb and Smith (**7**) in an earlier experiment made an absolute measurement which they estimated to be correct to within 10 per cent. This absolute measurement was used in putting the relative cross-sections on an absolute scale. The best theoretical calculations all lie within 10 per cent of this cross-section, and the dipole velocity result with the 20-parameter H^- wave function and exchange free waves bears the closest resemblance in shape to the experimental curve.

It seems likely that the error in the best theoretical results might be less than the 10 per cent error possible in the absolute experimental results. Figs. 1 (*a*) and 1 (*c*) compare the theoretical results (20-parameter H^- function, exchange free waves, dipole length and dipole velocity formulae) with the experimental results, the absolute values being determined by the theoretical results and the curves being fitted at 5,280 A. In Fig. 1 (*b*) a similar comparison is made with Chandrasekhar and Elbert's work.

The closest agreement is seen to be in the dipole velocity results of Fig. 1 (*a*). At low energies agreement is not so good; this is most probably due to the neglect of polarization in the exchange approximation. The dipole length formula gives the poorest agreement, this is probably due to the fact that the largest contribution to the integrals comes from functions at large distances, i.e. where the H^- function is less reliable and where the effect of polarization may be important in the free waves.

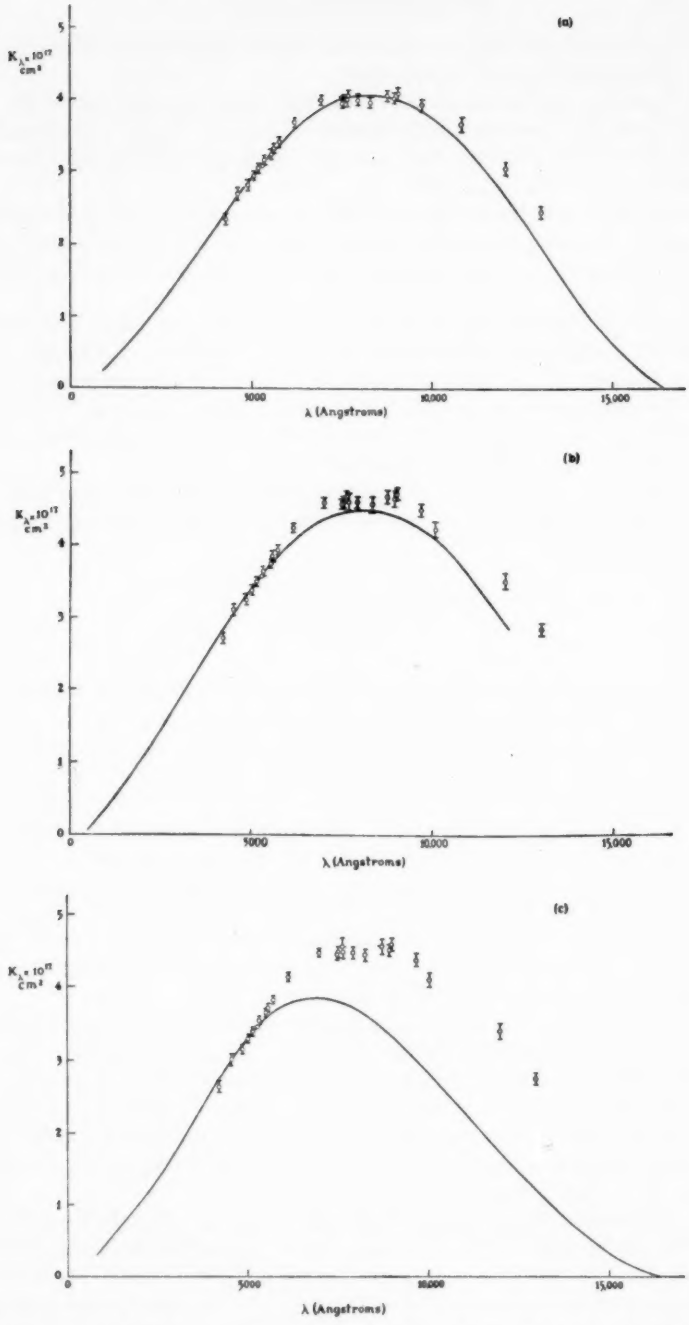

FIG. 1.—*Photo detachment cross sections. A comparison of theoretical and experimental results. All theoretical calculations use the 20-parameter H^- wave function and the experimental values are normalized to agree with those calculated for 5280 A.*

(*a*) *Calculations using the dipole velocity formula and exchange free wave functions.*

(*b*) *Calculations using the dipole velocity formula and central field free wave functions.*

(*c*) *Calculations using the dipole length formula and exchange free wave functions.*

The favourable agreement with experiment gives an indication of the reliability of the free wave functions for determining the elastic scattering cross-section for electron collisions with hydrogen atoms.

The best values for the absorption cross-section are most probably the experimental values given in Fig. 1 (*a*), normalized using theoretical results.

Acknowledgments.—The author is indebted to Dr M. J. Seaton for suggesting this problem and for his continual encouragement and advice. He is grateful to Dr S. J. Smith for interesting discussions. He is also indebted to Mr W. and Mrs J. Lawson for computational assistance and would like to extend his thanks to the English Electric Company for the use of the DEUCE computer at their London Computing Service and in particular to Dr V. E. Price and Mr J. Wollgar. This work was supported by the Atomic Energy Research Establishment (Harwell), to whom thanks are due for permission to publish.

Department of Physics,
University College London:
1960 *January.*

References

(1) B. H. Bransden, A. Dalgarno, T. L. John, and M. J. Seaton, *Proc. Phys. Soc.*, **71**, 877, 1958.
(2) S. Chandrasekhar and F. H. Breen, *Ap. J.*, **103**, 41, 1946.
(3) S. Chandrasekhar, *Ap. J.*, **102**, 223, 1945.
(4) S. Chandrasekhar, *Ap. J.*, **128**, 114, 1958.
(5) S. Chandrasekhar and D. D. Elbert, *Ap. J.*, **128**, 633, 1958.
(6) S. J. Smith and D. S. Burch, *Phys. Review Letters*, **2**, 165, 1959.
(7) L. M. Branscomb and S. J. Smith, *Phys. Rev.*, **98**, 1028, 1955.

COLLISION BROADENING AND SHIFT IN THE λ6573 LINE OF CALCIUM

W. R. Hindmarsh

(Communicated by the Director, University Observatory, Oxford)

(Received 1960 April 2)

Summary

The collision broadening and shift of the line Ca 6573 A due to an external pressure of helium have been measured. The half-intensity damping width of the line was found to be $1{\cdot}42 \pm 0{\cdot}07 \times 10^{-20}$ cm^{-1} per atom per cc of helium, and the shift $0{\cdot}19 \pm 0{\cdot}05 \times 10^{-20}$ cm^{-1} per atom per cc of helium towards the violet. The ratio of broadening to shift is 7·5. This result is shown to be consistent with the hypothesis that short-range repulsive forces between calcium and helium atoms are predominantly responsible for the broadening and shift. No deduction about collision broadening and shift in stellar atmospheres can be made from these laboratory results, but it is suggested that a study of more highly excited lines may yield astrophysically relevant results.

Introduction.—The experimental study of collision broadening and shift in spectral lines is of interest for three main reasons. First, the problem is of some importance in physics, and the recent flow of theoretical papers on the subject (e.g. **1**, **2**) indicates that there are still features of the theory which are obscure and uncertain. Secondly, with the aid of a tested and reliable theory, information concerning interatomic forces may be deduced from measured values of the broadening and shift. While it is possible to estimate theoretically the order of magnitude of the long-range attractive forces of the van der Waals type, almost nothing is known, except for pairs of very simple atoms, of the short-range repulsive forces between atoms. As was shown in a previous paper (**3**), and is further illustrated in this paper, these short-range forces may in certain circumstances be an important cause of collision broadening and shift. Thirdly, the damping constant of Fraunhofer lines is an important parameter in the theory of line formation in stellar atmospheres. It has so far proved impossible to measure this quantity directly in the laboratory, because of the difficulty of creating in the laboratory an atmosphere of atomic hydrogen at low pressures in imitation of the conditions in stellar atmospheres. Collison shifts also may be important in some stellar spectra, particularly those of white dwarf stars. To make reliable deductions of the stellar damping constant and shift from laboratory data an experimentally verified theory of collision broadening and shift is required, together with some detailed information concerning interatomic forces. The present paper represents a further contribution to this end.

Experimental method.—The intercombination line of calcium, λ6573, $4s^2\ ^1S_0 - 4s4p\ ^3P_1$ was formed in absorption in an atmosphere of helium, and the collision broadening and shift were determined.

The experimental technique and the apparatus were identical with those used previously in the investigation of Ca λ4227, $4s^2\ ^1S_0 - 4s4p\ ^1P_1$ (3). The absorption tube had to be heated to about 650 °C in order to give a concentration of calcium vapour sufficient to form an absorption line of suitable intensity. Helium pressures of 5, 40 and 70 cm of mercury were used. The continuous spectrum was provided by a tungsten strip-filament lamp, and the necessary high resolving power by a Babcock grating mounted in the new Oxford solar spectrograph and used in the fourth order. This gave the dispersion of 4·17 mm per A. The reference line employed in the measurement of the shift was Hg 4358 A in the sixth order of the grating spectrum, and was excited in a mercury 198 isotope lamp. This line fell about 10 cm distant from the line Ca 6573 on the plate. Ilford R40 plates were used. These required an exposure time of 15 minutes when the spectrograph slit was 0·077 mm wide. The plates were calibrated for intensity measurement in the usual way. 4 plates for the measurement of the shift between 5 and 40 cm mercury and 4 for the shift between 5 and 70 cm mercury were measured. For the determination of the broadening at 5, 40 and 70 cm mercury 7, 4 and 3 plates respectively were used.

Measurement of the shift.—The measuring procedure was the same as that used in (3). Table I shows the results obtained. The quoted error is in each case the standard deviation of the mean. The pressure has been converted into particle density with the use of the measured temperature, which was 930 °K for the 5 and 40 cm mercury plates and 903 °K for the 5 and 70 cm mercury plates.

TABLE I

Shift between $0{\cdot}52 \times 10^{18}$ and $4{\cdot}16 \times 10^{18}$ atoms per cc of helium 10^{-3} cm^{-1}	Shift between $0{\cdot}53 \times 10^{18}$ and $7{\cdot}49 \times 10^{18}$ atoms per cc of helium 10^{-3} cm^{-1}
− 0·5	+ 5·3
+12·0	+10·3
+12·0	+ 3·7
+ 8·2	+25·9
Mean +7·9 ± 2·1	Mean +11·3 ± 4·4
(−3·4 ± 0·9 mA)	(− 4·9 ± 1·9 mA)

From these results we find that the shift per helium atom per cc is

$$\beta/N = +0{\cdot}19 \pm 0{\cdot}05 \times 10^{-20}\ \text{cm}^{-1}\,\text{cm}^3$$

where the positive sign indicates that the shift is towards the violet.

Measurement of the damping coefficient.—The line profiles were found from microphotometer tracings of the plates, and from these profiles the atomic absorption coefficient (apart from a constant factor) was obtained as a function of wavelength. The absorption coefficient contours were fitted to Voigt profiles at the 0·5 and 0·1 intensity widths, and the tables of van de Hulst and Reesinck (4) used to deduce the damping and Gaussian components of the profiles. The individual plate measures are shown in Table II, where the errors are again standard deviations of the mean.

TABLE II

5 cm helium pressure $0{\cdot}53 \times 10^{18}$ atoms helium per cc		40 cm helium pressure $4{\cdot}16 \times 10^{18}$ atoms helium per cc		70 cm helium pressure $7{\cdot}55 \times 10^{18}$ atoms helium per cc	
Damping half-intensity width cm^{-1}	Gaussian half-intensity width cm^{-1}	Damping half-intensity width cm^{-1}	Gaussian half-intensity width cm^{-1}	Damping half-intensity width cm^{-1}	Gaussian half-intensity width cm^{-1}
0·047	0·076	0·127	0·046	0·163	0·072
0·071	0·046	0·099	0·060	0·171	0·049
0·048	0·065	0·098	0·067	0·139	0·108
0·060	0·057	0·085	0·089	...	...
0·071	0·044	...	...	...	...
0·062	0·048	...	...	...	...
0·058	0·062	...	...	...	...
Means					
0·059	0·057	0·102	0·066	0·158	0·076
±0·004	±0·004	±0·008	±0·008	±0·008	±0·012

Fig. 1 shows the plot of the damping half-intensity width against number density of helium atoms. The equation of the least squares straight line through the points is

$$\Delta\nu = 1{\cdot}42 \times 10^{-20} N + 0{\cdot}048.$$

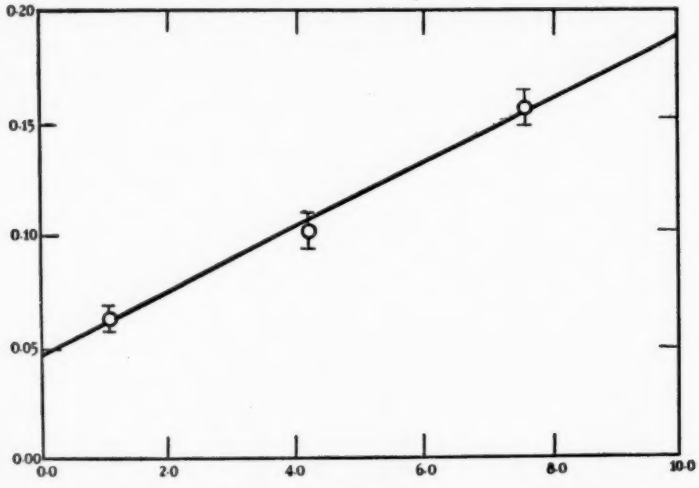

FIG. 1.—*Plot of damping half-intensity width against number density of helium atoms. Ordinates are damping half-widths in cm^{-1} and abscissae are in units of 10^{18} atoms of helium per cc.*

The intercept $0{\cdot}048\,cm^{-1}$ at $N=0$ is the apparatus function contribution to the damping width, so that the collision broadening gives a half intensity width of

$$2\gamma = 1{\cdot}42 \pm 0{\cdot}07 \times 10^{-20} N\,cm^{-1}$$

where γ is the damping constant of the line in cm^{-1}. The mean of all the values of the Gaussian half-intensity width is $0{\cdot}067 \pm 0{\cdot}005\ cm^{-1}$. This is due to the Doppler width of the line and the apparatus function of the spectrograph.

Discussion of the results.—A valuable parameter for the comparison of theory and experiment is the ratio $2\gamma/|\beta|$. The above measurements yield the result

$$10{\cdot}6 > 2\gamma/|\beta| > 5{\cdot}6$$

with the most probable value $2\gamma/|\beta| = 7{\cdot}5$. The value predicted by the Lindholm theory for long-range attractive forces whose potential varies as the inverse sixth power of the distance between the interacting atoms is $2\gamma/|\beta| = 2{\cdot}76$. Furthermore, it is very probable that the attractive force would give a red shift. On the other hand, short-range repulsive forces would most probably give a violet shift, and, assuming that the potential of this force varies as the inverse twelfth power of distance, the Lindholm theory predicts $2\gamma/|\beta| = 6{\cdot}70$. The results lead to the conclusion that, if we accept the Lindholm theory as reliable, then in Ca 6573 A the entire collision broadening and shift are due to the short-range repulsive forces. This contrasts with the case of Ca 4227 A formed in a helium atmosphere, where short-range and long-range forces were found to be of comparable importance, and produced a very small resultant shift.

No information can be deduced from these measurements about collision broadening and shift in the Fraunhofer line λ6573. It is certain that long-range forces are more important when the perturbing atoms are hydrogen than when they are helium, but how important they are relative to the short-range forces it is impossible to say. In order to gain useful information for astrophysical purposes it is necessary to find spectral lines for which long-range forces are the predominant cause of broadening in a helium atmosphere, for then the use of the laboratory results for a helium atmosphere to predict the damping constant and collision shift for an atomic hydrogen atmosphere can be put on a sound theoretical basis. It is probable that such lines will be the more highly excited lines of, e.g., the calcium spectrum, and it is proposed to investigate these in the future.

University Observatory,
Oxford:
1960 *April* 1.

References

(1) Baranger, M., *Phys. Rev.*, **111**, 481, 1958; **111**, 494, 1958; **112**, 855, 1958.
(2) Kolb, A. C., and Griem, H., *Phys. Rev.*, **111**, 514, 1958.
(3) Hindmarsh, W. R., *M.N.*, **119**, 11, 1959.
(4) van de Hulst, H. C., and Reesinck, J. J. M., *Ap. J.*, **106**, 121, 1947.

THE MAGNESIUM b LINES IN LATE-TYPE STARS

T. J. Deeming

(Communicated by the Director of the Cambridge Observatories)

(Received 1960 February 1)

Summary

The absorption lines of Mg I at λ 5167–84A have been measured photoelectrically in 539 G0–K5 stars. The results show an increasing absorption with advancing spectral type and a negative absolute luminosity effect. No significant differences are found between the strong and weak line groups of Miss Roman, or between weak-CN and strong-CN stars. High velocity class III stars have slightly stronger Mg than normal. It is suggested that the Mg b lines can be used as a good criterion of the MK luminosity class for stars with $B-V$ between 0·70 and 1·30, and as a fairly good criterion of MK spectral type between G8 and K5.

---

1. Much less work has been done on stellar spectra at wave-lengths above 5000 A than in the range 3500–5000 A and the only previous work of any extent on the magnesium b triplet at $\lambda\lambda$ 5167·3, 5172·7, 5183·6 is that of Thackeray (**1, 2**), who measured by photographic photometry equivalent widths and central intensities of a number of lines, including λ 5183·6, in 80 late-type stars. He seems to have been the first to give a substantial quantitative account of the negative absolute magnitude effect shown by this line, although this had been reported briefly by Öhman (**3**) a few years before Thackeray's first paper appeared.

The three-channel spectrophotometer at the coudé focus of the 36-inch reflector of the Cambridge Observatories which has been described by Griffin and Redman (**4**), offers an admirable method for the observation of almost any strong feature in a stellar spectrum for wave-lengths from about 4000 to 6000 A. Here it has been used for the more extensive measurement of the Mg b lines with a view to their possible use as criteria of luminosity, spectral type or population type in late-type stars.

The Mg b lines can be detected in main sequence stars as early as A0 but this programme is restricted to stars in the range G0–K5, where the lines are rather strong and easily measurable.

2. The spectrometer and the technique of observation and reduction are exactly as described by Griffin and Redman (**4**). Integrated intensities have been measured in each of three adjacent regions of the spectrum with wave-length limits

A 5110·4–5139·8 A,
B 5160·2–5189·0 A,
C 5214·4–5243·0 A.

These wave-lengths were checked during each night's observation and kept constant to better than $\pm$ 1 A, but it was found experimentally that errors in

wave-length adjustment of up to 5 A did not materially affect the results. The effects of stellar radial velocity on the results were therefore assumed to be negligible.

The magnesium b triplet lies in the central channel, and if A, B and C respectively are the integrated intensities in each of the channels then the ratio (A + C)/B forms a measure of the absorption in the central channel referred to the mean of the other two. The excess of absorption in the central channel is mostly due to the magnesium lines. Following Griffin and Redman we use not A, B and C themselves but A/A_L, B/B_L, C/C_L, where A_L, B_L, C_L are measures made with a lamp, interpolated to the time of the star observation. The "magnesium ratio" r is $(A/A_L + C/C_L) \div B/B_L$. The advantages of using this particular combination of measurements have been fully discussed by Griffin and Redman and all their arguments apply equally to this programme.

539 stars with spectra between Go and K5 have been measured and the ratio r formed for each star. These results are quoted in Table I which shows (1) Henry Draper number, (2) Mg b ratio r. The value quoted is generally the mean of six separate observations taken in pairs on three different nights. The r.m.s. error of one of these observations is ±0·05 and of the mean about ±0·02, i.e. one per cent. (3) Adopted spectral type, mostly by Miss Roman (**5, 6**) on the MK system; otherwise from the General Catalogue of Radial Velocities (**13**). (4) Colour index $B-V$ by Johnson *et al.* (**7, 8, 9, 25**). (5) Total space velocity in km/sec relative to the local standard of rest, from Miss Roman's papers. (6) The notes indicate members of the strong lines (s) and weak line (w) groups of stars of Miss Roman. Giants for which Griffin and Redman find a CN ratio more than 0·08 above normal for the appropriate spectral type and luminosity class are called strong CN stars and are indicated by CN+. Giants with a CN ratio more than 0·05 below normal are called weak CN stars and are indicated by CN−.

TABLE I

HD	r	Spectrum	$(B-V)$	Q	Notes
166	2·44	dG8	0·75		
417	2·27	Ko III	0·97	88	
443	2·44	dG9			
613	2·51	K4 III	1·44	46	
1400	2·62	dK5			
2774	2·36	K2 III	1·15	40	
2901	2·46	K2 III			CN−
2925	2·28	Ko III	0·92	146	CN−
3346	2·68	K5 III		50	
3457	2·49	K4 III	1·32	145	
3546	2·23	G8 III	0·88	129	CN−
3627	2·58	K3 III		18	
3651	2·64	Ko V	0·86		
3712	2·34	Ko II–III		6	s
3765	2·82	K2 V	0·93	73	
3817	2·18	G8 III	0·88	22	s
3989	2·71	K5 III	1·52	55	
4502	2·39	K1 II			
4628	2·70	dK4	0·88		
4656	2·67	K5 III		39	

TABLE I—*continued*

HD	r	Spectrum	$(B-V)$	Q	Notes
4817	2·49	cK5			
5234	2·36	K2 III		32	
5286	2·53	sgK1			
5395	2·26	G8 III–IV		56	w
5516	2·22	G8 III–IV	0·93	24	s
5916	2·17	G8 III–IV	0·90	95	
6186	2·25	Ko III	0·89	41	w
6497	2·50	K2 III	1·18	131	
6582	2·38	G5 VI	0·71	150	
6833	2·20	K1 III	1·18	235	CN−
7087	2·19:	Ko III		17	s
7106	2·35	Ko III–IV		31	s
7318	2·26	Ko III		12	CN+, s
8207	2·38	Ko III–IV		17	s
8491	2·34	Ko III		20	
9057	2·30	Ko III		17	
9138	2·58	K4 III	1·37	155	
9270	2·18	G8 III	0·98	16	CN+, s
9166	2·61	K3 III		20	CN+
9352	2·41	cK1			
9408	2·27	Ko III		30	w
9712	2·46	K1 III			
9927	2·50	K3 III	1·28	26	CN+
10072	2·21	G8 III		32	w
10307	2·23	G2 V	0·63	32	s
10380	2·49	K3 III		26	
10476	2·58	K1 V	0·84	46	
10486	2·49	K2 IV			
10761	2·22	Ko III		26	s
10780	2·55	Ko V	0·81		
10975	2·27	Ko III	0·97	83	
11559	2·30	Ko III		30	w
11749	2·30	Ko III	1·06	120	
11909	2·23	K1 p			
12533	2·39	K2 III		18	
12929	2·36	K2 III	1·15	18	
13520	2·54	K4 III		52	
13530	2·28	Ko III	0·93	165	CN+
13611	2·12	G8 II			
14770	2·23	G8 III		16	s
14872	2·61	K4 III		7	CN−
15596	2·32	Ko III	0·90	115	
15694	2·44	K3 III		17	
15656	2·66	K5 III		48	
16161	2·15	G8 III	0·86	28	s
16160	2·95	K3 V	0·99	90	
16024	2·47	cK5			
17361	2·41	K1 III		42	s
17506	2·43	K3 Ib			
17709	2·68	K5 III		19	

TABLE I—*continued*

HD	r	Spectrum	$(B-V)$	Q	Notes
18449	2·49	K2 III		51	
18970	2·26	Ko II–III		83	w
19476	2·32	Ko III		42	w
19656	2·30	K1 III		24	s
19787	2·35	K2 III		32	
19735	2·63	K5 III	1·43	104	
20123	2·14	G5 II			
20468	2·35	K2 II			
20277	2·28	sgG8			
20618	2·27	sgG5			
20644	2·50	K3 II–III		15	
20893	2·43	K3 III		32	
21120	2·18	G8 III	0·89	45	s
21552	2·47	K3 III		29	CN−
21754	2·26	Ko II–III		13	s
22072	2·43	dG7			
23183	2·31	Ko III	1·01	120	
23841	2·49	K2 III	1·21	92	CN−
25604	2·32	Ko III		13	CN+, s
25893	2·56	dK2			
25975	2·41	K1 III	0·95	113	
26311	2·38	cK5			
27022	2·18	G5 III	0·81	33	w
27371	2·33	Ko III	0·99	30	CN+, s
42° 939	2·53	dK5			
27348	2·29	G8 III		41	
27382	2·39	K1 III		42	w
27697	2·27	Ko III	0·98	31	CN+, s
27971	2·31	K1 III		42	w
28100	2·19	G8 III		20	s
28292	2·43	K2 III		25	
28305	2·29	Ko III	1·03	31	CN+, w
28307	2·26	Ko III		32	
29038	2·65	K3 III	1·18	101	
29139	2·68	K5 III	1·51	41	
29317	2·34	Ko III		44	s
30504	2·59	K4 II			
30834	2·38	K3 III	1·41	33	CN−
31421	2·44	K2 III		26	
31767	2·33	K2 II			
31782	2·40	Ko III	0·80	137	
32923	2·28	G4 V		36	
33554	2·66	K5 III		26	
33856	2·43	K3 III		24	CN+
34334	2·50	K3 III		64	CN−
34255	2·37	cK4			
34559	2·21	G8 III		27	w
34575	2·38	dG6			
35186	2·60	K4 III		30	
35620	2·50	K2IIIp			

TABLE I—*continued*

HD	π	Spectrum	$(B-V)$	Q	Notes
37160	2·33	G8 IIIp	0·95	126	CN−
37171	2·73	K5 III	1·55	107	CN−
37394	2·59	dK1	0·84		
37601	2·43	sgG9			
37984	2·29	K1 III	1·16	101	CN−, w
37981	2·44	K1 IV			
38230	2·68	K1 V	0·83		
38656	2·29	G8 III	0·94	31	w
38751	2·35	G8 III		4	
39003	2·32	Ko III		21	CN+, s
39400	2·33	cK2			
39587	2·25	Go V	0·59	30	s
40035	2·32	Ko III	0·99	19	CN−, w
40460	2·24	K1 III	1·02	120	
40801	2·40	Ko III	0·97	119	CN−
41636	2·39	Ko III	1·05	77	
41597	2·24	G8 III		47	w
41927	2·38	K2 II–III		9	
43039	2·39	G8 III	1·03	98	
43380	2·49	K2 III	1·11	82	
44990	2·12	cG6			
44708	2·55	K4 III		15	CN−
45088	2·73:	dK3			
45416	2·22	K1 II			
45410	2·33	sgG8			
46480	2·35	sgG7			
47174	2·29	K3 III		40	
47731	2·15	G5 Ib			
47914	2·71	K5 III	1·45	60	
48433	2·40:	K1 III		4	s
48432	2·26	Ko III		20	w
48682	2·20	Go V		43	s
48781	2·28	K1 III		25	CN+, s
49161	2·54	K4 III		33	
49293	2·25	Ko III		9	CN+, s
49520	2·41	K3 III	1·27	99	
51219	2·39:	G8 V	0·70	45	
51440	2·41	K2 III	1·23	76	CN−
52005	2·44	cK4	1·54		
52071	2·43	K2 III	1·25	111	CN−
52960	2·44	K3 III		7	
54371	2·31	dG6			
54563	2·43	dG7			
54719	2·38	K2 III		14	CN+
54716	2·56	K4 II–III		57	
55280	2·40	K2 III		83	CN−
56224	2·46	K1 III	1·17	117	
57264	2·34	Ko III		33	w
57727	2·27	G8 III		28	CN−, w
57669	2·33	Ko III		18	CN+

TABLE I—*continued*

HD	r	Spectrum	$(B-V)$	Q	Notes
58207	2·30	Ko III		19	w
58367	2·18	G8 III	1·01	24	s
58972	2·46	K3 III		41	CN−
59148	2·34	K2 III		23	
59294	2·36	K2 III		31	
60318	2·29	Ko III		28	w
60522	2·75	Mo III		38	
62044	2·46	K1 III		58	s
62285	2·62:	K5 III		10	
62345	2·19	G8 III	0·93	9	s
62509	2·27	Ko III	1·00	33	w
62721	2·62	K5 III	1·45	106	
63410	2·26	G8 III	0·95	106	CN−
65345	2·31:	Ko III	0·91	103	w
65583	2·48	G8 V	0·70	103	
66141	2·48	K2 III	1·25	91	CN−
66216	2·40	K2 III		20	
69267	2·57	K4 III	1·48	10	
70272	2·61	K5 III		30	
71115	2·22	G8 II			
71597	2·53:	K2 III	1·16	125	CN−
71952	2·44	sgKo			
72184	2·47	K2 III	1·11	92	
72292	2·50	K3 III		24	
72324	2·22	G9 III	1·02	110	CN+
73593	2·34	G8 IV			
74442	2·41	Ko III		42	w
74739	2·22	G8 II			
75506	2·19	Ko III		37	CN−, w
75732	2·56	dKo			
76219	2·28:	G8 II–III		17	s
76294	2·22	G8 III		17	
76291	2·47	K1 IV	1·09	81	
77996	2·30	K2 II–III		16	
77912	2·18	G8 Ib–II			
78235	2·23	G8 III		24	w
78479	2·54	K3 III	1·21	114	CN+
78515	2·27	Ko III		27	s
79096	2·42	dG7			
79354	2·65:	K5 III		29	CN−
79452	2·20	G6 III	0·86		CN−
79969	2·92	dK4	0·89		
81146	2·44	K2 III		23	
81192	2·32	G8 III	0·94	203	CN−
82308	2·65	K5 III		21	
82395	2·24	Ko III		34	w
82381	2·39	K3 III		17	
82394	2·25	cG7			
82443	2·42	dG9			
82635	2·24	G8 III		24	s

TABLE I—*continued*

HD	r	Spectrum	(B−V)	Q	Notes
82741	2·34	Ko III		25	CN−, w
82885	2·43	G8 IV–V	0·75	37	
83240	2·27	K1 III		17	w
83425	2·47	K3 III	1·30	91	CN−
83805	2·25	G8 III		34	w
84453	2·36	Ko IV	0·95	36	
85503	2·53	K2 III		31	CN+
87837	2·53	K4 III		40	
89269	2·27	dG5			
89484	2·31	Ko III		32	
90250	2·35	K1 III	1·09	100	
90572	2·45	sgKo			
90537	2·30	G8 III–IV		14	s
91011	2·30	sgKo			
91612	2·23	G8 II–III	0·93	113	w
92095	2·43	K3 III	1·27	99	
92424	2·44	K2 III		42	CN+
92523	2·49	K3 III		16	CN−
94084	2·32	K2 III	1·11	62	
94132	2·47	dG9			
94264	2·37	K1 III	1·03	59	w
94247	2·46	K3 III		20	CN−
94600	2·32	K1 III		30	w
94549	2·36	dG8			
94669	2·40	K2 III	1·13	56	CN−
95345	2·34	K1 III		25	w
95689	2·25	Ko III	1·06	8	s
96436	2·30	sgG7			
96833	2·29	K1 III	1·13	11	w
97561	2·35	G7 IV	0·75	152	
97907	2·38	K3 III		21	CN−
98262	2·40	K3 III	1·38	22	CN−
98824	2·30	K1 III–IV		108	
99196	2·68	K4 III	1·38	98	
99491	2·49	dKo			
99648	2·22	G8 II–III	1·00	40	s
100470	2·35	Ko III	1·05	103	
100696	2·27	Ko III		75	w
101484	2·28	Ko III		13	w
101501	2·37	G8 V	0·69	1	
101673	2·36	K3 III		31	
102224	2·33	Ko III		17	w
102328	2·54	K3 III		28	
103095	2·43	G8 VI	0·75	315	
104556	2·42	G8 V	0·86	46	
104979	2·24	G8 III		67	w
105043	2·45	K2 III		52	CN−
105475	2·22	dG9			
105631	2·46	dK1			
105963	2·64	dK2			

TABLE I—*continued*

HD	r	Spectrum	(B−V)	Q	Notes
106714	2·22	Ko III		26	CN−, w
106760	2·39	K1 III		47	s
107328	2·37	Ko III	1·13	112	
107383	2·26	G8 III		73	w
107469	2·36	dKo			
107950	2·15	G7 III		28	s
108225	2·24	G8 III–IV		5	w
108381	2·34	K1 III–IV		14	
109317	2·23	Ko III			w
110833	2·73	dKo	0·85		
111028	2·33	K1 IV	0·99	97	
111067	2·47	K3 III		63	
112033	2·22	G8 III		6	s
112989	2·30	K1p			
113092	2·31	G8 III		64	
113226	2·16	G9 III		29	s
113996	2·58	K5 III		46	
114960	2·61	K5 III	1·40	78	CN+
115004	2·25	Ko III		14	CN+, s
117176	2·26	dG5	0·71		
117876	2·28	Ko III	0·96	107	CN−
118643	2·44	cK3			
119425	2·42	K2 III	1·10	133	
120477	2·67	K5 III		29	
120539	2·50	K4 III		32	
121146	2·49	sgK2			
121710	2·49	K3 III		45	
123977	2·26	Ko III		95	
124679	2·28	Ko III		59	w
124897	2·43	K2 IIIp	1·23	71	CN−
125351	2·32	K1 III		21	s
125560	2·53	K3 III		58	CN+
127665	2·44	K3 III	1·29	37	
128165	2·92	K3 V			
128750	2·33	sgK2			
128902	2·49	K4 III	1·48	104	CN−
129312	2·19	G8 III		19	CN+, w
129336	2·18	G8 III	0·94	124	
129580	2·40	dKo			
129972	2·17	Ko III			s
131111	2·31	Ko III–IV	1·02	78	w
131156	2·36	G8 V	0·76		
131507	2·51	K4 III		98	
131511	2·49	dK1	0·75		
132132	2·34	sgK1			
133124	2·59	K4 III		36	
133208	2·18	G8 II–III	0·95	13	s
133165	2·26	Ko III		13	s
133582	2·39	K2 III		34	
134190	2·16	G8 III		52	w

TABLE I—*continued*

HD	r	Spectrum	$(B-V)$	Q	Notes
135722	2·25	G8 III	0·96	43	
136726	2·47	K4 III		18	
136512	2·27	Ko III	1·02	79	
136514	2·42	K3 III		56	
137759	2·38	K2 III	1·17	14	
137704	2·50	K4 III	1·40	100	CN−
138481	2·58	K5 III	1·59	21	
139195	2·26	Kop			
139341	2·62	dK4			
139641	2·27	G8 IV		20	s
140538	2·35	dG5	0·68		
140573	2·46	K2 III	1·17	34	CN+
141714	2·18	G5 III–IV		14	w
141680	2·29	G8 III	1·02	35	w
141992	2·65	K5 III		49	
142091	2·42	Ko III–IV		80	s
142574	2·76	K4 III	1·59	93	CN−
142980	2·53	K1 IV	1·14	82	
143107	2·39	K3 III	1·23	28	
143666	2·25	Ko III		66	w
143761	2·26	G2 V	0·60	49	w
144287	2·50	G8 V	0·77	108	
144579	2·33:	dG8	0·73		
145001	2·24	G8 III		12	s
145000	2·38	K2 III			
145148	2·43	Ko IV	1·02	97	
145328	2·36	Ko III–IV	1·00	90	w
145675	2·57	dK1			
145958	2·38	dKo	0·73		
147677	2·24	Ko III		41	s
147767	2·58	K5 III		40	
148293	2·32	K2 III		10	CN+
148387	2·23	G8 III	0·91	7	s
148513	2·54:	K4 IIIp		54	
148653	2·45	dK2			
148856	2·06	G8 III	0·91	12	s
148897	2·10	G8p			
149161	2·53	K5 III	1·50	92	
150449	2·30	K1 III		21	s
151101	2·26	K1p			
150997	2·15	G8 III–IV		33	s
151217	2·64	K5 III		18	
151937	2·28:	K1 II–III	1·25	167	
152326	2·32	K2 II–III		13	
152391	2·38	G6 V	0·77		
152812	2·43	K2 III		70	
153210	2·41	K2 III	1·14	63	CN+
154345	2·37	dKo	0·73		
154278	2·29	K1 III	1·02	68	CN−
154733	2·55	K4 III	1·30	122	

TABLE I—*continued*

HD	r	Spectrum	(B−V)	Q	Notes
155410	2·42	K3 III		41	
156283	2·43	K3 II			
156681	2·57	K4 II–III	1·55	64	
157999	2·36	K3 II			
158633	2·41	dK1	0·76		
158899	2·51	K4 III		15	
159966	2·20	K0 III		87	w
160346	2·70	dK3	0·96		
161074	2·65	K4 III		70	CN−
161096	2·45	K2 III	1·16	28	
161198	2·54	dG8			
161797	2·28	G5 IV	0·75	43	
162076	2·33	sgG5			
162211	2·44	K2 III		13	
163217	2·36	K3 III		28	
163588	2·39	K2 III	1·18	23	
163770	2·34	K1 II			
164058	2·48	K5 III	1·52	14	
163993	2·34	K0 III		26	s
164349	2·19	K0 II–III		5	
164922	2·48	K0 V	0·80	43	
165341	2·55:	K0 V	0·86	24	
165760	2·15	G8 III–IV		21	s
166208	2·31	K0p			
166229	2·47	K2 III		68	
166620	2·72	K2 V	0·87		
167042	2·37	K1 III		152	
167193	2·49	K4 III		72	
168322	2·28	G8 III		131	CN−
168532	2·46	K4 II			
168775	2·36	K2 III		8	CN+
168656	2·16	G8 III		27	s
169191	2·28	K3 III		44	
169414	2·37	K2 III		76	
170693	2·34	K2 III		62	
171779	2·17	K0 III		7	CN+, s
173780	2·41	K3 III		13	
175306	2·25	K0 II–III		53	
175225	2·24	dG8			
175535	2·15	G8 III		32	s
176411	2·30	K2 III		34	
176527	2·35	K2 III		28	CN−
176670	2·31	K3 II			
179094	2·37	K1 IV			
180006	2·17	G8 III		25	CN+
180610	2·42	K2 III		35	
180809	2·15	K0 II			
181276	2·19	K0 III	0·95	28	s
180972	2·29	K2 II–III			
182293	2·53	K3 III		174	CN−

TABLE I—*continued*

HD	r	Spectrum	$(B-V)$	Q	Notes
182488	2·35	Ko V	0·82		
182572	2·24	G8 IV	0·78	149	
182762	2·18	Ko III		43	w
184010	2·24	sgG8			
184398	2·22	K2 II–III			
184467	2·59	K1 V		34	
184406	2·56	K3 III		92	
185194	2·12	G8 III		22	CN+, s
185351	2·31	Ko III		60	w
185622	2·53	cK5			
185662	2·49	dK4			
185734	2·25	G8 III–IV		27	s
185958	2·23	G8 II			
186120	2·29	sgKo			
186486	2·15	G8 III		17	w
186675	2·19	G8 III		33	s
188056	2·48	K3 III		39	CN+
188310	2·28	Ko III		38	w
188512	2·32	G8 IV	0·86	31	w
188753	2·31	dKo			
188947	2·25	Ko III		18	w
189319	2·67	K5 III		22	
190147	2·22	K1 II–III		21	
190360	2·29	G6 IV		126	
190403	2·69	K1 V	0·82	92	
190608	2·36	K2 III		41	
191026	2·32	Ko IV		47	
191046	2·26	Ko III		126	CN–
191785	2·64	K1 V		80	
192577	2·34	K2 II			
192806	2·50	K3 III		30	CN–
192909	2·48	K3 Ib–II			
192944	2·21	G8 III		34	w
193092	2·48	K4 II			
194013	2·24	G8 III–IV		18	w
194317	2·46	K3 III		40	
194526	2·65	K5 III		59	
195506	2·42	K2 III		121	CN–
195987	2·48	G9 V		58	
196725	2·34	K3 Ib			
196755	2·16	G5 IV		74	
196758	2·27	K1 III		42	w
197752	2·38	K2 III		45	
197912	2·32	Ko III		22	w
197913	2·34	dG9			
198149	2·35	Ko IV	0·92	108	
197989	2·30	Ko III	1·03	49	s
198134	2·50	K3 III		13	
198387	2·36	dKo			
198809	2·21	G8 III		47	s

TABLE I—*continued*

HD	r	Spectrum	$(B-V)$	Q	Notes
199191	2·26	G8 III		260	CN−
199169	2·45	K4 III		26	
199253	2·22	K0 III		7	w
199580	2·38	K1 IV		126	
200905	2·53	K5 Ib	1·64		
201051	2·25	sgK1			
201091	2·97	K5 V	1·19	80	
201092	2·81	K7 V	1·38	80	
201251	2·47	K4 II			
202109	2·20	G8 II			
203344	2·39	K0 III–IV		124	
203504	2·34	K1 III	1·10	89	w
204771	2·26	K0 III		41	w
205435	2·20	G8 III	0·88	41	
205512	2·28	K1 III		91	CN+
205941	2·25	dG8		189	
206067	2·23	K0 III		40	w
206952	2·34	K0 III		44	CN+, w
206778	2·32	K2 Ib	1·58		
206936	2·15	G5 Ib	1·18		
207089	2·34	K0 Ib			
207134	2·45	K3 III		157	
209747	2·66	K4 III		90	
209960	2·65	K4 III		33	
209945	2·53	K5 III		17	
210745	2·32	K1 Ib			
210889	2·31	K2 III		16	
211073	2·46	K3 III		7	
211076	2·53	K4 III		11	
211388	2·32	K3 II–III		6	
212466	2·29	G8 Ia			
212496	2·23	G9 III		67	CN−, w
212943	2·27	K0 III		100	w
213310	2·50	M0 Ib–II+A			
213893	2·73	K5 III		114	
214868	2·40	K3 III		23	
215373	2·26	K0 III		30	w
215549	2·39	K1 III–IV		202	
215665	2·19	G8 II–III	0·95	16	s
216131	2·23	K0 III		26	s
216228	2·34	K1 III		35	s
216206	2·16	G4 Ib			
216946	2·57	K5 Ib			
218029	2·43	K3 III		8	CN+
218031	2·28	K0 III		76	w
218101	2·33	G8 IV		41	
218356	2·39	K0 IIp			
218395	2·33	sgK0			
219134	2·88	K3 V	1·01		
219615	2·28	G8 III		222	

TABLE I—*continued*

ND	r	Spectrum	$(B-V)$	Q	Notes
219668	2·46	sgKo			
219916	2·26	Ko III		11	CN−, w
219945	2·28	Ko III			w
219962	2·35	K2 III		135	
220009	2·41	K2 III		46	CN−
220363	2·50	K3 III		2	
220954	2·29	K1 III		48	CN+
221115	2·25	G8 III		25	w
221345	2·42	Ko III		168	
221354	2·64	Ko V		79	
221585	2·29	G8 IV		143	
221639	2·40	sgG9			
221673	2·45	K4 III		23	
222107	2·42	G8 III–IV	1·02	69	
222842	2·42	Ko III		10	w
223047	2·19	G5 Ib			
223165	2·35	K1 III		26	w

3. *Results*

3.1. *Variation of r with spectral type and colour index.*—Fig. 1 gives the mean run of the Mg ratio r with spectral type for each of the four principal luminosity classes, dwarfs, subgiants, giants and supergiants. The MK luminosity classes II–III, and III–IV have been included in the giants and the class IV–V has been included in the dwarfs, so that only fairly well attested subgiants have been treated separately. All luminosity classes show a marked increase of r

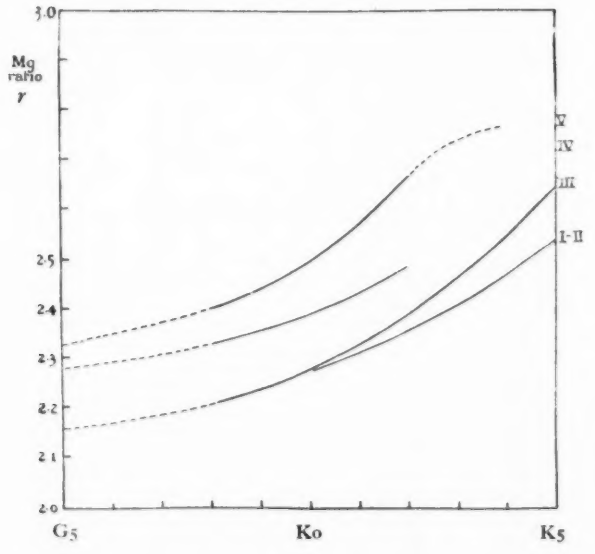

FIG. 1.—*The mean run of r with spectral type for each of the principal luminosity classes.*

with advancing spectral type. The r.m.s. scatter from these mean curves is about 0·06 per star, except for dwarfs, where it is about 0·12. The chief cause of the greater spread for dwarfs appears to be less accurate spectral classifications. For dwarfs also there are signs of a systematic difference between MK types and others, in the sense that the MK type tends to be a little earlier. It should be noted that if the class V curve in Fig. 1 uses only stars with MK types a smoother run is obtained, although only 23 stars are then available from G8 to K5. Further, in that case the curve lies higher, the difference in r being about 0·02 at G8, 0·05 from K0 to K2, and perhaps 0·15 at K4. The evidence therefore is that the use of MK types gives a better separation of class V from class III stars.

The colour index $(B-V)$ is in some respects a more satisfactory parameter than spectral type and it is important to find the behaviour of r with $(B-V)$ for those stars for which the colour index is known. There are 158 such stars on the programme. Fig. 2 (*a*) shows r plotted against $(B-V)$ for stars of all luminosity classes, and in order that a fair comparison should be made, Fig. 2 (*b*) contains a diagram with the same stars as appear in 2 (*a*), but with spectral type as abscissa. It should be emphasized that this diagram contains less than one-third of the total number of stars used to obtain the curves of Fig. 1.

In the case of luminosity class III stars there is a linear relation between r and $(B-V)$, within the errors imposed by the scatter of individual star values:

$$\text{For Class III, } r=0{\cdot}622(B-V)+1{\cdot}677, \quad 0{\cdot}85<(B-V)<1{\cdot}55.$$

The r.m.s. scatter in r per star about this line is 0·08, which is slightly greater than the scatter for the same luminosity class in the (r, spectral type)-relation.

There are also approximately linear relations between r and $(B-V)$ for class IV and class V stars, although there are not enough data to determine them well. In the case of class V stars there is a suggestion of a maximum for r in the vicinity of $(B-V)=1{\cdot}0$, but there are not enough points to give any certainty of this. We may note that there is possibly a maximum at K4 or K5 in the (r, spectral type)-relation, although again this needs much more data for confirmation.

3.2. *Variation of r with absolute magnitude.*—The discovery by Thackeray of the negative absolute magnitude effect shown by the Mg b lines is confirmed by the present measurements. The increased absorption in dwarfs can be seen in Figs. 1 and 2. If we anticipate the later calibration of our ratio scale in terms of Thackeray's equivalent widths, of λ 5183·6, the only line of the triplet which he measured, we find that the increase in equivalent width passing from a typical K0 III star to, say, 54 Psc, a K0 V star, is 0·3 A, or about 25 per cent.

In the range of surface temperatures covered by our measures, and within the range of absolute magnitude covered by classes III to V, the b lines increase in strength both with decreasing temperature and with decreasing intrinsic luminosity of the star. At constant spectral type class V stars are hotter than those of class III, but at constant $(B-V)$ the two are of approximately equal temperature, so that we might expect a plot of r against $(B-V)$ to show a greater separation of dwarfs from giants than a plot of r against spectral type. This is indeed what is observed. The change in equivalent width from a class III star of colour $(B-V)=1{\cdot}00$ to a class V star of the same colour is 1·8 A, an increase of over 100 per cent. This assumes that we are allowed to extrapolate the linear relationship between r and equivalent width beyond the domain of overlap of Thackeray's measurements with ours.

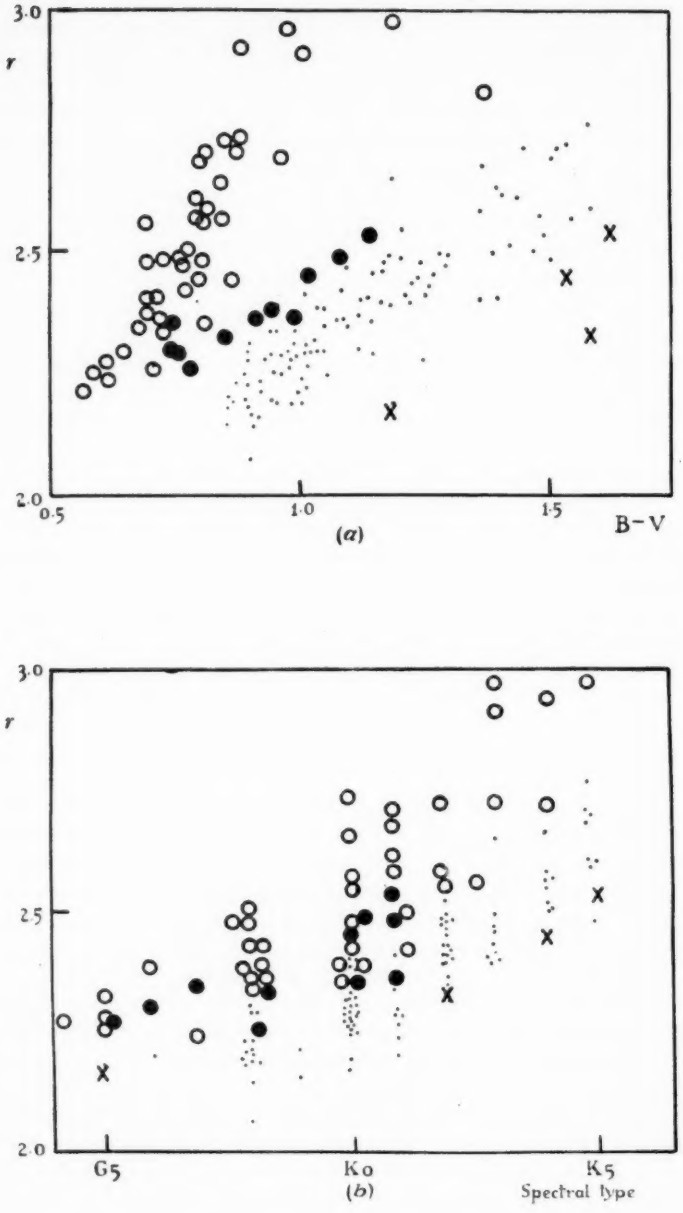

FIG. 2.—*(a) Mg ratio r as a function of (B−V).*

(b) The same stars as appear in (a) but with spectral type as abscissa. Crosses indicate supergiants; dots, giants; filled circles, subgiants; and open circles, dwarfs.

Fig. 1 shows that subgiants have absorption intermediate between that of giants and dwarfs and that supergiants have the same or somewhat weaker absorption than giants. We note that when the abscissa is colour (Fig. 2 (*a*)) there seems to be a better separation of giants and supergiants, but there are then only four supergiants available. Until we pass K3 the giant and dwarf curves in Fig. 1 (spectrum as abscissa) run more or less parallel, but the subgiants appear to be nearer to dwarfs in the late G types and to giants in the early K's. And in Fig. 2 (*a*) (colour as abscissa) a somewhat similar trend is shown, with subgiants merging with dwarfs near $(B-V)=0{\cdot}6$. It should be pointed out that we have Mg ratios for only 39 subgiants, that MK types are available for about half of these only, and $(B-V)$ values for even fewer. Lack of data is clearly the chief difficulty here.

3.3. *The Mg ratio r as a criterion of spectral type and of absolute magnitude.*— We have seen that r is a function of spectral type and of absolute magnitude so that we can use it either to determine spectral type if the luminosity class is known, or to determine luminosity if we know the spectral type or colour. The latter problem is generally the more important.

The purely observational r.m.s. error of an Mg ratio from six measurements is $\pm 0{\cdot}02$. For luminosity class III this would produce an error of about 0·04 in the deduced spectral class or $0^{m}{\cdot}03$ in $(B-V)$. But the scatter arising from measurement errors is small relative to that arising from the intrinsic scatter of individual stars, which corresponds to about 0·12 of a spectral class (perhaps rather more for dwarfs), or $0^{m}{\cdot}12$ in $(B-V)$.

The error of determination of a spectral type, provided the luminosity class is known, compares favourably with the errors of the MK system itself or with the accuracy obtainable from analogous measures of the G band (**4**) and further, except possibly in luminosity class V, the b lines avoid the ambiguity in the G band type arising from the maximum near K2, so that they could with profit be incorporated into a scheme of spectral classification, at least as far as K5. In general there does not seem much useful purpose in using the b line measures to deduce a $(B-V)$ colour. One needs prior information of the luminosity class and the resulting colour determination is not particularly precise relative to the errors obtained in straightforward good photoelectric photometry. For instance Morgan and Johnson (**7**) claim a probable error of $\pm 0^{m}{\cdot}009$ in $(B-V)$. Given the climate it would appear preferable to measure $(B-V)$ directly.

We do not have enough MK spectral types for the dwarfs, nor do we have enough measures of $(B-V)$ to obtain comparable results for dwarfs, but there seems to be no *a priori* reason why we should not expect similar accuracy for the determination of spectral types of class V stars also, at least to K2 or K3.

The possibility of using r as a luminosity criterion is more attractive, especially if we know the colour of the star concerned. It is evident from Fig. 2 (*a*) that if we know the colour of a star in the range $(B-V)=0{\cdot}70$ to $1{\cdot}30$ then the Mg ratio will provide an almost unequivocal determination of luminosity class. Almost, because we are not yet certain of the behaviour of subgiants in the diagram, and because the separation of points on the supergiant side of the class III stars is not good. (In part this may merely be an indication that the supergiants do not form a well separated sequence of their own and that there are many intermediate stars which have generally been given luminosity class II on the

MK system.) The very large scatter in the later-type dwarfs make prediction of luminosity rather uncertain if only spectral type is known. However the separation when colour is used instead is so good that it would seem better to estimate spectral type from a measured $(B-V)$ and to use the colour with a measured ratio r to give a luminosity class, rather than to estimate spectral type directly and try to obtain a luminosity classification on that basis alone with no direct colour measurement.

It is unfortunate that not enough good absolute magnitudes exist for stars in general for us to determine directly whether the scatter in our measurements can be ascribed to a real spread in the absolute magnitudes of the class III stars in the solar neighbourhood, a "cosmic scatter". The use of spectroscopically determined absolute magnitudes to resolve this question is not permissible as there may be some effects which cause changes in line intensities without there being any real changes in absolute magnitude, and such effects may influence both the Mg b lines and the lines customarily used for absolute magnitude determination, so that a spurious correlation might be obtained. It is found that there is no correlation between the Mg ratio (with the effects of spectral type and luminosity class removed) and the spectroscopic absolute magnitudes of Young and Harper (**10**), although this cannot be taken as conclusive evidence that the scatter in r is not due to scatter in absolute magnitude. Further measures of r in a number of galactic clusters may help to elucidate the "cosmic scatter" problem.

It seems then that if we have a measurement of $(B-V)$ in the range 0·7 to 1·3, the Mg b ratio provides a good criterion of luminosity class, but that for the moment we are not justified in supposing that it will give accurate determination of absolute magnitude. If we know spectral type but not colour index we can still make a separation of luminosity classes but the distinction is in this case not quite so clear.

3.4. *Population type differences, high velocity effects.*—N. G. Roman in her paper on the spectra of F5–K5 stars (**5**) discusses certain groups of stars which she says are characterized respectively by weak or strong Fraunhofer lines, the two groups tending to have high and low velocities respectively. Griffin and Redman have pointed out that for stars near K0 the designation "weak-line" in fact means strong λ4227 Ca I and G band, "strong line" means weak λ4227 and G band. Miss Roman also discusses stars having unusually weak or strong CN, giving them respectively the designations "weak CN" or "4150". Since Griffin and Redman's measures appear to give more complete information on this latter point, for present purposes we shall take "weak CN" to refer to giant stars with CN anomalies less than −0·05 and "strong CN" to refer to stars with CN anomalies greater than +0·08. In Table I "weak line" stars have been marked w, "strong line" s, "weak CN" CN−, "strong CN" stars CN+. The differences from the mean for the appropriate spectral class have been taken for the class III stars which belong to one or other of these groups. The mean value of the "Mg anomaly" for each group is given in Table II. The r.m.s. scatter in each case is such that we cannot regard any of these groups as having an "Mg anomaly" very significantly different from zero. There is a hint of very slightly weak Mg among "strong line" stars, to parallel the weak λ4227 of Ca I, and a suggestion of very slightly stronger Mg for stars having weak CN.

TABLE II

Mean anomalies for weak line, strong line, weak CN and strong CN stars

Stars	Mean anomaly	r.m.s. scatter per star
weak line	$-0{\cdot}003 \pm 0{\cdot}006$	0·049
strong line	$-0{\cdot}016 \pm 0{\cdot}009$	0·066
weak CN	$+0{\cdot}014 \pm 0{\cdot}009$	0·064
strong CN	$+0{\cdot}005 \pm 0{\cdot}010$	0·059

Fig. 3(*a*) shows a plot of the Mg anomaly, evaluated using spectral type, against space velocity (relative to the local standard of rest) according to Miss Roman. There is no sign that the Mg ratio is systematically less for high velocity stars; on the contrary there is a slight tendency for high velocity stars to show greater r (67 high velocity stars of luminosity class III give an "Mg anomaly" $+0{\cdot}034 \pm 0{\cdot}009$). Such a trend would be consistent with the idea that high velocity stars show more of the characteristics of under-luminous stars. In Fig. 3(*b*) the Mg anomalies have been taken with respect to $(B-V)$. Unfortunately this restricts the number of stars considerably, but again there is a slight tendency for a greater r at higher velocity.

To summarize, there are no certain variations of the Mg ratio with other spectral characteristics usually denoted by "weak line", "strong line", "weak CN", "4150"; there is possibly a slight increase with space velocity.

4. *Correlation of Mg ratio with Thackeray's 1939 measurements.*—Our measurements cover a much larger wave-length range than did Thackeray's, and inevitably we take in absorption lines of other elements, chiefly Fe, and in the later types we include a certain amount of molecular absorption by TiO, MgH, C_2. The two sets of measurements are therefore comparable only to a limited extent, but since the line $\lambda 5183{\cdot}6$ which Thackeray measured is attributable almost solely to Mg I, we may use his measurements to check whether our measures are affected to any considerable degree by these other lines or bands.

We have 55 stars in common with Thackeray and Fig. 4 gives a comparison of his measures with ours. The correlation appears to be satisfactory and supports the view that what we have been measuring is in fact primarily Mg I absorption. The regression line can be represented by

$$W = (3{\cdot}26 \pm 0{\cdot}03)r - (5{\cdot}88 \pm 0{\cdot}07)$$

where r is the Mg ratio and W is the equivalent width of $\lambda 5183{\cdot}6$ in Angstrom units. This diagram omits two values (for α Tau and 5 Lac) for which Thackeray introduced corrections for TiO absorption. This relation may be found useful if our Mg ratios are to be compared with the predictions of a model stellar atmosphere.

5. *Theoretical interpretations of Mg intensities.* Until now we have not been concerned with any reasons for the effects discussed. The analysis has been on an empirical basis and the results derived for the variations of r with luminosity or with spectral peculiarities of various kinds will remain valid whatever the physics is behind the "Mg ratio". In what follows we shall be concerned with the interpretation of r and the physical basis of the variation of r in stars of different types and luminosities.

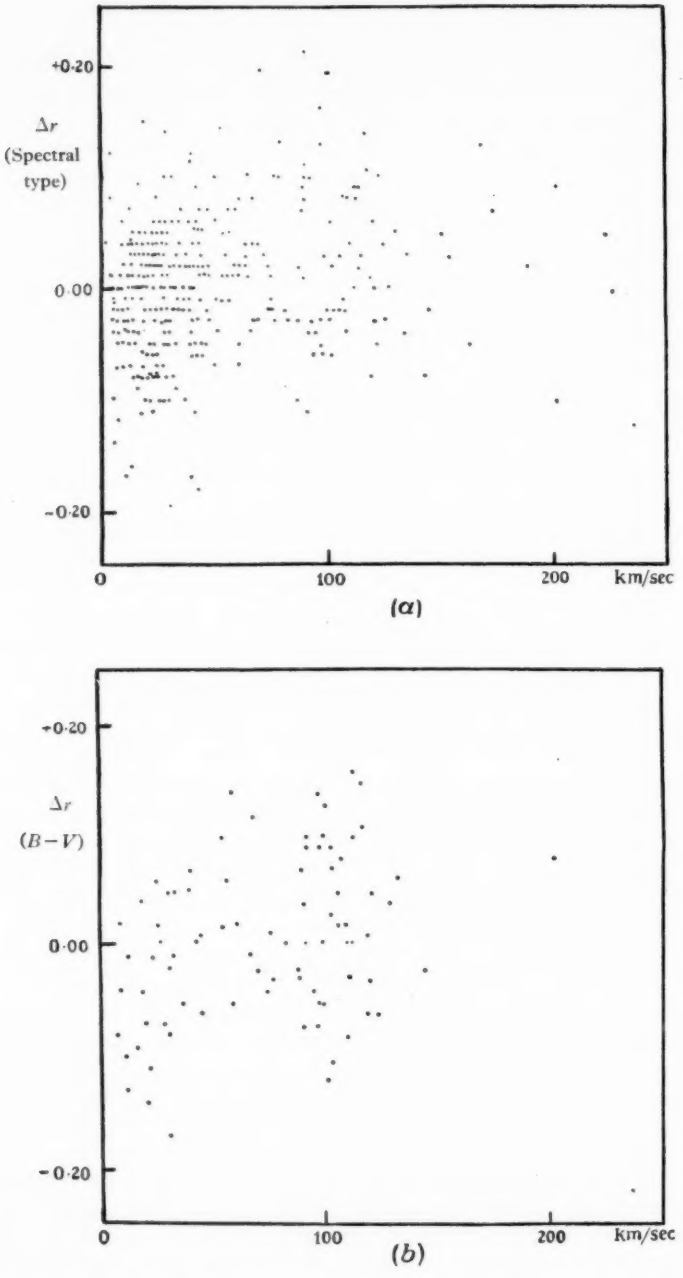

FIG. 3.—(*a*) *Mg anomalies, evaluated using spectral type, plotted against space velocity as computed by Miss Roman.*

(*b*) *The same, evaluated using* $B-V$ *colours.*

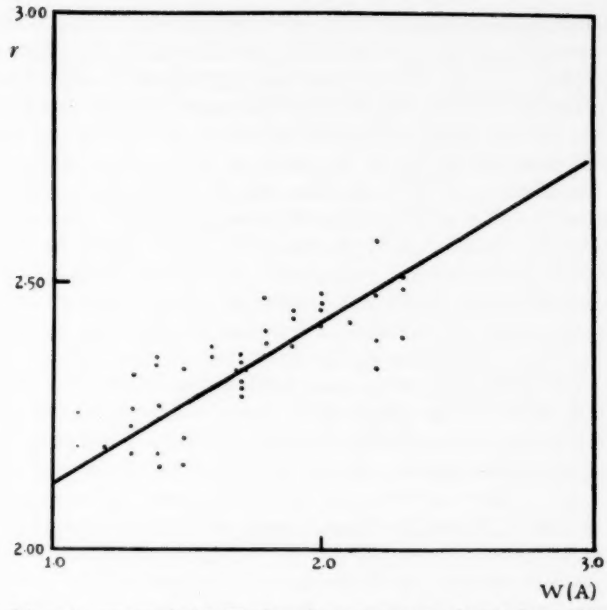

FIG. 4.—*Mg ratios compared with Thackeray's measurements of equivalent widths of* 5183*A*.

5.1. First we wish to know whether the absorption that has been measured is primarily due to magnesium or whether there is an appreciable contribution due to molecular absorption by TiO which is known to occur strongly from K5 onwards, or from MgH which has been reported in K stars by Öhman (**3**) and by Davis (**12**). Code (**11**) reports that in population II K giants there exists a dip in the continuum near the region we have measured which is not present in late-type dwarfs. The origin of this dip is not assigned and Code does not make it clear whether this is a feature peculiar to population II spectra. Furthermore the diagrams of continua which he publishes are for two stars of strongly differing spectral types, HD 103095, G8 VI and HD 128902, K4 III, so that one cannot be sure what the result of comparing a giant and a dwarf of the same spectral type would be.

It happens that we have measured both these stars, finding an Mg ratio 2·43 for HD 103095 and 2·49 for HD 128902. We would expect this intensity dip to tend to increase the Mg ratio: in fact HD 103095 has a somewhat lower Mg ratio than we should expect of its spectral type and HD 128902 whose Mg ratio should perhaps be somewhat increased, shows an unusually low ratio for a K4 III star. Presumably this dip is due to some molecular band absorption, probably TiO; in any case TiO bands should show in the tracing of HD 128902, if they are going to affect the Mg ratio appreciably. Since we find little if any effect of this dip, we conclude that it, and molecular absorption, have not affected the Mg measurements to any appreciable extent. This is confirmed by the correlation we find between r and Thackeray's equivalent width. (The point at $W = 2{\cdot}7$ A, $r = 2{\cdot}58$ in Fig. 4 is δ And and although it seems to suggest that the Mg ratio is too high for the equivalent width, this particular value for W is rather uncertain according to Thackeray.)

5.2. Assuming that r represents a measurement of the behaviour of the Mg b lines, we now wish to interpret this behaviour in terms of the physical properties of the atmosphere of the various types and magnitudes of stars which we have measured. The behaviour of Mg 5183·6 with spectral type has been predicted by Aller (**13**) and by Russell (**14**) on the basis of the Boltzmann and Saha formulae together with some allowance for variation of continuous absorption. Russell predicts a maximum at G9 V and Aller one at $T = 4250\,^{\circ}\mathrm{K}$. If we interpret this temperature as the reversing layer temperature and follow Allen ((**15**), p. 189), the spectral type would be K2 V–K3 V. The only suggestion of a maximum that the present measurements show is at $(B-V) = 1{\cdot}10$ or at K4 V but this is based on only two stars, 61 Cygni A and B at $(B-V) = 1{\cdot}19$ and 1·38 respectively. 61 Cygni B is the only dwarf in Table I with an MK type later than K5—Morgan classifies it as K7 V. Öhman (**3**) gives a reproduction of a Mount Wilson spectrogram of this star, together with a microphotometer tracing showing the (0, 0) band of MgH. The spectrum is considerably depressed to the short wave-length side of λ 5200 and this would perhaps have the effect of reducing the ratio r by reducing the light in channel A. Thus we should not put too much weight on to 61 Cyg B in deciding whether or not there is a maximum. Certainly we can say that there is no sign of a maximum at G9 as Russell predicts and any maximum is unlikely to be as early as K3 as Aller predicts, although the star with the highest measured r, HR 753, has an MK type of K3 V. The theoretical difficulty is to know how the continuous absorption coefficient varies along the spectral sequence and what part, if any, molecular absorption plays in determining it.

5.3. A similar difficulty is encountered in trying to explain why the Mg b lines are stronger in dwarfs than in giants. The reduction in electron pressure in the giants and the consequent greater ionization produces a change in the right direction but appears to be several orders of magnitude too small. From a detailed comparison of the spectra of α Boo and 70 Oph A, Miss S. A. van Dijke (**16**) deduces that lines of excitation potentials less than about 2·7 volts are stronger in giants while lines of E.P. greater than 2·7 volts are stronger in dwarfs. The actual dividing potential depends on the element and its state of ionization, but is in general in the range 2·5–3·0 volts. The excitation potential of the lower states of the Mg b triplet is 2·7 volts which is just on the dividing line, so that we cannot easily say whether the Mg b lines are in agreement with the tendency indicated by Miss van Dijke's measurements. The lines of Mg I which she measured, with E.P. 4·3 volts were found to be stronger in the dwarf. Aller and Stoddard (**17**) find for Mg 3838 a similar variation with spectral type and absolute magnitude to that which we find for the Mg b lines, and point out that this disagrees with the theory of Pannekoek (**18**). The line 3838 belongs to the triplet $\lambda\lambda$ 3829·4, 3832·3, 3838·3 which arises from the same lower level as do the b lines (**19**), but the other triplets from this level are too far in the ultra-violet to be observed successfully. Nevertheless the similar behaviour of λ 3838 and λ 5183 suggests that the negative absolute magnitude effect arises principally from differences in the populations of the $3P^0$ level, or from differences in the continuous absorption, rather than from some anomaly in the region of the b lines, possibly due to TiO or MgH. The Ca I triplet analogous to the b lines is at $\lambda\lambda$6162·2, 6122·2, 6102·2. These lines are reported by Miss Burwell (**20**) to

be stronger in dwarfs than in giants, the differences increasing with advancing spectral type. No data appear to exist on the triplets Sr I λλ 7070·1, 6878·4, 6791·1, and Ba I λλ 7905·8, 7392·4, 7195·2.

As was pointed out by Öhman (**21**), it is known from studies at eclipses that Ca and Mg appear very high up in the solar chromosphere (e.g. S. A. Mitchell (**22**) gives 6000 km for Mg 3838, 3500 km for Mg 5184, 1000 km for Ca 6162). In addition Christie and Wilson (**23**) in a study of the 1934 eclipse of ζ Aurigae studied the behaviour of the Mg triplet λλ 3829, 3832, 3838, and found that the behaviour with height in the atmosphere of the K star is markedly different from that of other lines, showing a minimum at $0{\cdot}05R_K$ and a maximum about $0{\cdot}08R_K$ (pp. 448 to 453). Miss van Dijke (**16**) considers that there is evidence for a stratification of elements in the atmosphere of α Boo, similar to that observed in the Sun, although the data on this point do not include magnesium. All this suggests that the difference of Mg b intensities between giants and dwarfs, and the similar behaviour of the 3830 A Mg I triplet and the 6130 A Ca I triplet, may possibly be related to peculiarities in the distribution with respect to height in the stellar atmosphere of the atoms concerned. A similar idea was put forward by Lindblad (**24**) many years ago.

5.4. The foregoing discussion has been restricted to giants and dwarfs because for subgiants and supergiants there are insufficient data to draw any certain conclusions. The peculiar position of ε Peg at $(B-V)=1{\cdot}58$, $r=2{\cdot}32$ in Fig. 2 (*a*) suggests that perhaps interstellar reddening could be an important factor for supergiants. However according to Morgan, Harris and Johnson (**8**) ε Peg is not noticeably reddened with respect to the other supergiants 9 Peg and ξ Cyg.

The behaviour of subgiants is more interesting. Although there are relatively few stars available for discussion, there is a tendency for them in earlier types to resemble dwarfs, as far as Mg absorption is concerned, and in the later types to resemble the giants. This is borne out by Fig. 2 (*a*), where although there are only 11 subgiants, they form a well defined sequence. This behaviour is perhaps what would be expected on the basis of current ideas on evolution, as the later-type subgiants are supposed to be among the oldest stars in the solar neighbourhood and are presumably structurally similar to giants (A well-known example is δ Eri which unfortunately was not measured because it was too far south to be accessible with the 36-inch telescope at Cambridge.) The early-type subgiants cannot long have left the main sequence, so that they should still bear a similarity to dwarfs.

The increase of Mg absorption in high velocity stars is not well enough established to merit extensive comment here. We would merely point out that if lines in the blue–violet part of a spectrum are weak then there is a tendency for the assigned spectral type to be too early and the measured colour will be too blue for the true effective temperature of the star. In this case the Mg absorption would appear to be too high for the measured $(B-V)$ or spectral type.

6. *Stars with peculiar Mg b lines.*—There are a few stars which stand out from the general run of r with spectral type and $(B-V)$ in Figs. 1 and 2. We give notes on some of these, but we would emphasize that this list is not exhaustive. Note that space velocities are based on assumed absolute magnitudes which may need correction.

(i) HD 6833

K1 III, $(B-V)=1{\cdot}18$, CN ratio 2·03, Mg ratio 2·20, space velocity 235 km/sec. The weak Mg at first suggests a supergiant but this is ruled out by the weak CN. It may be that we have the beginnings of an indication of metal deficiency in an extremely high velocity star.

(ii) HD 29038

K3 III, $(B-V)=1{\cdot}18$, CN ratio 2·03, Mg ratio 2·65, space velocity 101 km/sec. A class III star of this spectral type and colour would normally have a much stronger CN and much weaker Mg. A class V star would have this CN but stronger Mg. Class IV stars are rare in spectral types as late as K3.

(iii) HD 31782

Ko III, $(B-V)=0{\cdot}80$, CN 1·93:, Mg 2·40. The colour, CN, and Mg all suggest that this star is a dwarf and not a giant.

(iv) 54 Her (HD 152879)

K4 III, $(B-V)=1{\cdot}41$, CN 2·23, G band 2·86, Mg 2·25, space velocity 74 km/sec. The CN and G band are normal. The Mg is very low both for this spectral type and for this colour.

(v) β Her (HD 148856)

G8 III, $(B-V)=0{\cdot}91$, CN 2·23, G band 2·71, Mg 2·06. The colour and G band are normal, the CN is slightly strong for the spectral type, the Mg ratio has the lowest value measured for any star.

7. *Suggestions for further work.*—It would be helpful to measure the Mg ratio in a greater number of stars, particularly in subgiants, which could easily be the subject of a large investigation, designed to clarify their position in relation to class III and V stars. It would also be of interest to measure the analogous red calcium and strontium triplets to see whether they behave in the same way as the Mg b lines.

The results show that as a luminosity criterion the Mg ratio is much more effective when used in conjunction with colours than with spectra. There are, unfortunately, only a comparatively small number of stars in the sky for which $(B-V)$ colours are available. Accurate colour work cannot profitably be attempted in this country but in a good climate the data could be obtained fairly rapidly for comparatively bright stars such as are considered here, without elaborate apparatus.

Acknowledgments.—The author wishes to thank Professor R. O. Redman, who suggested and supervised this work; Mr D. W. Beggs, who designed and maintained the electronic equipment; and Mr G. A. H. Walker, who gave much assistance at the telescope.

The Observatories,
Cambridge:
1960 *January.*

References

(1) A. D. Thackeray, *M.N.*, **99**, 492, 1939.
(2) ——— *M.N.*, **109**, 436, 1949.
(3) Y. Öhman, *Stockholm Obs. Ann.*, **12**, No. 8, 1936.
(4) R. F. Griffin and R. O. Redman, *M.N.*, **120**, 287, 1960.
(5) N. G. Roman, *Ap. J.*, **116**, 122, 1952.
(6) ——— *Ap. J. Supp.*, **2**, 198, 1955.
(7) H. L. Johnson and W. W. Morgan, *Ap. J.*, **117**, 322, 1953.

(8) W. W. Morgan, D. L. Harris, and H. L. Johnson, *Ap. J.*, **118**, 92, 1954.
(9) H. L. Johnson, and C. F. Knuckles, *Ap. J.*, **126**, 113, 1957.
(10) R. K. Young and W. E. Harper, *Publ. D.A.O.*, **3**, No. 1, 1924.
(11) A. Code, *P.A.S.P.*, **71**, 118, 1959.
(12) D. N. Davis, *Ap. J.*, **86**, 109, 1937.
(13) L. Aller, *Astrophysics*, I: "The Atmospheres of the Sun and Stars", p. 84, Ronald Press Co., N.Y., 1953.
(14) H. N. Russell, *Ap. J.*, **78**, 239, 1933.
(15) C. W. Allen, *Astrophysical Quantities*, Athlone Press, London, 1955.
(16) S. E. A. van Dijke, *Ap. J.*, **104**, 27, 1946.
(17) L. H. Aller and L. G. Stoddard, *Ap. J.*, **85**, 54, 1938.
(18) A. Pannekoek, *Publ. Astr. Inst. Amsterdam*, **4**, 1935.
(19) W. Grotrian, *Handbuch der Astrophysik III*, p. 533, 1930.
(20) Cora G. Burwell, *P.A.S.P.*, **42**, 351, 1930.
(21) Y. Öhman, *Stock. Obs. Ann.*, **12**, No. 3, 1936.
(22) S. A. Mitchell, *Ap. J.*, **105**, 1, 1947.
(23) W. H. Christie, and O. C. Wilson, *Ap. J.*, **81**, 426, 1935.
(24) B. Lindblad, *Stock. Obs. Ann.*, **12**, No. 2, 1936.
(25) J. B. Oke, *Ap. J.*, **130**, 487, 1959.

THE ABUNDANCE OF OXYGEN IN THE PLANETARY NEBULA NGC 7027

A. Burgess and M. J. Seaton

(Received 1959 October 24)

Summary

The abundances of O^0, O^+ and O^{+2} are determined from [O I], [O II] and [O III] forbidden lines and the abundances of O^{+3}, O^{+4} and O^{+5} from O III, O IV and O V recombination lines. In the recombination calculations cascade from all upper levels is taken into account. It is found that O^{+3} is the most abundant oxygen ion and that the abundance of O^{+5} is small. The chemical abundance ratio is found to be $N(O)/N(H) = 1{\cdot}2 \times 10^{-3}$.

---

1. *Introduction.*—Since gaseous nebulae are optically thin in the observed emission lines the numbers of emitting atoms or ions are proportional to the observed line intensities. In this respect the problem of determining the chemical composition of a nebula is simpler than that of determining the composition of a stellar atmosphere. The main difficulties in the nebular problem are, first, that there are large departures from thermodynamic equilibrium and a great deal of atomic data is therefore required in order to interpret observed line intensities and, secondly, that for many chemical elements the ionic abundances can be deduced from observations for only one or two stages of ionization and approximate estimates must be made for all other stages (**1, 2, 3, 4**).

Aller, Bowen and Minkowski (**5**) have made a particularly detailed study of the line intensities in the spectrum of the planetary nebula NGC 7027. Atomic oxygen is represented by lines of [O I], [O II], O II, [O III], O III, O IV, and O V. The [O I], [O II] and [O III] forbidden lines are excited by electron impact. Using calculated collision cross-sections and transition probabilities the abundances of O^0, O^+ and O^{+2} may be deduced from the forbidden line intensities. Most of the permitted lines are excited by radiative recombination but the Bowen fluorescent mechanism (**6**) (resonant absorption of He II Lyα in the transition $O^{+2}\ 2p^2\ ^3P_2 \rightarrow 2p3d\ ^3P_2$, possibly due to a chance coincidence in wave-length) excites the strong O III lines. The main work of the present paper is the calculation of recombination spectra for O III, O IV and O V and the deduction of abundances for O^{+3}, O^{+4} and O^{+5}. Our results determine the total oxygen abundance without any significant correction for unobserved stages of ionization and provide information about the ionization equilibrium which is useful for the determination of abundances of other elements.

For the calculation of recombination spectra one must consider not only direct captures on a given level but also captures on all higher levels followed by cascade. Calculations of reasonable accuracy have been made previously

only for H I, He I and He II (see (**7**)). In order to be able to make such calculations for complex ions we have developed an approximate general method for the calculation of recombination rates (**8**) and have obtained improved methods of performing the cascade calculations (**9**).

2. *General remarks on the calculation of recombination spectra.*—Let the energy levels be denoted by subscripts $i = 1, 2, 3, \ldots$ in order of increasing excitation energy. We consider the usual cases, Case A for an optically thin nebula and Case B for a nebula optically thick for lines ending on the $i = 1$ ground state. Let the radiative transition probabilities be denoted by A_{ij}. For Case A the probability that population of i is followed by a direct radiative transition to j is

$$P_{ij} = A_{ij}/A_i \tag{2.1}$$

where

$$A_i = \sum_{k=1}^{i-1} A_{ik} \qquad \text{(Case A)}. \tag{2.2}$$

For Case B transitions to $i = 1$ are counterbalanced by absorptions from $i = 1$ and the effective value of P_{ij} is therefore $P_{ij} = A_{ij}/A_i$ where now

$$A_i = \sum_{k=2}^{i-1} A_{ik} \qquad \text{(Case B)}. \tag{2.3}$$

Let C_{ij} be the probability that population of i is followed by a transition to j when all cascade routes are taken into account and let $C_{ii} = 1$. Then (**9**)

$$C_{ij} = \sum_{k=j}^{i-1} P_{ik} C_{kj}. \tag{2.4}$$

Let $N_e N_+ \alpha_k$ be the number of captures on k per unit volume per unit time, N_e being the electron density and N_+ the density of recombining ions. The number arriving on i due to capture and cascade is

$$N_e N_+ \sum_{k=i}^{\infty} \alpha_k C_{ki} \tag{2.5}$$

and of these a fraction P_{ij} give the $i \to j$ line. The number of quanta per unit volume per unit time emitted in the line is

$$\mathcal{Q}_{ij} = N_e N_+ \alpha_{ij} \tag{2.6}$$

where the *effective recombination coefficient* is

$$\alpha_{ij} = P_{ij} \sum_{k=i}^{\infty} \alpha_k C_{ki}. \tag{2.7}$$

For Cases A and B we use the notation $\alpha_{ij}^{(A)}$, $\alpha_{ij}^{(B)}$. It sometimes happens that some of the $\alpha_{ij}^{(B)}$ are much greater than the $\alpha_{ij}^{(A)}$; this is the case if

$$A_{i1} \gg \sum_{k=2}^{i-1} A_{ik} \tag{2.8}$$

or if a similar inequality holds for upper states which are important for populating level i by cascade. If $\alpha_{ij}^{(B)}$ is only a little larger than $\alpha_{ij}^{(A)}$ then the resonant line quanta, $k \to 1$, need be scattered only a small number of times to effect the conversion from Case A to Case B but when $\alpha_{ij}^{(B)}$ is much greater than $\alpha_{ij}^{(A)}$ many more scatterings are required for the Case B limit to be approached.

At first sight it would seem that the question of whether Case A or Case B applies could be settled by estimating the optical depths for resonant line scattering, but that the problem is more complicated may be demonstrated by considering

the efficiencies of fluorescent mechanisms. The essential ideas concerning the O III fluorescent mechanism may be understood by considering O^{+2} to be an atom with three levels, $i = 1$, 2 and 3. He II Lyα happens to have a wave-length practically identical with that of the $3 \rightarrow 1$ line. Absorption of a single He II Lyα quantum may be followed by re-emission of $3 \rightarrow 1$ radiation or by emission of observable $3 \rightarrow 2$ radiation. It will be shown (Section 7.4) that these two processes have probabilities $P_{31} = 0{\cdot}983$ and $P_{32} = 0{\cdot}017$. Let $\mathcal{N}$ (He II, Lyα) be the number of He II Lyα quanta produced in the nebula and let $\mathcal{N}(3, 2)$ be the number of $3 \rightarrow 2$ quanta escaping from the nebula. Define the overall efficiency of the fluorescent mechanism as

$$\mathscr{R} = \frac{\mathcal{N}(3, 2)}{\mathcal{N}(\text{He II Ly}\alpha)} . \tag{2.9}$$

If each He II Lyα quantum can escape from the nebula after being scattered n times by O^{+2} it is readily shown that

$$\mathscr{R} = (1 - P^n_{31}) \tag{2.10}$$

which approaches unity for n large. The condition that $\mathscr{R}$ should be close to unity is essentially the same as the condition that Case B should apply for the recombination spectrum.

For NGC 7027 the O III resonant line optical depth is $\tau_{13} \sim 10^4$ (Section 7.1). If scattering by O^{+2} were alone considered we would have $n \sim \tau_{13}{}^2 \sim 10^8$ and hence $\mathscr{R} = 1$. Allowance for scattering by He^+ would cause n to be larger still. But from the observed spectrum $\mathscr{R}$ may be deduced and we obtain $\mathscr{R} = 0{\cdot}43$ (Section 7.4). Using a slightly different method, it is shown elsewhere (**10**) that $\mathscr{R} \simeq 0{\cdot}3$ for both the O III and N III fluorescent efficiencies in a number of nebulae. Putting $\mathscr{R} = 0{\cdot}43$ in (2.10) gives $n = 33$. The large discrepancy between $n \sim 10^8$ and $n = 33$ must be due to some physical processes having been overlooked. The following might be considered: (i) absorption of O III resonance quanta in ionizing H atoms; (ii) the Zanstra effect (**11**) of scattering with redistribution of frequency; (iii) the wave-length difference of 0·019 Å between the centres of the He II Lyα line and the O III absorption line.

3. *Energy levels, transition probabilities and recombination coefficients*

3.1. *Energy levels.*—Let E_i be the energy of level i measured in Rydbergs (13·60 eV or 109737 cm^{-1}) and let E_i be negative for bound states and zero at the series limit ($i \rightarrow \infty$). The energy parameter ϵ_i is defined by

$$E_i = z^2 \epsilon_i \tag{3.1}$$

where z is the residual charge; $z = m + 1$ for the ion X^{+m}. The effective quantum number ν_i is defined by

$$\epsilon_i = -\frac{1}{\nu_i{}^2} \tag{3.2}$$

and the quantum defect μ_i by

$$\nu_i = n_i - \mu_i$$

where n_i is the principal quantum number. For a given spectral series the quantum defects may be expressed as a series in ϵ_i:

$$\mu_i = a + b\epsilon_i + c\epsilon_i{}^2 + \ldots . \tag{3.3}$$

Assuming LS coupling, the recombination coefficients $\alpha(\gamma SLJ)$ are proportional to $(2J + 1)$ and the level populations $N(\gamma SLJ)$ determined by recombination and cascade will also be proportional to $(2J + 1)$. We may

therefore neglect J quantum numbers in the recombination calculations and consider only centres of gravity of spectral terms:

$$E(\gamma SL) = \frac{\sum_J (2J+1)E(\gamma SLJ)}{(2S+1)(2L+1)}. \tag{3.4}$$

3.2. *Transition probabilities.*—The quantal formula for A_{ij} is

$$A_{ij} = \left(\frac{\alpha^4 c}{6a_0}\right) z^4 \mathscr{A}_{ij} \tag{3.5}$$

where

$$\left(\frac{\alpha^4 c}{6a_0}\right) = 2{\cdot}6774 \times 10^9 \text{ sec}^{-1} \tag{3.6}$$

(α being the fine structure constant, c the speed of light and a_0 the Bohr radius) and where

$$\mathscr{A}_{ij} = (\epsilon_i - \epsilon_j)^3 z^2 \frac{S_{ij}}{\omega_i} \tag{3.7}$$

S_{ij} being the line strength (**12**) in atomic units and ω_i the statistical weight of level i. For a single jumping electron

$$\mathscr{A}_{ij} = (\epsilon_i - \epsilon_j)^3 C(i \to j) |z(n_i l_i | r | n_j l_j)|^2. \tag{3.8}$$

The coefficients $C(i \to j)$, which have been discussed in a previous paper (**8**), have the properties:

(i) $$\omega_i C(i \to j) = \omega_j C(j \to i) \tag{3.9}$$

(ii) For the transitions $O^{+4}\ 1s^2 2snl \to 1s^2 2sn'l'$ and $O^{+3}\ 1s^2 2s^2 nl \to 1s^2 2s^2 n'l'$,

$$C(l \to l') = l_> / (2l+1) \tag{3.10}$$

where $l_>$ is the larger of l, l'.

(iii) For the transitions $O^{+2}\ 2pnlSL \to 2pn'l'SL'$ the coefficients $C(plL \to pl'L')$ are given in Table I. They satisfy the sum rule

$$\sum_{L'} C(plL \to pl'L') = C(l \to l'). \tag{3.11}$$

(iv) For $2pnlSL \to 2p^2 SL'$,

$$C(plL \to p^2 L') = 2C(plL \to ppL'). \tag{3.12}$$

TABLE I

l	L	l'	L'	$C(plLp \to l'L')$
0	1	1	0	1/9
			1	1/3
			2	5/9
1	0	2	1	2/3
1	1	2	1	1/6
			2	1/2
1	2	2	1	1/150
			2	1/10
			3	14/25

Most of the integrals $(n_i l_i | r | n_j l_j)$ were obtained from the Bates and Damgaard tables (**13**); in this approximation $z(n_i l_i | r | n_j l_j)$ depends on the effective quantum numbers ν_i, ν_j but does not depend explicitly on z. For a few transitions lying outside the range of the Bates and Damgaard tables the tables of Burgess and Seaton (**8**) were used; for $|\nu_i - \nu_j|$ not small these two sets of tables give results which are practically identical.

For transitions to $2p^2$ it is important to include the term involving $\zeta = 1 + \partial\mu/\partial\nu$ in the normalization of the $2p$ radial function (**14**). When this factor is included it has been shown (**8**) that good results are obtained for photo-ionization from $2p^2$ and equally good results may be expected for bound–bound transitions $2p^2 - 2pnl$. In practice this means that the values of $\mathscr{A}(2p^2 - 2pnl)$ obtained from the Bates and Damgaard tables must be divided by (**14**)

$$\zeta = (\nu - 1)(\nu + 2)/\nu(\nu + 1) \tag{3.13}$$

where ν is the effective quantum number for the $2p$ electron in the $2p^2$ configuration.

3.3. *Recombination coefficients.*—For recombination to level i,

$$\alpha_i = \frac{1}{c^2}\left(\frac{2}{\pi}\right)^{1/2}(mkT)^{-3/2}\frac{\omega_i}{\omega_+}\,e^{I_i/kT}\int_{I_i}^{\infty}(h\tilde{\nu})^2 a_i(\tilde{\nu})e^{-h\tilde{\nu}/kT}\,d(h\tilde{\nu}) \tag{3.14}$$

where ω_+ is the statistical weight of the recombining ion, I_i the threshold ionization energy and $a_i(\tilde{\nu})$ the cross-section for photo-ionization by radiation of frequency $\tilde{\nu}$. The photo-ionization cross-section is given by (**8**)

$$a_i = \frac{4\pi\alpha a_0^2}{3}\left(\frac{I_i + z^2\epsilon'}{I_i^2}\right)\sum_{L'l'} C_{l'L'}\left|g(\nu_i l_i, \epsilon' l' \mu'_{l'L'})\right|^2 \tag{3.15}$$

where I_i is in Rydbergs, $z^2\epsilon'$ is the ejected electron energy in Rydbergs,

$$C_{l'L'} = C(i \to i_+ l' L') \tag{3.16}$$

where i_+ specifies the state of the ion, l' the angular momentum of the ejected electron and L' the total angular momentum of ion plus ejected electron. The quantity $\mu'_{l'L'}$ is the extrapolated quantum defect for the $i_+ n' l' L'$ series. The $g(\nu_i l_i, \epsilon' l' \mu'_{l'L'})$ are obtained from the tables of Burgess and Seaton (**8**).

From (3.14) and (3.15),

$$\alpha_i = \left(\frac{2\pi^{1/2}\alpha^4 a_0^2 c}{3}\right)\frac{\omega_i}{\omega_+}\frac{z}{\nu_i^2}\lambda^{1/2}D_i(\lambda) \tag{3.17}$$

where $(2\pi^{1/2}\alpha^4 a_0^2 c/3) = 2{\cdot}8128 \times 10^{-15}\,\mathrm{cm^3\,sec^{-1}}$, $\lambda = (hRcz^2/kT) = 157\,890\,z^2/T$ and

$$D_i(\lambda) = \lambda\sum_{L'l'} C_{l'L'}\int_0^{\infty}(1 + \nu_i^2\epsilon')^3\left|g(\nu_i l_i, \epsilon' l' \mu'_{l'L'})\right|^2 e^{-\epsilon'\lambda}\,d\epsilon'. \tag{3.18}$$

For photo-ionization from $2p\nu lL$ the final state is $2p\epsilon' l' L'$ with $l' = l \pm 1$ and $L' = l', l' \pm 1$. It was found that the amount of calculation could be substantially reduced without significant loss of accuracy on replacing $\mu'_{l'L'}$ by

$$\overline{\mu'_{l'}} = \frac{\sum_{L'} C_{l'L'}\mu'_{l'L'}}{\sum_{L'} C_{l'L'}}. \tag{3.19}$$

Using the relations (3.9), (3.11) we then have

$$\sum_{L'} C_{l'L'}\left|g(\nu_i l_i, \epsilon' l' \overline{\mu'_{l'}})\right|^2 = C(l_i \to l')\left|g(\nu_i l_i, \epsilon' l' \overline{\mu'_{l'}})\right|^2. \tag{3.20}$$

Using the Burgess and Seaton expression for g, one obtains the expansion in powers of λ^{-1}:

$$D_{nl}(\lambda) = \sum_{l' = l \pm 1} C(l \to l')\left|g(\nu l, o l' \overline{\mu'_{l'}})\right|^2 \tag{3.21}$$

$$\times\{1 - \lambda^{-1}[(2\gamma_{ll'} - 3)\nu^2 + 2\pi(b' + \alpha_{ll'}\nu + \beta_{ll'}\nu^2)\tan\pi(\nu + a' + \chi_{ll'})] + O(\lambda^{-2})\} \tag{3.22}$$

where

$$\mu' = a' + b'\epsilon'.$$

4. *The* O III *recombination spectrum.*—The O^{+2} ion has ground configuration $1s^2 2s^2 2p^2$ with spectral terms ^3P, ^1D and ^1S. Assuming all O^{+3} ions to be in the ground state, $1s^2 2s^2 2p$, recombination will populate O^{+2} states $2pnl\,^1L$ and $2pnl\,^3L$. We require the effective recombination coefficients for the O III lines belonging to the transitions $2p3p \to 2p3s$.

Table II gives the O^{+2} quantum defects $\mu(2pnlSL)$ obtained from observed energy levels (**15**). This includes the constants a and b in the linear extrapolation formulae $\mu = a + b\epsilon$. Extrapolated values of μ, given in brackets, are used when the energy level has not been observed. States nl with $l \geqslant 3$ may be taken to be hydrogenic.

TABLE II

O^{+2} *quantum defects* $\mu(2pnlSL)$

Singlets

	l	s	p			d		
	SL	^1P	^1S	^1P	^1D	^1P	^1D	^1F
n								
2		...	0·429	...	0·472	...	...	...
3		0·591	0·235	0·451	0·309	0·009	0·112	0·022
4		0·582	0·241	0·425	0·297	0·012	0·117	0·022
5		0·574	(0·244)	(0·412)	(0·292)	0·011	0·115	0·021
6		(0·576)	(0·246)	(0·407)	(0·289)	(0·011)	0·114	(0·021)
	a =	0·573	0·249	0·395	0·284	0·011	0·114	0·020
	b =	−0·102	+0·108	−0·362	−0·175	0·000	0·000	0·000

Triplets

	l	s	p			d		
	SL	^3P	^3S	^3P	^3D	^3P	^3D	^3F
n								
2		...	...	0·506	...	...	...	...
3		0·627	0·393	0·368	0·424	0·049	0·077	0·110
4		0·610	0·371	0·308	0·401	0·049	0·060	0·110
5		0·604	(0·362)	(0·285)	(0·392)	(0·049)	0·077	0·110
6		(0·600)	(0·357)	(0·273)	(0·387)	(0·049)	0·077	(0·110)
	a =	0·594	0·347	0·247	0·377	0·049	0·077	0·110
	b =	−0·186	−0·316	−0·840	−0·313	0·000	0·000	0·000

Table III gives the elements $C_{k,3pSL}$ of the cascade matrices. For Case B triplets we exclude transitions to $2p^3\,^3P$ and for Case B singlets we exclude transitions to $2p^2\,^1D$ but include transitions to $2p^2\,^1S$.

Table IV gives values of $D_k(\lambda)$. For the triplets the integrals in (3.18) were evaluated numerically for temperatures of 1×10^4 and 2×10^4 °K. Only one rather weak singlet line is observed and the $D_k(\lambda)$ for the singlets were therefore calculated a little less accurately, for 1×10^4 °K, using the expansion (3.22).

TABLE III

The cascade matrix C_{ij}

Singlets

	Case A			Case B		
i j	$3p$ ^{1}S	$3p$ ^{1}P	$3p$ ^{1}D	$3p$ ^{1}S	$3p$ ^{1}P	$3p$ ^{1}D
$4s$ ^{1}P	·0297	·0704	·1511	·0766	·1814	·3894
5	·0229	·0594	·1202	·0516	·1729	·3757
6	·0202	·0537	·1112	·0432	·1638	·3811
$3p$ ^{1}S	1·0000	...	...	1·0000	...	...
4	·0119	·0343	·0538	·0286	·0742	·1384
5	·0150	·0146	·0172	·0196	·0314	·0530
6	·0184	·0116	·0119	·0218	·0230	·0369
$3p$ ^{1}P	...	1·0000	...	...	1·0000	...
4	·0008	·0082	·0035	·0018	·2812	·0234
5	·0054	·0188	·0240	·0115	·2576	·1222
6	·0072	·0249	·0327	·0153	·2563	·1562
$3p$ ^{1}D	...	...	1·0000	...	...	1·0000
4	·0062	·0162	·0342	·0159	·1137	·6362
5	·0025	·0086	·0209	·0063	·0853	·6422
6	·0027	·0097	·0251	·0073	·0865	·6456
$3d$ ^{1}P	·0022	·0148	·0003	·0023	·0156	·0003
4	·0262	·0022	·0009	·0275	·0040	·0012
5	·0322	·0060	·0016	·0339	·0076	·0033
6	·0333	·0083	·0019	·0351	·0109	·0049
$3d$ ^{1}D	...	·0180	·0010	...	·9479	·0521
4	·0000	·0365	·0254	·0003	·5530	·3722
5	·0001	·0524	·0303	·0017	·5471	·3558
6	·0001	·0596	·0312	·0021	·5301	·3404
$3d$ ^{1}F	...	...	·0048	...	...	1·0000
4	·0000	·0000	·0184	·0018	·0131	·9581
5	·0000	·0001	·0257	·0024	·0275	·9225
6	·0001	·0002	·0282	·0034	·0395	·9018
$4f$	·0004	·0094	·0026	·0004	·3491	·4672
5	·0020	·0106	·0070	·0024	·3235	·4824
6	·0026	·0119	·0095	·0033	·3172	·4899
$5g$	·0004	·0094	·0026	·0004	·3491	·4672
6	·0011	·0099	·0046	·0013	·3385	·4740
7	·0015	·0104	·0058	·0018	·3328	·4774
$6h$	·0004	·0094	·0026	·0004	·3491	·4672

From the $3p$ states the only possible transition is to $3s$ and therefore $P_{3p,3s}=1$. The expression for the effective recombination coefficient becomes

$$\alpha(3pSL', 3s) = 1{\cdot}677 \times 10^{-14} t^{-1/2} \sum_k \frac{\omega_k D_k(\lambda) C_{k,3pSL'}}{\nu_k^2} \qquad (4.1)$$

with $t = 10^{-4}T$. Putting $k = 2pnlSL$ we have to evaluate the sums

$$\sum_{n=3}^{\infty} \frac{D_n(\lambda) C_{n,3pSL'}}{\nu_n^2} \qquad (4.2)$$

TABLE III—(*continued*)

Triplets

	Case A			Case B		
i j	$3p\ ^3S$	$3p\ ^3P$	$3p\ ^3D$	$3p\ ^3S$	$3p\ ^3P$	$3p\ ^3D$
$4s\ ^3P$	·0465	·1437	·2190	·1136	·3512	·5353
5	·0363	·1093	·2214	·1037	·2904	·4802
6	·0311	·0939	·2176	·0997	·2856	·4484
$3p\ ^3S$	1·0000	...	...	1·0000	...	...
4	·0106	·0184	·0234	·3542	·2356	·0792
5	·0125	·0210	·0253	·3407	·2829	·0846
6	·0146	·0234	·0268	·3345	·2970	·0950
$3p\ ^3P$	...	1·0000	...	...	1·0000	...
4	·0137	·0399	·0577	·1300	·4418	·3212
5	·0074	·0225	·0314	·1255	·5352	·2408
6	·0058	·0187	·0200	·1277	·5597	·2211
$3p\ ^3D$	...	...	1·0000	...	...	1·0000
4	·0030	·0092	·4177	·0113	·0692	·4645
5	·0050	·0161	·4451	·0161	·1011	·5041
6	·0059	·0191	·4565	·0185	·1126	·5231
$3d\ ^3P$	·0101	·0059	·0007	·6068	·3524	·0407
4	·0145	·0136	·0008	·4663	·4381	·0445
5	·0208	·0186	·0021	·4484	·4326	·0769
6	·0254	·0221	·0031	·4280	·4209	·1010
$3d\ ^3D$	...	·0039	·0023	...	·6241	·3759
4	·0000	·0152	·0038	·0067	·7672	·1978
5	·0001	·0210	·0060	·0268	·7074	·2340
6	·0001	·0243	·0085	·0374	·6646	·2562
$3d\ ^3F$	...	...	1.0000	...	...	1·0000
4	·0004	·0013	·9194	·0016	·0096	·9260
5	·0007	·0020	·8801	·0074	·0258	·8946
6	·0009	·0027	·8364	·0105	·0374	·8562
$4f$	·0019	·0024	·4823	·1147	·2721	·6129
5	·0022	·0041	·4799	·1043	·2882	·5924
6	·0024	·0051	·4776	·1008	·2920	·5867
$5g$	·0019	·0024	·4823	·1147	·2721	·6129
6	·0020	·0032	·4812	·1103	·2793	·6038
7	·0021	·0036	·4799	·1078	·2822	·5989
$6h$	·0019	·0024	·4823	·1147	·2721	·6129

for each spectral series of given *lSL*. The contributions from $n \leqslant 6$ are obtained from Tables III and IV.

The elements of the cascade matrix tend to finite limits as $n \to \infty$ and from Table III it is seen that the elements vary slowly with n for all series in which

TABLE IV

Values of $D_n(\lambda)$ for O^{+2}

Singlets, $T = 1 \times 10^4$ °K

	l	s	p			d			f	g	h
	SL	^1P	^1S	^1P	^1D	^1P	^1D	^1F			
n											
3		1·065	3·70	2·54	3·39	2·46	4·10	2·59	...	...	...
4		0·745	2·44	1·615	2·23	2·70	3·63	2·78	1·20	...	...
5		0·615	1·88	1·25	1·74	2·57	3·05	2·63	1·64	0·60	...
6		0·486	1·56	1·04	1·46	2·40	2·67	2·43	1·74	1·02	0·29

Triplets, $T = 1 \times 10^4$ °K

	l	s	p			d			f	g	h
	SL	^3P	^3S	^3P	^3D	^3P	^3D	^3F			
n											
3		0·923	2·74	3·25	3·09	3·07	3·48	4·07	...	...	...
4		0·615	1·75	2·44	1·99	3·10	3·31	3·62	1·21	...	...
5		0·488	1·35	2·02	1·54	2·81	2·91	3·04	1·66	0·60	...
6		0·415	1·15	1·76	1·30	2·55	2·59	2·66	1·75	1·02	0·29

Triplets, $T = 2 \times 10^4$ °K

	l	s	p			d			f	g	h
	SL	^3P	^3S	^3P	^3D	^3P	^3D	^3F			
n											
3		0·929	2·81	3·30	3·14	2·87	3·28	3·88	...	...	...
4		0·628	1·82	2·48	2·05	2·91	3·14	3·47	1·05	...	...
5		0·504	1·42	2·05	1·60	2·63	2·76	2·92	1·44	0·49	...
6		0·438	1·21	1·79	1·36	2·40	2·46	2·55	1·54	0·81	0·23

the elements are fairly large. Also Table IV shows that the $D_n(\lambda)$ do not vary rapidly with n and the variation of the summand in (4.2) is largely determined by the factor $1/\nu_n^2$. The sum for $n \geqslant 7$ may therefore be estimated on fitting $D_n C_{n,i}$ to some slowly varying function,

$$D_n C_{n,i} = f(\nu_n) \tag{4.3}$$

and replacing the sum by an integral,

$$\sum_{n=7}^{\infty} \frac{D_n C_{n,i}}{\nu_n^2} \simeq \tfrac{1}{2} \frac{f(\nu_7)}{\nu_7^2} + \int_{\nu_7}^{\infty} \frac{f(\nu)}{\nu^2}\, d\nu. \tag{4.4}$$

We consider the functional form to be chosen for $f(\nu_n)$. Using the results of Burgess and Seaton (**8**) and asymptotic expansions obtained by Burgess (**16**) it may be shown that, for large n,

$$f(\nu_n) \sim \text{const.} \times \nu_n^{-p} \tag{4.5}$$

where p lies between 7/3 and about 0·7. The procedure employed in practice was to use either

$$f(\nu_n)=\frac{A}{\nu_n^{1.2}}+\frac{B}{\nu_n} \tag{4.6}$$

or

$$f(\nu_n)=\frac{C}{\nu_n}+\frac{D}{\nu_n^2} \tag{4.7}$$

according to which gave the best fit for $n=3$, 4, 5 and 6 and to determine the constants by fitting at $n=5$ and 6. It was found that the final results were not sensitive to the form chosen for $f(\nu_n)$.

The above methods were used for all states nl with $l\leqslant 3$ and for 5*g*, 6*g* and 6*h*. The contributions from $n>6$, $l>3$ were made using hydrogenic recombination data and making use of the fact that cascades from these levels to 3*p* must pass through one of the *ng* levels. From Table III we see that $C_{ng,3pSL'}$ varies slowly with n and may be replaced by some mean value $\bar{C}_{g,3pSL'}$. The contribution to the sum in (4.1) is therefore

$$\sum_{n=7}^{\infty}\sum_{l=4}^{n-1}\sum_{L=l,l\pm1}\frac{\omega_{SL}D_{nlSL}C_{nlSL,3pSL'}}{n^2}$$
$$=3(2S+1)\bar{C}_{g,3pSL'}\sum_{n=7}^{\infty}\sum_{l=4}^{n-1}\frac{(2l+1)D_{nl}}{n^2} \tag{4.8}$$

since, with $\omega_{SL}=(2S+1)(2L+1)$, the sum over L gives a factor $3(2S+1)(2l+1)$. For hydrogenic ions

$$\sum_{l=0}^{n-1}(2l+1)D_{nl}(\lambda)=\frac{2^4}{\sqrt{3}}\frac{\lambda}{n}S_n(\lambda) \tag{4.9}$$

(**16, 17**) and therefore

$$\sum_{n=7}^{\infty}\sum_{l=4}^{n-1}\frac{(2l+1)D_{nl}(\lambda)}{n^2}=\frac{2^4\lambda}{\sqrt{3}}\sum_{n=7}^{\infty}\frac{S_n(\lambda)}{n^3}-\sum_{n=7}^{\infty}\sum_{l=0}^{3}\frac{(2l+1)D_{nl}(\lambda)}{n^2}. \tag{4.10}$$

Values of $\sum S_n(\lambda)/n^3$ were obtained using the tables of Seaton (**17**) and values of $D_{nl}(\lambda)$ for $l=0$ to 3 were interpolated using equation (3.22) together with results previously obtained by Burgess (**15**). Values of

$$\sum_{l=0}^{3}(2l+1)D_{nl} \tag{4.11}$$

calculated for $n=7$ to 12 were fitted to expressions of the type $\dfrac{A}{n}+\dfrac{B}{n^2}+\dfrac{C}{n^3}$ which were used to complete the summation from $n=13$ to ∞. Results of these calculations, given in Table V, should be correct to within 5 per cent.

TABLE V

	$\lambda=142{\cdot}10$ $(T=1\times10^4,\ z=3)$	$\lambda=71{\cdot}05$ $(T=2\times10^4,\ z=3)$
$\sum_{n=7}^{\infty}\sum_{l=4}^{n-1}\frac{(2l+1)D_{nl}(\lambda)}{n^2}$	6·25	4·35
$\sum_{n=7}^{\infty}\sum_{l=0}^{3}\frac{(2l+1)D_{nl}(\lambda)}{n^2}$	2·95	2·53

Table VI gives the effective recombination coefficients for the $3p \rightarrow 3s$ multiplets. For 4 of the 6 multiplets the intensities for Case B exceed those for Case A by an order of magnitude, the reason being that in Case B a large contribution to the $3p$ populations comes from cascade through the *nd* states but in Case A the *nd* states have large probabilities of decay to $2p^2$. Of the two exceptional multiplets, $3p\,^1S \rightarrow 3s\,^1P$ is weak for both Cases and $3p\,^3D \rightarrow 3s\,^3P$ is strong for both Cases. The reason for the weakness of $3p\,^1S \rightarrow 3s\,^1P$ is that, of the *2pnd* terms, only $2pnd\,^1P$ gives direct transitions to $2p3p\,^1S$ but in both Cases we assume the nebula to be thin for $2pnd\,^1P \rightarrow 2p^2\,^1S$, which effectively depopulates $2pnd\,^1P$. The reason for the great strength of $3p\,^3D \rightarrow 3s\,^3P$ is that $2pnd\,^3F$ cannot undergo direct transitions to $2p^2\,^3P$ and is therefore very effective, even in Case A, for populating $2p3p\,^3D$.

TABLE VI

O III *effective recombination coefficients*

Singlets

Values of $10^{14}\alpha_{3p\,^1L,\ 3s\,^1P}(O^{+2})$

	Case A	Case B
L	$T = 10^4\,^\circ K$	$T = 10^4\,^\circ K$
S	1·07	1·21
P	3·15	26·1
D	4·98	42·4

Triplets

Values of $10^{14}\alpha_{3p\,^3L,\ 3s\,^3P}(O^{+2})$

	Case A	Case B	
		$T = 1 \times 10^4$	$T = 2 \times 10^4\,^\circ K$
L	$T = 10^4\,^\circ K$		
S	2·91	27·3	16·4
P	9·10	79·3	48·1
D	124·3	153·9	86·3

In Section 7.5 we shall estimate the recombination contribution to the [O III] forbidden line intensities. Case B gives an upper limit to $\alpha(2p^2\,^1S \rightarrow 2p^2\,^1D)$ since it is assumed that each recombination on an excited singlet configuration eventually leads to population of $2p^2\,^1S$. We obtain

$$\alpha(2p^2\,^1S \rightarrow 2p^2\,^1D) = \frac{A(^1S \rightarrow {}^1D)}{A(^1S \rightarrow {}^1D) + A(^1S \rightarrow {}^3P)} \times \{\alpha(2p^2\,^1S) + \sum_{n \geqslant 3} \sum_{lL} \alpha(2pnl\,^1L)\}\,.$$

For $T = 10^4\,^\circ K$ this gives $\alpha(2p^2\,^1S \rightarrow 2p^2\,^1D) = 87{\cdot}0 \times 10^{-14}\,cm^3\,sec^{-1}$.

5. O IV *and* O V *recombination lines.*—Calculations of effective recombination coefficients have been made for the lines O IV $1s^2 2s^2 3d\,^2D_{5/2} \rightarrow 1s^2 2s^2 3p\,^2P_{3/2}$ and O V $1s^2 2s 3p\,^1P \rightarrow 1s^2 2s 3s\,^1S$.

For O IV we have

$$\alpha_{3d,3p} = P_{3d,3p} \sum_{nl} \alpha_{nl} C_{nl,3d} \qquad (5.1)$$

where $P_{3d,3p}=1$ for Case B and $P_{3d,3p}=0{\cdot}002$ for Case A. The sum over *nl* in (5.1) will be much less sensitive to whether Case A or Case B is assumed. This sum was evaluated for Case B using hydrogenic data, an approximation which will introduce little error since only the *ns* and *np* series are appreciably non-hydrogenic and these contribute only 1·4 per cent to the total summation. The calculations were made for $T=(16/9)\times 10^4$ °K, the reason for this choice being that the hydrogenic α_{nl} used in the O III calculations could again be used ($T=10^4$ and $z=3$ giving the same value of λ as $T=(16/9)\times 10^4$ and $z=4$). Also $T=(16/9)\times 10^4$ happens to be close to the correct electron temperature for NGC 7027. From these calculations we obtained $\alpha_{3d,3p}{}^{(B)}=2{\cdot}1\times 10^{-12}\,\mathrm{cm^3\,sec^{-1}}$ and $\alpha_{3d,3p}{}^{(A)}\sim 4\times 10^{-15}\,\mathrm{cm^3\,sec^{-1}}$. These figures must be multiplied by 0·6 to obtain the coefficients for the line $^2D_{5/2}\rightarrow{}^2P_{3/2}$.

Since the O V $3^1P\rightarrow 3^1S$ line is very weak the measured intensity will be uncertain and an elaborate calculation would not be justified. For small (T/z^2) a large contribution to the effective recombination rates comes from highly excited states, which are closely hydrogenic. Let us define

$$C_{n,3p}=\sum_l \alpha_{nl}C_{nl,3p}/\sum_l \alpha_{nl}\,. \tag{5.2}$$

Then for Case B,

$$\alpha_{3_1P,3_1S}\simeq \tfrac{1}{4}\sum_{n=3}^{\infty}\alpha_n C_{n,3p} \tag{5.3}$$

where α_n is calculated for a hydrogenic ion. Using values of $C_{nl,3p}$ calculated for O V singlets and values of α_{nl} calculated from hydrogenic data with $(T/z^2)=0$ (**16**) we obtain:

n	3	4	5	6
$C_{n,3p}$	0·40	0·13	0·18	0·19

We took $C_{n,3p}=0{\cdot}20$, independent of n, and evaluated $\sum_3^{\infty}\alpha_n$ for $T=1{\cdot}7\times 10^4$ °K and $z=5$ (**17**) to obtain $\alpha_{3_1P,3_1S}=4\times 10^{-13}\,\mathrm{cm^3\,sec^{-1}}$, a figure which should be correct to within a factor of two.

6. *Data for NGC 7027*

6.1. *Relative intensities.*—Intensities are denoted by $I(\lambda)$ relative to the Hβ intensity $I(4861)=100$. The relative quantum emission rates are defined by $q(\lambda)=(\lambda/4861)I(\lambda)$. We use I_o for observed intensities, I_c for intensities corrected for reddening and I_r for calculated recombination intensities.

The intensities of Aller, Bowen and Minkowski (**5**) have been discussed in a previous paper (**7**). It was found that a reddening constant, $c=1{\cdot}22$, could be chosen so as to obtain agreement between I_c and I_r for the stronger lines of H I, He I and He II but that there was then poor agreement for the weak lines and in the infra-red. Suggested explanations in terms of physical processes in the nebula appear to be unsatisfactory and the possibility has been considered that the intensity anomalies are due to systematic errors in the measurements. In the present paper we shall assume that this is the case. We take the true relative emission rates to be given by $q(\lambda)=\xi q_c(\lambda)$ where $\xi=\xi_1(I_o)\xi_2(\lambda)$ and where the correction factors ξ_1 and ξ_2 are given in (**7**). For all the lines considered in the present paper, values of I_o, I, q_c, ξ and q are given in Table VII.

TABLE VII

Relative intensities and emission rates for NGC 7027

λ	Transition	$J \to J'$	I_o	I_c	q_c	ξ	q	
3300	O III $3p\ ^3S \to 3s\ ^3P$	1→0	3·5	11·4	7·7	0·8	6·2	65·9
3312		1→1	11·3	36·6	24·9	1·0	24·9	
3341		1→2	16·0	50·6	34·8	1·0	34·8	
3412	O IV $3d\ ^2D \to 3p\ ^2P$	$\frac{5}{2} \to \frac{3}{2}$	1·1	3·3	2·3	0·37	0·9	
3726	[O II] $^2D \to {}^4S$	$\frac{3}{2} \to \frac{3}{2}$	9·4	22·3	17·1	1·0	17·1	24·7
3729		$\frac{5}{2} \to \frac{3}{2}$	4·6	10·9	8·4	0·9	7·6	
3755	O III $3p\ ^3D \to 3s\ ^3P$	2→1	1·4	3·3	2·5	0·42	$1·0_5$	7·8
3757		1→0	0·8	1·9	1·5	0·30	$0·4_5$	
3760		3→2	3·8	8·8	6·8	0·83	5·6	
3774		1→1	0·7	1·6	1·2	0·29	$0·3_5$	
3791		2→2	0·7	1·6	1·2	0·29	$0·3_5$	
4363	[O III] $^1S \to {}^1D$	0→2	21	30·5	27	1·0	27	
4686	He II 4→3	...	45	50	48	1·0	48	
4861	H I 4→2	...	100	100	100	1·0	100	
4959	[O III] $^1D \to {}^3P$	2→1	420	390	400	1·0	400	1490
5007		2→2	1170	1055	1090	1·0	1090	
5112	O V 3 $^1P \to 3\ ^1S$	1→0	0·5	0·4	0·4	0·2	0·08	
5577	[O I] $^1S \to {}^1D$	0→2	1·5	0·9	1·0	0·5	0·5	
5592	O III $3p\ ^1P \to 3s\ ^1P$	1→1	1·1	0·7	0·8	0·4	0·3	
5755	[N II] $^1S \to {}^1D$	0→2	12	6·8	8·1	1·0	8·1	
6300	O I $^1D \to {}^3P$	2→2	20	8·5	11	1·1	12	18
6364		2→1	10	4	5	1·1	6	
6548	[N II] $^1D \to {}^3P$	2→1	80	32·9	44·4	1·1	49	197
6584		2→2	240	99·4	134·8	1·1	148	
7320 7330	[O II] $^2D \to {}^2P$	...	77	21	31	1·4	4·3	

6.2. *The electron temperature and electron density.*—The following ratios depend on the electron temperature T_e and electron density N_e (**18, 19**):

$$\left.\begin{aligned} \rho''[\mathrm{O\,I}] &= \frac{q(6300)+q(6364)}{q(5577)} \\ \rho''[\mathrm{O\,II}] &= \frac{q(3726)+q(3729)}{q(7320)+q(7330)} \\ \rho[\mathrm{O\,II}] &= \frac{q(3729)}{q(3726)} \\ \rho''[\mathrm{O\,III}] &= \frac{q(4959)+q(5007)}{q(4363)} \\ \rho''[\mathrm{N\,II}] &= \frac{q(6548)+q(6584)}{q(5755)} \end{aligned}\right\} . \qquad (6.1)$$

Fig. 1 gives the T_e, N_e relations obtained using the observed ratios and atomic data from (**19**), (**20**) and (**21**). The ratio ρ''[O I] may be uncertain since $I(5577)$ is weak and could include a contribution from airglow radiation but it is satisfactory that ρ''[O I] in fact gives good agreement with the other curves.

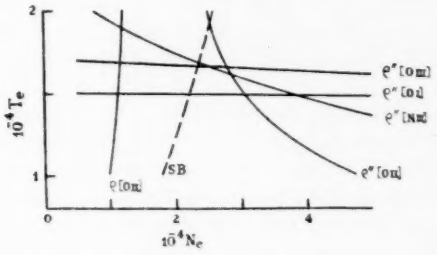

FIG. 1.—*T_e, N_e relations for NGC 7027 from the forbidden line ratios (equations (6.1)) and from the surface brightness, SB (equation (6.2)). We adopt $T_e = 1{\cdot}7 \times 10^4$ °K and $N_e = 2{\cdot}2 \times 10^4$ cm^{-3}.*

In Fig. 1 we include the curve calculated from the relation

$$\log N_e = 5{\cdot}97 + \tfrac{1}{2}\log S_\beta - \tfrac{1}{2}\log(Ar) + \tfrac{1}{2}\log(t^{3\cdot2}/b_4 e^{x}{}_4) + \tfrac{1}{2}c \qquad (6.2)$$

where S_β is the observed Hβ surface brightness in ergs cm^{-2} sec^{-1}, A the nebular radius in seconds of arc, r the distance in parsecs and $t = 10^{-4}T_e$. We use values of S_β, A and r from (**22**), $b_4 e^{x}{}_4$ from (**16**) and c from (**7**).

The different T_e, N_e relations are seen to give reasonably concordant results but ρ[O II] gives a density lower than that obtained by the other methods; this difference may be due to local condensations (**19**). From the results of Fig. 1 we adopt $T_e = 1{\cdot}7 \times 10^4$ °K and $N_e = 2{\cdot}2 \times 10^4$ cm^{-3}.

6.3. *Abundances from forbidden lines.*—The effective recombination coefficient for a line $n \to n'$ in the spectrum of an ion X^{+m} we denote by $\alpha_{n,n'}(X^{+m})$. The absolute emission rate for the Hβ line is

$$\mathcal{Q}(4861) = N_e N(\mathrm{H}^+)\alpha_{4,2}(\mathrm{H}^0) \qquad (6.3)$$

where, using Case B for H I, $\alpha_{4,2}(\mathrm{H}^0)$ in cm^3 sec^{-1} is $2{\cdot}99 \times 10^{-14}$ for $T_e = 1 \times 10^4$ °K and $1{\cdot}595 \times 10^{-14}$ for 2×10^4 °K (**16**). For the $i \to j$ forbidden line of some ion B we have

$$\mathcal{Q}_{ij} = N_i(B)A_{ij}. \qquad (6.4)$$

The total ion density $N(B)$ is expressed in terms of the excited state density $N_i(B)$ using relations of the type (**19**)

$$N_i(B) = \frac{N(B)P(i)}{S} \qquad (6.5)$$

where

$$S = \sum_j P(j) \qquad (6.6)$$

the sum being over all ground configuration states.

The quantum emission rate relative to $q(4861) = 100$ is

$$\frac{q_{ij}}{100} = \frac{N_i(B)A_{ij}}{N_e N(\mathrm{H}^+)\alpha_{4,2}(\mathrm{H}^0)}. \qquad (6.7)$$

We are interested in the total numbers of ions in the ionized region and may therefore equate $N(H^+)$ to the total hydrogen density $N(H)$. From (6.5) and (6.7) we obtain

$$\frac{N(B)}{N(H)} = \frac{q_{ij}}{100} \cdot \frac{SN_e}{A_{ij}P(i)} \cdot \alpha_{4,2}(H^0). \tag{6.8}$$

Abundance ratios O^0/H, O^+/H and O^{+2}/H are given in Table X. For [O I] and [O III], $P(i)/S$ is approximately proportional to N_e and the abundance ratios insensitive to N_e but, because the [O II] lines are more highly forbidden, O^+/H is more sensitive to N_e.

7. *Interpretation of the O III line intensities*

The O III lines are excited both by fluorescence and by recombination. We shall show how the contributions from these two processes may be separated. From the recombination contribution we obtain the O^{+3} abundance and from the fluorescent contribution we obtain the overall efficiency of the fluorescent mechanism. We also consider the contribution to forbidden line intensities due to recombination. But first of all we calculate the optical depths for O III resonance lines.

7.1. *Optical depths.*—The optical depths for absorptions from the $2p^2\,{}^1D$ and ${}^1S$ metastable states are deduced from observed absolute intensities. The optical depth for $i \to k$ absorption is

$$\tau_{ik} = \int_{R_0}^{R_1} N_i \kappa_{ik}\, dR \tag{7.1}$$

where R_0 is the inner radius of the nebula, R_1 the outer radius and κ_{ik} the absorption coefficient. Suppose that $i \to j$ emission is observed and that this is forbidden-line radiation for which the nebula is optically thin. Let F_{ij} be the flux of $i \to j$ quanta at the surface of the nebula ($F_{ij} = S_{ij}/h\nu_{ij}$ where S_{ij} is the surface brightness). Then

$$F_{ij} = \frac{\int N_i A_{ij}\, dV}{4\pi R_1^2} \tag{7.2}$$

where the integral is over the nebular volume. From this we obtain

$$\int_{R_0}^{R_1} N_i\, dR = \mathscr{G} F_{ij}/A_i \tag{7.3}$$

where $\mathscr{G}$ is a geometrical factor. For N_i uniform in $R_0 \leqslant R \leqslant R_1$ we have $\mathscr{G} = 3R_1^2/(R_1^2 + R_1R_0 + R_0^2)$. From (7.1) and (7.3),

$$\tau_{ik} = \mathscr{G}\kappa_{ik}F_{ij}/A_{ij}. \tag{7.4}$$

For thermal Doppler broadening the absorption coefficient at the line centre is

$$\kappa_{ik} = \frac{\pi e^2}{m\tilde{\nu}_{ik}} \left(\frac{M}{2\pi kT}\right)^{1/2} f(k,i) \tag{7.5}$$

where $\tilde{\nu}_{ik}$ is the frequency and M the ion mass and where, in the notation of Section 3.2,

$$f(k,i) = \tfrac{1}{3}(\epsilon_k - \epsilon_i) C(i \to k) |\langle i|r|k\rangle|^2. \tag{7.6}$$

Table VIII gives optical depth for lines ending on $2p^2\,{}^1D$ calculated using the measured Hβ surface brightness (**22**), multiplied by 10^c to correct for extinction, and relative emission rates of Table VII. It is seen that the nebula is optically thick for some, but not all, of these lines.

TABLE VIII

Optical depths $\tau(2p^2\,{}^1\mathrm{D}\rightarrow 1pnl\,{}^1\mathrm{L})$ *for* O III *lines in NGC* 7027

	l	*s*	*d*		
	^{1}L	^{1}P	^{1}P	^{1}D	^{1}F
n					
3		10·4	0·77	20·7	70·6
4		1·3	0·24	5·8	21·4

Using relative emission rates of Table VII and calculated transition probabilities (**21**) we obtain

$$\frac{N(2p^2\,{}^1\mathrm{D})}{N(2p^2\,{}^1\mathrm{S})} = 4600 \tag{7.7}$$

and using equations of the type (6.5) we obtain

$$\frac{N(2p^2\,{}^3\mathrm{P})}{N(2p^2\,{}^1\mathrm{D})} = 730. \tag{7.8}$$

The nebula is therefore optically thin for transitions ending on $2p^2\,{}^1$S and optically thick for those ending on $2p^2\,{}^3$P.

The optical depth for the absorption line $2p^2\,{}^3\mathrm{P}_2\rightarrow 2p3d\,{}^3\mathrm{P}_2$ is of importance for the fluorescent mechanism. Expressing the population in the form (6.5) we obtain, using collision strengths from (**23**) and transition probabilities calculated from (**24**),

$$\left.\begin{aligned} P(^3\mathrm{P}_0) &= x^2 + 0{\cdot}46x + 0{\cdot}08 \\ P(^3\mathrm{P}_1) &= 3x^2 + 1{\cdot}5x \\ P(^3\mathrm{P}_2) &= 5x^2 + 0{\cdot}18x \end{aligned}\right\} \tag{7.9}$$

with $x = 10^{-2}N_e/T_e^{1/2}$. This gives 1·0 : 3·0 : 3·9 for the ratios of the $2p^2\,{}^3\mathrm{P}_{0,1,2}$ populations. For the optical depth we obtain finally

$$\tau(2p^2\,{}^3\mathrm{P}_2,\, 2p3d\,{}^3\mathrm{P}_2) = 2{\cdot}2 \times 10^4. \tag{7.10}$$

7.2. *Separation of fluorescent and recombination emission rates.*—We denote fluorescent emission rates by q_f, recombination rates by q_r and corrected observed rates by $q = q_f + q_r$. From Table VII we have

$$\frac{q(3p\,{}^3\mathrm{S}\rightarrow 3s\,{}^3\mathrm{P})}{q(3p\,{}^3\mathrm{D}\rightarrow 3s\,{}^3\mathrm{P})} = 8{\cdot}5. \tag{7.11}$$

The corresponding ratio for recombination is 0·18 (Case B) or 0·023 (Case A) and the ratio for fluorescence is

$$\frac{q_f(3p^3S\rightarrow 3s\,{}^3\mathrm{P})}{q_f(3p\,{}^3\mathrm{D}\rightarrow 3s\,{}^3\mathrm{P})} = \frac{C_{3d\,{}^3\mathrm{P},\,3p\,{}^3\mathrm{S}}}{C_{3d\,{}^3\mathrm{P},\,3p\,{}^3\mathrm{D}}} = 14{\cdot}9 \tag{7·12}$$

it being noted that $\sum_{J'} A(SLJ\rightarrow S'L'J')$ does not depend on J. The fluorescent ratio (7.12) is equal to the ratio of the $3d\rightarrow 3p$ transition probabilities and should be determined accurately. Since the observed ratio is intermediate between

the recombination and fluorescent ratios the relative contributions of the two processes may be determined. For Case B we obtain:

	$q(3p\,^3S\rightarrow 3s\,^3P)$	$q(3p\,^3D\rightarrow 3s\,^3P)$
Fluorescent	65·3	4·4
Recombination	0·6	3·4
Observed	65·9	7·8

Since $q_r(3p\,^3S\rightarrow 3s\,^3P)$ is always small, the deduced value of $q_r(3p\,^3D\rightarrow 3s\,^3P)$ is practically independent of whether Case A or Case B is assumed.

Having separated the fluorescent and recombination contributions by considering the relative intensities of the two multiplets we may check that theory agrees with observation for the fine structure intensities within the multiplets. For recombination we use the fact that $N(SLJ)$ is proportional to $(2J+1)$ (Section 3.1). It is here assumed that the states $O^{+3}2p\,^2P_{1/2}, {}^2P_{3/2}$ are populated in the 1 : 2 statistical weight ratio. The density of NGC 7027 should be high enough to ensure that this is a good approximation. The position when this condition is not satisfied has been discussed in (**25**). For the fluorescent mechanism we solve the problem of cascade from $3d\,^3P_2$ taking J quantum numbers into account.

The comparison of fine structure emission rates is given in Table IX. The agreement between theory and observation is seen to be very good. For $3p\,^3S\rightarrow 3s\,^3P$ the upper state has no fine structure and the agreement therefore provides a check only on the intensity measurements and on the basic assumption of LS coupling. The $3p\,^3D\rightarrow 3s\,^3P$ multiplet is more interesting. Here the fluorescent and recombination mechanisms give quite different fine structure intensities. It is seen that the combination of q_f and q_r which gives the observed intensity ratio for the two multiplets also gives the observed relative intensities for the components of the $^3D\rightarrow{}^3P$ multiplet.

TABLE IX

Quantum emission rates for O III $2p3p\rightarrow 2p3s$ *in NGC 7027*

	J	J'	q Obs.	q Calc.	q_f	q_r
$3p\,^3S_J-3s\,^3P_{J'}$	1	0	6·2	7·4	7·3	0·1
	1	1	24·9	22·0	21·8	0·2
	1	2	34·8	36·5	36·2	0·3
			65·9	65·9	65·3	0·6
$3p\,^3D_J-3s\,^3P_{J'}$	3	2	5·6	5·3	3·7	1·6
	2	2	0·3$_5$	0·5	0·2	0·3
	2	1	1·0$_5$	1·3	0·5	0·8
	1	2	...	0·0	0·0	0·0
	1	1	0·3$_5$	0·3	0·0	0·3
	1	0	0·4$_5$	0·4	0·0	0·4
			7·8	7·8	4·4	3·4
$3p\,^1P_J-3s\,^1P_{J'}$	1	1	0·3	0·6 (B) 0·06 (A)	0·0 0·0	0·6 (B) 0·06 (A)

In Table IX we include the emission rates for the singlet line, $3p\,^1\mathrm{P}\rightarrow 3s\,^1\mathrm{P}$, to which the fluorescent mechanism does not contribute. It is satisfactory that the observed emission rate is intermediate between those calculated for Cases A and B.

7·3. *The O^{+3} abundance.*—The abundance ratio is determined from

$$\frac{N(\mathrm{O}^{+3})}{N(\mathrm{H})} = \frac{q_r(3p\,^3\mathrm{D}\rightarrow 3s\,^3\mathrm{P})}{100}\cdot\frac{\alpha_{4,2}(\mathrm{H}^0)}{\alpha_{3p\,^3\mathrm{D},3s\,^3\mathrm{P}}(\mathrm{O}^{+2})}. \tag{7.13}$$

Using $q_r(3p\,^3\mathrm{D}, 3s\,^3\mathrm{P}) = 3{\cdot}4$, values of $\alpha_{4,2}(\mathrm{H}^0)$ quoted in Section 6.3 and values of $\alpha_{3p\,^3\mathrm{D},3s\,^3\mathrm{P}}$ for Case B from Table VI we obtain $N(\mathrm{O}^{+3})/N(\mathrm{H}) = 0{\cdot}64\times 10^{-3}$. This result is practically independent of the assumed value of T_e (we obtain $0{\cdot}65\times 10^{-3}$ for $T_e = 1\times 10^4\,^\circ\mathrm{K}$ and $0{\cdot}63\times 10^{-3}$ for $T_e = 2\times 10^4\,^\circ\mathrm{K}$) and is not sensitive to whether Case A or Case B is assumed for O III triplets (the O^{+3} abundance would be increased by a factor of 1·24 if Case A were assumed).

7·4. *The efficiency of the fluorescent mechanism.*—The probability that absorption of a single He II Lyα photon by O^{+2} will give fluorescent lines is

$$\sum_L C^{(A)}_{3d\,^3\mathrm{P},3p\,^3\mathrm{L}} = 0{\cdot}0167. \tag{7.14}$$

This is the quantity P_{32} used in Section 2.

The total emission rate for fluorescent quanta is

$$\mathcal{Q}_f(\mathrm{O\,III}) = \sum_L \mathcal{Q}_f(3d\,^3\mathrm{P}_2\rightarrow 3p\,^3\mathrm{L}). \tag{7.15}$$

The overall efficiency of the fluorescent mechanism is

$$\mathscr{R} = \frac{\mathcal{Q}_f(\mathrm{O\,III})}{\mathcal{Q}(\mathrm{He\,II\ Ly}\alpha)}. \tag{7.16}$$

From the cascade theory of Section 4 we obtain

$$\mathcal{Q}_f(\mathrm{O\,III}) = 1{\cdot}65\,\mathcal{Q}_f(3p\,^3\mathrm{S}\rightarrow 3s\,^3\mathrm{P}) \tag{7.17}$$

and for the He II Lyα emission rate we have

$$\mathcal{Q}(\mathrm{He\,II\ Ly}\alpha) = \frac{\alpha_{2p,1s}(\mathrm{He}^+)}{\alpha_{4,3}(\mathrm{He}^+)}\,\mathcal{Q}(\mathrm{He\,II}, 4\rightarrow 3). \tag{7.18}$$

Case B should certainly apply for He^+. We then have

$$\alpha_{2p,1s}(\mathrm{He}^+) = (1-X)\sum_{n=2}^{\infty}\alpha_n(\mathrm{He}^+) \tag{7.19}$$

where X, which is approximately equal to 0·3, is the fraction of excited state recombinations which populate $2s$ (**16**). Using data from (**7**) and (**17**) we obtain

$$\frac{\alpha_{2p,1s}(\mathrm{He}^+)}{\alpha_{4,3}(\mathrm{He}^+)} = 0{\cdot}19, \tag{7.20}$$

practically independent of T_e. The fluorescent efficiency is therefore

$$\mathscr{R} = 0{\cdot}19\times 1{\cdot}65\times\frac{q_f(3p\,^3\mathrm{S}\rightarrow 3s\,^3\mathrm{P})}{q(\mathrm{He\,II}, 4\rightarrow 3)} \tag{7.21}$$

and substitution of $q_f(3p\,^3\mathrm{S}\rightarrow 3s\,^3\mathrm{P}) = 65{\cdot}3$ and $q(\mathrm{He\,II},\ 4\rightarrow 3) = 48$ gives $\mathscr{R} = 0{\cdot}43$.

7·5. *The recombination contribution to forbidden line intensities.*—It is usually assumed that collisional processes alone are responsible for forbidden line excitation. We are now in a position to check that this is justified. We have

$$q_r(2p^2\,^1\mathrm{S}\rightarrow 2p^2\,^1\mathrm{D}) = \frac{\alpha_{2p^2\,^1\mathrm{S},2p^2\,^1\mathrm{D}}}{\alpha_{3p\,^3\mathrm{D},3s\,^3\mathrm{P}}}\times q_r(3p\,^3\mathrm{D}\rightarrow 3s\,^3\mathrm{P}). \tag{7.22}$$

In Section 4 we obtained an upper limit of $87 \times 10^{-14}\,\mathrm{cm^3\,sec^{-1}}$ for $\alpha_{2p^2\,{}^1S,2p^2\,{}^1D}$. For the same temperature, $T_e = 10^4$ °K, we have $\alpha_{3p\,{}^3D,3s\,{}^3P} = 154 \times 10^{-14}\,\mathrm{cm^2\,sec^{-1}}$. With $q_r(3p\,{}^3D \rightarrow 3s\,{}^3P) = 3{\cdot}4$ we therefore obtain $q_r(2p^2\,{}^1S \rightarrow 2p^2\,{}^1D) \leqslant 1{\cdot}9$. Comparison with the observed rate, $q(2p^2\,{}^1S \rightarrow 2p^2\,{}^1D) = 27$, shows recombination to be unimportant.

8. *Abundances of* O^{+4} *and* O^{+5}

8.1. *The* O^{+4} *abundance.*—Recombination of O^{+4} ions in the $1s^2 2s^2$ ground configuration will populate O^{+3} levels with configuration $1s^2 2s^2 nl$. This could give the observed O IV line, $3\,{}^2D_{5/2} \rightarrow 3\,{}^2P_{3/2}$, λ 3412. A further weak O IV line observed by Aller, Bowen and Minkowski (**5**),

$$1s^2 2s2p(^3P)3d\,{}^4F_{9/2} \rightarrow 1s^2 2s2p(^3P)3p\,{}^4D_{7/2}, \quad \lambda\,3737,$$

would not be expected in the recombination spectrum. It would be worth looking for the other members of the multiplet in order to check the identification.

We use the $3\,{}^2D_{5/2} \rightarrow 3\,{}^2P_{3/2}$ line to obtain the O^{+4} abundance. Using $\alpha_{3\,{}^2D_{5/2},\,3\,{}^2P_{3/2}} = 1{\cdot}2 \times 10^{-12}\,\mathrm{cm^3\,sec^{-1}}$ calculated for Case B and $T_e = 1{\cdot}78 \times 10^4$ °K (Section 3.5) we obtain $N(O^{+4})/N(H) = 0{\cdot}14 \times 10^{-3}$. The O^{+4} abundance would be greater by a factor of order 10^3 if Case A were assumed. Since the O III triplet resonance lines have central optical depths of order 10^4 (Section 7.1), and since the number of O^{+3} ions exceeds the number of O^{+2} ions by a factor of about 4, the optical depths will certainly be very large for the O IV resonance lines and we may expect Case B to be approached but the discussion of fluorescent efficiencies (Section 2) suggests that the O^{+4} abundance may exceed that calculated for Case B by a factor of 2 or 3.

We adopt an O^{+4} abundance twice as large as that calculated for Case B.

8.2. *The* O^{+5} *abundance.*—A single weak O V line is observed, $3\,{}^1P \rightarrow 3\,{}^1S$, λ 5112. Using $\alpha_{3\,{}^1P,\,3\,{}^1S} = 4 \times 10^{-13}\,\mathrm{cm^3\,sec^{-1}}$ calculated for Case B and $T_e = 1{\cdot}7 \times 10^4$ °K we obtain $N(O^{+5})/N(H) = 0{\cdot}04 \times 10^{-3}$.

As in the case of O^{+4}, we adopt an abundance for O^{+5} which is twice as large as that calculated for Case B.

9. *Summary and discussion*

9.1. *Summary.*—Table X summarizes our results for the oxygen ion abundances. The chemical abundance ratio for NGC 7027, $N(O)/N(H) = 1{\cdot}2 \times 10^{-3}$,

TABLE X

X	$10^3 N(X)/N(H)$	$10^{18} a_{\nu_0}^{\tau}(X)$	$\tau_0(X)$	*I.P.* (eV)
O^0	0·0035	7·6	0·09	13·60
O^+	0·010	8·1	0·29	35·17
O^{+2}	0·15	3·5	1·8	54·93
O^{+3}	0·64	1·1	2·5	77·35
O^{+4}	0·28	0·9	0·44	113·86
O^{+5}	0·08	0·32	0·05	138·06
	1·2			

agrees closely with the chemical abundance ratios obtained for atmospheres of early type stars (**26, 27**). In Table X we include estimates of the optical depths for photo-ionization of the oxygen ions. These are calculated from

$$\tau_0(X) = 1{\cdot}6 \times 10^{17} N(X) a_{\nu_0}^{\tau}(X) \qquad (9.1)$$

where $1{\cdot}6 \times 10^{17}$ cm is taken to be the radius of the nebula (**22**) and where the $a_{\tilde{\nu}_0}$ are the threshold photo-ionization cross-sections, calculated from formulae given in (**8**) and (**20**).

9.2. *Discussion of sources of error.*—For the total oxygen abundance the main uncertainty is in the observed intensities. Only further observational work can decide whether we are justified in introducing the correction factor ξ which brings the measured H I, He I and He II intensities into agreement with theory. If this factor is not introduced it is difficult to obtain any value for the O/H abundance ratio since we then have no satisfactory theory for the H I spectrum. If we had not introduced the correction factor but had still assumed the recombination theory for the strong H I lines we would have obtained a ratio $N(\mathrm{O})/N(\mathrm{H}) = 2{\cdot}6 \times 10^{-3}$.

The main uncertainties on the theory side are concerned with the question of how closely Case B is approached for O III, O IV and O V. Improved calculations will be possible when a satisfactory theory has been obtained for the efficiencies of the fluorescent mechanism. So far as the total oxygen abundance is concerned it is very fortunate that, for reasons explained in Section 4, the effective recombination coefficient for O III $3p\,^3\mathrm{D} \rightarrow 3s\,^3\mathrm{P}$ is not sensitive to whether case A or Case B is assumed. The abundance of O^{+3}, which is the most abundant oxygen ion, should therefore be determined fairly accurately. The abundances of O^{+4} and O^{+5} are determined a good deal less accurately but, so long as departures from Case B are not much greater than we have assumed, this does not introduce serious uncertainty in the final chemical abundance ratio. Further improvement in the accuracy of the O^{+4} and O^{+5} abundances is still very desirable since a quantitative study of the ionization equilibrium for oxygen should eventually provide important information about the stellar ultra-violet radiation field.

9.3. *The determination of oxygen abundances in other nebulae.*—It would be of interest to determine O/H abundance ratios for a number of nebulae. The ions O^{+4} and O^{+5} do not make a large contribution to the total oxygen abundance in NGC 7027 and since this object has particularly large abundances of highly ionized atoms we may expect that O^{+4} and O^{+5} may be neglected in most nebulae. The main need is to determine O^{+3} abundances from recombination lines in addition to O^0, O^+ and O^{+2} from forbidden lines. The O^{+3} abundance is best obtained from the O III multiplet $3p\,^3\mathrm{D} \rightarrow 3s\,^3\mathrm{P}$. The wave-length interval 3750 A to 3800 A contains all five lines of the O III multiplet and, in addition, three H I lines and two He II lines. In NGC 7027 these ten lines all have comparable intensities and this may also be expected in other high excitation nebulae. Further careful spectrophotometry of this 50 A interval in selected nebulae would be of considerable interest. From the relative intensities of the O III lines the fluorescent and recombination contributions may be separated. The ratio of O III recombination intensities to H I intensities then gives the $\mathrm{O}^{+3}/\mathrm{H}$ abundance ratio and the ratio of O III fluorescent intensities to He II intensities give the efficiency of the fluorescent mechanism.

Department of Physics,
University College London,
W.C.1:

1959 *October.*

References

(1) L. H. Aller and D. H. Menzel, *Ap. J.*, **102,** 239, 1945.
(2) L. H. Aller, *Ap. J.*, **120,** 401, 1954.
(3) L. H. Aller and R. Minkowski, *Ap. J.*, **124,** 110, 1956.
(4) L. H. Aller, *Ap. J.*, **125,** 84, 1957.
(5) L. H. Aller, I. S. Bowen and R. Minkowski, *Ap. J.*, **122,** 62, 1955.
(6) I. S. Bowen, *Publ. A.S.P.*, **46,** 146, 1934.
(7) M. J. Seaton, *M.N.*, **120,** 326, 1960.
(8) A. Burgess and M. J. Seaton, *M.N.*, **120,** 121, 1960.
(9) M. J. Seaton, *M.N.*, **119,** 90, 1959.
(10) M. J. Seaton, *Rep. Progr. Phys.*, **23,** 313, 1960.
(11) H. Zanstra, *Bull. Astr. Inst. Neth.*, **9,** 1, 1949.
(12) E. U. Condon and G. H. Shortley, *Theory of Atomic Spectra*, p. 98, Cambridge, 1935.
(13) D. R. Bates and A. Damgaard, *Phil. Trans. Roy. Soc. A*, **242,** 101, 1949.
(14) M. J. Seaton, *M.N.*, **118,** 504, 1958.
(15) C. E. Moore, *Atomic Energy Levels*, Vol. 1, 1949, and appendix to Vol. 3, 1958 National Bureau of Standards, Washington.
(16) A. Burgess, *M.N.*, **118,** 477, 1958.
(17) M. J. Seaton, *M.N.*, **119,** 81, 1959.
(18) M. J. Seaton, *M.N.*, **114,** 154, 1954.
(19) M. J. Seaton and D. E. Osterbrock, *Ap. J.*, **125,** 66, 1957.
(20) M. J. Seaton, *Rev. Mod. Phys.*, **30,** 979, 1958.
(21) R. H. Garstang, *M.N.*, **111,** 115, 1951.
(22) L. H. Aller, *Gaseous Nebulae*, p. 149, Chapman and Hall, London, 1956.
(23) M. J. Seaton, *Proc. Roy. Soc. A*, **218,** 400, 1953.
(24) G. H. Shortley, L. H. Aller, J. G. Baker and D. H. Menzel, *Ap. J.*, **93,** 178, 1941.
(25) G. H. Shortley and D. H. Menzel, *Ap. J.*, **91,** 307, 1940.
(26) G. Traving, *Zs. f. Astr.*, **36,** 1, 1955 and **41,** 215, 1957.
(27) R. Cayrel, *Thèses*, Paris, 1957.

VARIABLE STARS IN NGC 2257

*J. B. Alexander**

(Communicated by the Radcliffe Observer)

(Received 1959 November 30)

Summary

From the blink-comparison of plates taken at the Radcliffe Observatory over a period of about six years, 28 variables have been discovered in the globular cluster NGC 2257 which is on the outskirts of the Large Magellanic Cloud. Visual estimates of the brightness of these variables have been made on a step basis relative to a sequence. For six variables with a large amplitude of light-variation, periods ranging from 0·51 to 0·69 days have been derived, and the light-curves obtained are like those of Bailey *a* and *b* type RR Lyrae variables in the galaxy. It has not been possible from the available material to work out the periods of the many variables with a much smaller range of light-variation, but at least some of these stars have the gradual rise to maximum found in Bailey *c* type variables.

1. *Introduction.*—The globular cluster NGC 2257 (R.A. $6^h\,29^m\cdot9$, Dec. $-64^\circ\,27'$; 1950) was first regarded as a possible outlying member of the Large Magellanic Cloud by Shapley and Mohr (**1**), who assigned to it an integrated photographic magnitude of $12^m\cdot4$. The degree of central concentration is not high (see Plate 1), and on good plates taken with the Radcliffe 74-inch reflector it is possible to resolve some stars at the centre of the cluster at a magnitude corresponding to the minima of the RR Lyrae variables. No determination of the integrated colour of the cluster has yet been made.

Variable stars were first found in the cluster by Dr A. D. Thackeray in 1953. A series of plates extending from September 1953 to May 1959 have been taken with a view to the further discovery of variables, and, if possible, to the eventual determination of periods and light-curves. There exist 66 plates, mostly of 30 min exposure, taken on Kodak 103a-O (without filter) at the Newtonian focus of the Radcliffe 74-inch reflector. Of these, 37 were taken by Dr A. D. Thackeray, 25 by Dr A. J. Wesselink, 1 by Dr T. D. Kinman and the remaining 3 by the writer. There is also one 30 min exposure in the yellow which is sufficient to show that the brightest stars in the cluster are not blue.

2. *The blink-comparisons.*—Twelve pairs of plates were examined by the writer in the blink comparator which is on loan to the Radcliffe Observatory from the Royal Observatory, Cape. On the basis of this survey, 16 stars were considered with certainty to be variables, and a further 11 stars were regarded as likely variables. Of this latter group, 7 were afterwards considered to be certain variables when the various estimates of brightness described in Section 3 had been made.

Some idea of the degree of completeness of the examination can be obtained as follows. The 23 certain variables are divided into two groups according to whether the amplitude of the observed light-variations is less than or more than eight steps on the scale described in Section 3. The blinking was done in such a way that a method described by Van Gent (**2**) can be applied, and the results of this analysis are given in Table I. Group 1 is the large amplitude group.

* On secondment from the Royal Greenwich Observatory, Herstmonceux.

TABLE I

	Predicted number in cluster*	Number found in survey
Group 1	8·0	8
Group 2	16·6	15

The probability of the discovery of a variable from the blink-comparison of one pair of plates (i.e. the quantity α in van Gent's notation) is 0·53 for Group 1 and 0·18 for Group 2.

Although the cluster is not very heavily concentrated towards its centre, it is likely that several variables have been missed in the blinking because of crowding, but no allowance is made for this effect in any simple statistical method such as that used above. This is to some extent confirmed by what follows below.

The blinking done by the writer was carried out independently of any other investigation. Dr A. R. Sandage has also searched the plates for variables, and an unpublished list of 19 certain variables found by him contains 5 not discovered by the writer. There are therefore 28 stars in all regarded as certain variables in at least one of the two surveys. These are indicated by numbers in Plate 1. There are four C.P.D. stars in the field of the plates, and these have been used to obtain the approximate distances of the variables east and north (ΔX and ΔY respectively) of an origin near the centre of the cluster. These are given in Table II below. The letters refer to the comparison stars mentioned in the next section.

TABLE II

Positions of variables in NGC 2257 for 1950 (seconds of arc)

Variable	ΔX	ΔY	r	Variable	ΔX	ΔY	r
1	+27	+45	52	15	−55	−14	57
2	−41	−28	50	16	−35	+ 7	36
3	+28	−24	37	17	+35	−51	62
4	+99	+28	103	18	+14	−19	24
5	+51	−22	56	19	+ 9	+56	57
6	+18	−41	45	20	−60	−90	108
7	−26	−21	33	21	+25	+72	76
8	−64	+17	66	22	+15	−83	84
9	−50	−15	52	23	−24	−32	40
10	+63	−34	72	24	+47	+19	51
11	+ 2	+20	20	25	−18	−20	27
12	−33	+70	77	26	+115	+31	119
13	−44	+ 5	44	27	+ 9	−21	23
14	−51	−12	52	28	+ 6	−18	19

Comparison	ΔX	ΔY	r
A	+52	+46	69
B	− 1	+70	70
C	− 5	+47	47
D	+20	+60	63
E	+59	+42	72

* Evaluated from Van Gent's equation $N = \frac{A_1 G_1 \cdot}{\alpha n}$ α is the probability of the discovery of a variable on one pair of plates. n is the total number of pairs which are blinked. If we denote by a_i the number of variables which are found a total of i times during the course of the n blink comparisons, then A_1 and G_1 are defined by the relations:

$$A_1 = a_1 + a_2 + \ldots + a_n$$

$$G_1 = \frac{a_1 + 2a_2 + \ldots n a_n}{a_1 + a_2 + \ldots a_n} \cdot$$

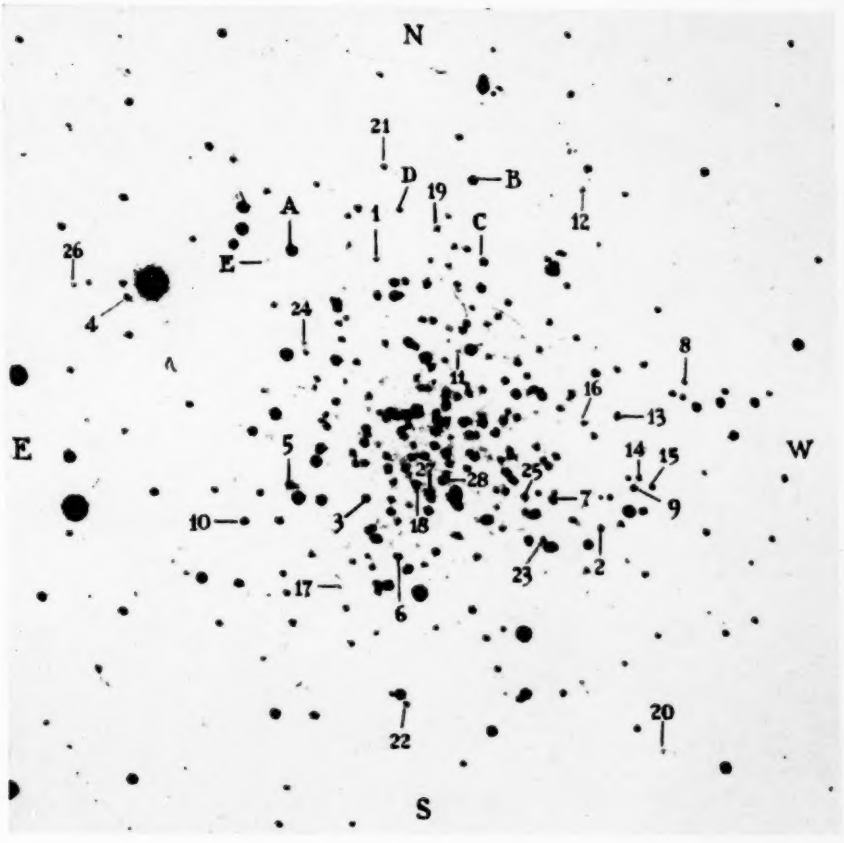

NGC 2257 in blue light with variable and comparison stars indicated. Scale of reproduction: 1″·9/mm.

3. *The visual estimates.*—Estimates of the brightness of the variable stars relative to a sequence were made on all the plates by means of visual inspection with an eyepiece. The five sequence stars A, B, C, D and E are shown in Plate 1 and their positions are given in Table II. The gap between successive sequence stars was taken to be either four or six steps, the interval being kept fixed from plate to plate. A star equal in brightness to the brightest sequence star A is assigned the number 0, and the corresponding values for the other sequence stars are given below.

Sequence Star	A	B	C	D	E
Step	0	6	10	16	20

Estimates have been made at least once on each plate of all the stars regarded as certain or likely variables in the blink surveys. In many cases, owing to the quality of the seeing, all that can be said is that a variable is fainter than a certain sequence star.

No photoelectric calibration of this sequence exists at present.

4. *Individual results.*—Owing to the spacing of good plates, it is very difficult to find the periods of the variables from the estimates. One serious problem is the difficulty of obtaining good conditions for observing on consecutive nights during the summer months at Pretoria. Moreover, plates have to be taken when the cluster is at rather a low altitude if a reasonably long series of observations is to be obtained in a night.

Periods have been derived for six variables with large amplitudes of light-variation and steep rises giving well-defined maxima. The elements for these variables are given below:

TABLE III

Elements of six variables in NGC 2257

Variable	Maximum at JD 2436000+	P^{-1} days^{-1}	P days
1	280·29	1·85047	0·54040
2	254·43	1·97767	0·50565
5	280·34	1·82884	0·54679
6	281·31	1·45843	0·68567
7	254·38	1·77141	0·56452
14	695·26	1·97287	0·50688

The corresponding light-curves for these variables are plotted in Fig. 1. At the time when the estimates described in Section 3 were made, in many cases it was felt that there was some doubt about the estimate due either to the general quality of the images on the plate or to the effects of crowding. Such step-estimates are plotted as open circles in the figure.

It should be borne in mind that these light-curves will differ from the true light-curves due to the effect of the finite exposure time. In particular, the steeply rising portions of the Bailey *a* type light-curves will be in reality somewhat steeper than they appear in Fig. 1.

Various details for the 28 variables are given below:

V1. $P=0{\cdot}54040$ days. A Bailey *a* type light-curve.
V2. $P=0{\cdot}50565$ days. A Bailey *a* type light-curve.
V3. The step-estimates vary from 12 to 18.
V4. A nearby bright star makes estimation very difficult. Amplitude of light-variation appears to be large.

V5. $P=0{\cdot}54679$ days. There is a fairly bright star nearby, and there is also a very close faint star which is only resolved in conditions of excellent seeing. The estimates are therefore very difficult, and refer to the total light of the variable and its faint neighbour. This should be borne in mind especially when the fainter portions of the light-curve are compared with the corresponding parts of those of the other variables.

V6. $P=0{\cdot}68567$ days. This is the longest period of the six which have been derived. The amplitude of the light-variation and the asymmetry of the light-curve are both markedly less than for any of the other five variables.

V7. $P=0{\cdot}56452$ days. Nearby star makes estimation rather difficult. A Bailey *a* type light-curve.

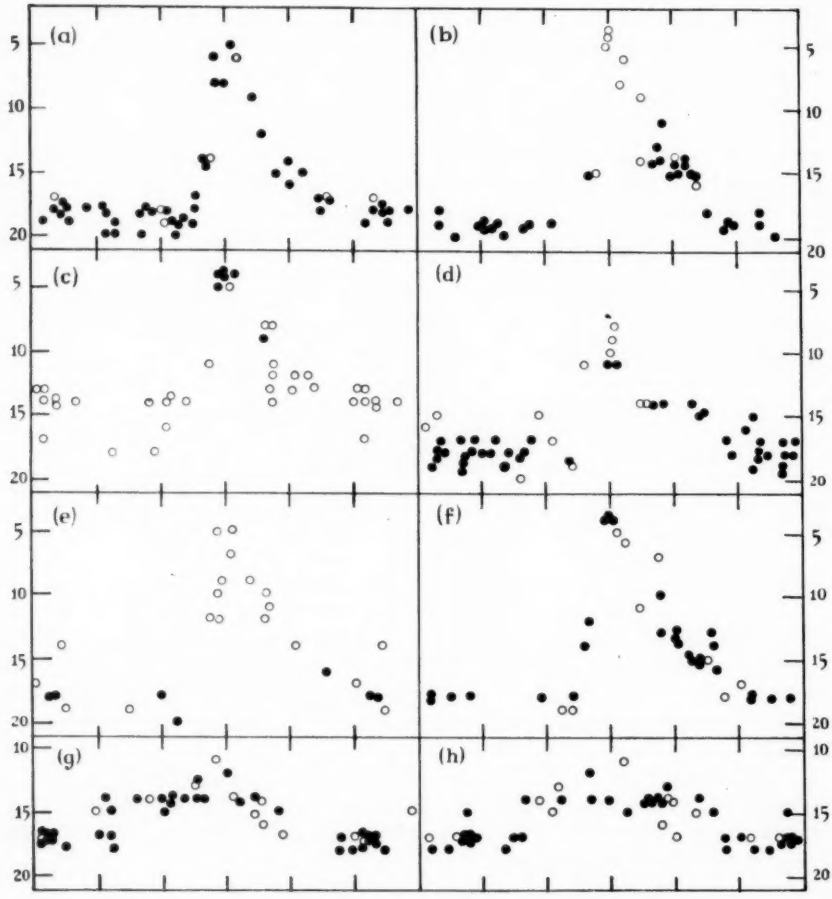

FIG. 1.—*Light-curves of variable stars in NGC 2257. Abscissae: phase with 0·2P overlap right and left. Ordinates: step-estimates relative to sequence.*

(*a*) $V1$; $P^{-1}=1{\cdot}85047$.
(*b*) $V2$; $P^{-1}=1{\cdot}97767$.
(*c*) $V5$; $P^{-1}=1{\cdot}82884$.
(*d*) $V6$; $P^{-1}=1{\cdot}45843$.
(*e*) $V7$; $P^{-1}=1{\cdot}77141$.
(*f*) $V14$; $P^{-1}=1{\cdot}97287$.
(*g*) $V15$; $P^{-1}=4{\cdot}00418$.
(*h*) $V15$; $P^{-1}=3{\cdot}00418$.

V8. Step-estimates from 12 to 18.
V9. Step-estimates from 13 to 18.
V10. Step-estimates from 13 to 18. It would appear to have a gradual rise to maximum.
V11. A close bright star makes estimation difficult. Step-estimates vary from 10 to 19. The rise to maximum appears to be fairly steep.
V12. Step-estimates from 12 to 19.
V13. Step-estimates from 10 to 17.
V14. $P = 0{\cdot}50688$ days. A Bailey *a* type light-curve.
V15. The observations are satisfied tolerably well both by a period of 0·249739 days and by one of 0·332870 days (see Fig. 1). It is by no means certain that the true period is either of the two possibilities above.
V16. Step-estimates from 12 to 18.
V17. Step-estimates from 13 to 18.
V18. Step-estimates from 13 to 19.
V19. Step-estimates from 14 to 18.
V20. Step-estimates from 13 to 18.
V21. Step-estimates from 12 to 17.
V22. Step-estimates from 14 to 18.
V23. Nearby bright star makes estimation extremely difficult.
V24. Estimation difficult. Step-estimates from 14 to 18.
V25. Step-estimates from (9) to 16.
V26. Step-estimates from (6) to 18. The light-curve has a steep rise to maximum.
V27 Two nearby stars make estimation extremely difficult. Amplitude of light-variation appears to be large.
V28. Very close to a fairly bright star. Certainly a variable of large amplitude.

5. *Discussion.*—A recent survey of the red globular clusters in the Large Magellanic Cloud has been made by Hodge (**3**). Although NGC 2257 is just outside the region he considers, he remarks that the clusters probably extend beyond the limits of his search on the eastward side of the Cloud.

As no photoelectric calibration exists at present, it is not yet possible to give the magnitudes of any stars in NGC 2257. A very rough idea of the brightness of the variables can be obtained by comparing the plates of the cluster with those of NGC 1466 and NGC 1978 (both in the Large Magellanic Cloud) also taken with the Radcliffe 74-inch reflector. Since plates of these two clusters were taken in similar conditions to and in some cases on the same nights as NGC 2257, a comparison can be made. It seems that the mean magnitude of the RR Lyrae variables in NGC 2257 is the same as those in the other two clusters to within a third of a magnitude. (The median photographic magnitude of the RR Lyrae variables in NGC 1466 and NGC 1978 is $19^{m}{\cdot}2$ (**4**)).

Hence from the above there is no contradiction with the view that NGC 2257 is an outlying member of the Large Magellanic Cloud.

The position of the 28 variables is such that most of them must be regarded as members of the globular cluster NGC 2257. It is possible that one or two may be field stars in the Large Magellanic Cloud, but none of the variables is far enough away from the cluster centre to be in a position where cluster members are very scarce. NGC 2257 must therefore be regarded as being rich in variables. Of 72 globular clusters in the galaxy which had been searched for variables prior to 1955, in only 13 of them had more than 28 variables been found (**5**).

The six variables for which periods have been derived have light-curves like those of Bailey *a* and *b* type RR Lyrae variables in the galaxy. For the five Bailey *a* type variables with periods between 0·50 and 0·57 days the step-estimates of the maxima and minima differ little from star to star, and the amplitudes of light-variation are all about 14 or 15 steps (an exception being made for V5 where the minimum cannot be determined accurately). The five stars have very steep rises to maximum, but, since the apparent slope of the rising portion of the light-curve is very sensitive to small changes in the assumed period, no quantitative assessments of the asymmetry have been made.

V6, with a period of 0·69 days, has a smaller amplitude of light variation than the other five stars for which periods have been determined. Moreover, the much more gradul rise to maximum is typical of the Bailey *b* type variables found in the galaxy.

It is reasonable to assume that the other 22 variables found are all of the RR Lyrae type. Although periods have not been deduced for these, all show clear indications of a change in brightness during times of an hour or so. The median magnitudes of the smaller amplitude members are all about 15 or 16 on the step-scale used in the estimates.

It is interesting to compare NGC 2257 in the Large Magellanic Cloud with NGC 121 in the Small Magellanic Cloud (**6**). The latter is a globular cluster of somewhat smaller angular extent but with a much greater central concentration. Its known variable star population consists of two long-period variables and three RR Lyrae variables with periods between 0·50 and 0·64 days, there being apparently none of the small amplitude variables which are very abundant in NGC 2257. This difference between two individual clusters is, of course, no indication of any fundamental dissimilarity between the globular cluster systems of the two Magellanic Clouds. The variable star content of globular clusters in the galaxy varies enormously from cluster to cluster, and, in fact, from the available evidence neither NGC 2257 nor NGC 121 would appear to possess any extra-ordinary peculiarities compared with their counterparts in the galaxy.

Acknowledgments.—This investigation was made possible by a grant from the Department of Scientific and Industrial Research to the Radcliffe Trustees under a scheme sponsored by the Astronomer Royal. The writer is greatly indebted to Dr A. D. Thackeray, Dr A. J. Wesselink and Dr M. W. Feast for their valuable advice and assistance during this work.

Radcliffe Observatory,
Pretoria:
1959 *November* 6.

References

(1) H. Shapley and J. Mohr, *H.B.*, **889**, 13, 1932.
(2) H. van Gent, *B.A.N.*, **243**, 21, 1933.
(3) P. W. Hodge, Studies of the Large Magellanic Cloud, I (*Ap. J.*, in press).
(4) A. D. Thackeray and A. J. Wesselink, *Observatory*, **75**, 33, 1955.
(5) H. B. Sawyer, *Pub. D.D.O.*, Vol. **II**, No. 2, 1955.
(6) A. D. Thackeray, *M.N.*, **118**, 117, 1958.

A CATALOGUE OF Hα-EMISSION REGIONS IN THE SOUTHERN MILKY WAY

A. W. Rodgers, C. T. Campbell and J. B. Whiteoak

(Received 1959 December 10)

Summary

In connection with an Hα atlas of the Southern Milky Way being produced at Mount Stromlo, a catalogue has been made of the H II regions distributed about the galactic equator within galactic latitude limits ±15°, and extending from galactic longitude 190° to 12°. The results of this survey have been compared with those of previous surveys overlapping the region investigated.

In 1957, a survey programme of the Southern Milky Way for the detection of H II regions was initiated at Mount Stromlo Observatory by Professor B. J. Bok. This programme was carried out with a Meinel-Pearson 8-inch *f*/1 flat field Schmidt which was mounted as a counterweight to the 6-inch Farnham refractor used as the guiding telescope. The camera was delivered to Mount Stromlo in December 1957, when observations were commenced, the Milky Way programme being completed in April 1959.

Optical quality of photographic images depends in large part upon the quality of the objective filters used in the particular survey. The filters used here were Chance OR1 with Kodak 103a-E emulsion for the Hα plates, and Chance OY1 with Kodak 103a-D emulsion for the yellow comparison plates. The glass disks, each 8·25 inches in diameter, were 8 mm (OR1) and 5 mm (OY1) thick. After final adjustment of the camera it was found that the smallest well-exposed images on the 103a-E emulsion were 17 microns in diameter. This figure was regarded as acceptable in view of the limiting resolution imposed by the emulsion.

The measured colour transmissions of the filters are given in Table I.

TABLE I

Filter	Wavelength A	Hα						
		5600	5800	6000	6200	6400	6563	6600
Chance OR1, 9 mm	Transmission	0	0	0	0	6·5	52	61
Chance OY1, 5 mm	(per cent)	0	48	83	88	86		88

At wavelengths of 6300 A and 6364 A, where prominent night sky lines of [O I] occur, the transmission of the OR1 filter was less than 2 per cent.

The survey was carried out in two parts: in 1958, Hα and comparison plates were obtained on 26 centres of the region along the Lund galactic plane commencing at $l = 190°$ and extending to $l = 12°$ through southern declinations, together with 26 North and 26 South plates centred at $b = \pm 9°$. The plate centres are 7 degrees apart in longitude and the diameter of the coma-free field is 12 degrees. The area of the sky surveyed, then, is 194 degrees long and a maximum of 30 degrees wide.

The majority of the plates were obtained by Rodgers, the remainder by Campbell. The possible H II regions were detected by a blink comparison of the Hα and yellow plates. The plate pairs were exposed to approximately the same limiting stellar magnitude, which is near 14 on the visual scale. The exposure times averaged 20 minutes for the red plates and 7 minutes for the yellow. The blinking technique was preferred to the "negative–positive superposition" method used by Gum (**1**), being simpler and one that takes advantage of the excellent optical quality of the camera which may otherwise be lost in any copying process. The plates were blinked by Whiteoak, Rodgers and Campbell, and the positions, dimensions and estimated brightnesses of the H II regions are given in Tables II and III.

The columns of the Tables are:

1. Current catalogue number.
2. New galactic longitude, l^{II}.
3. New galactic latitude, b^{II}.
4. Old galactic longitude, l^{I}.
5. Old galactic latitude, b^{I}.
6. Right ascension, α_{1950}.
7. Declination, δ_{1950}.
8. Dimensions (minutes of arc).
9. Estimated brightness on a scale of bright (b), medium (m), or faint (f).
10. The number of the object in other catalogues.

The tables are followed by a list of remarks concerning individual nebulae. The coordinates have an estimated accuracy of ± 3 min of arc in right ascension and declination. Comparison is made with surveys of Gum (**1**), Sharpless (**2**), NGC (**3**), Hase and Shajn (**4**), and Bok, Bester and Wade (**5**). NGC or IC numbers in parentheses refer to clusters in emission regions. Catalogues in column 10 are designated thus: HS: Hase and Shajn; E: Sharpless; BBW: Bok, Bester and Wade; and G: Gum. Reduction from equatorial coordinates was effected using the computer SILLIAC of the University of Sydney.

Table II contains regions with dimensions greater than 4 min of arc, which are unambiguously H II regions. Table III contains objects with diameters less than 4 minutes, found to be bright on the Hα plates, some of which are stellar or semi-stellar and may include emission-line B stars, planetary nebulae, Wolf–Rayet stars or variable stars. The known variables listed in the Variable Star Catalogue of P. V. Kukarkin *et al.* (**6**) and detected in the survey have been omitted from Table III. In the higher latitude fields, only objects definitely found to be H II regions are noted in Table II.

It is our experience that in this survey we have reached fainter limiting emission measures in a given region of the sky than did Gum, primarily because of the increase in resolution of our camera. This has resulted in the detection of large areas of faint diffuse emission particularly in the region of Vela-Puppis. Gum (**7**) discovered large areas of Hα emission in Vela and Puppis, and Abt, Morgan and Strömgren (**8**) photographed this object at low altitude with an 8-inch, $f/1$ Schmidt camera. The nebula as defined by the latter work is inside the area of the present survey. We have found that the outlying fragments in Antlia and Pyxis are in fact joined to the brighter main body of the nebulae in Vela and Puppis, that faint emission fills the shell structure of the brighter part of the nebula near $07^h\,50^m$; $-45°$, and that there are extensions to the nebula,

to the outer parts in Antlia and Pyxis, near δ Canis Majoris, and near the galactic equator to longitude 249°. The overall dimensions of the nebula then become 27° × 42°, elongated along the galactic plane and symmetrical about it. Considerable difficulty lies in the adequate description and cataloguing of this nebula due to its size and complex brightness distribution. For this reason Table II lists only the extensions of the Vela-Puppis nebula found here but not described by Gum (**9**) or in the Yerkes survey of Abt, Morgan and Strömgren.

To give pictorial representation of these nebulae, Mount Stromlo Observatory is preparing a complete Hα atlas of the region surveyed, together with key charts giving right ascension, declination and new galactic coordinates based on the recent recommendations of the Commission 33b of the International Astronomical Union.

TABLE II

Table of regions greater than 4′ diam

No.	l^{II}	b^{II}	l^{I}	b^{I}	α_{1950}	δ_{1950}	Dimensions	Brightness	Comparison
					h m	° ′	(min of arc)		
1	223·0	−1·5	190·7	−0·2	07 02	−09 30	150×150	m	NGC 2327; HS 111,
	→226·9	→+0·3	→194·6	→+1·1	→07 14	→−12 24			113, 114; G 2, 3
2	223·8	−1·9	191·5	−0·6	07 02	−10 27	14×14	b	IC 2177; HS 109; G 1
4	224·4	+3·2	192·1	+4·6	07 21·5	−08 30	60×60	f	
5	227·8	−0·2	195·5	+1·1	07 16·1	−13 09	8×8	b	NGC 2359; HS 116; G 4
6	231·6	−4·3	199·2	−3·1	07 08·0	−18 24	12×10	b	G 5
7	232·6	+0·9	200·3	+2·2	07 29·5	−16 51	17×15	m	(NGC 2409)?; G 6
9	234·4	−12·2	201·9	−11·0	06 43	−24 20	90×30	f	
10	234·4	− 0·2	202·1	+ 1·0	07 29·0	−18 54	18×14	f	
11	234·6	−10·0	202·1	− 8·8	06 52	−23 35	60×20	f	
12	234·7	+ 0·9	202·4	+ 2·1	07 33·7	−18 42	6×3	b	G 7
13	234·8	− 0·1	202·5	+ 1·1	07 30·1	−19 18	12×10	m	
14	235·6	− 4·1	203·2	− 2·9	07 17·0	−21 50	6×4	m	(NGC 2367)
15	237·5	− 7·3	205·0	− 6·2	07 08	−25 00	300×300	f	
16	243·3	+ 0·6	211·0	+ 1·6	07 51·2	−26 15	33×33	b	(NGC 2467); G 9
19	253·8	− 0·5	221·5	+ 0·4	08 13·5	−35 42	48×40	b	G 10
20	254·5	0·0	222·2	+ 0·9	08 17·5	−36 00	10×10	m	NGC 2579; G 11
22	258·1	+12·1	226·1	+12·9	09 13·5	−31 10	45×45	m	
27	260·1	+ 0·5	227·8	+ 1·3	08 36·5	−40 12	100×100	m	G 14
32	261·6	+ 0·9	229·3	+ 1·6	08 43·0	−41 09	27×27	m	G 15
33	263·0	+ 1·4	230·7	+ 2·1	08 49·5	−41 54	95×80	m	G 17
35	264·6	+ 0·1	232·3	+ 0·8	08 49·7	−43 55	30×30	m	G 18
36	265·2	+ 1·4	232·9	+ 2·1	08 57·5	−43 33	12×6	m	G 20
37	267·0	+ 0·1	234·7	+ 0·7	08 58·5	−45 45	13×3	f	Part of NGC 2736
38	268·0	− 1·0	235·7	− 0·5	08 57·5	−47 16	40×40	m	G 22, 23 24,
40	269·3	− 1·4	236·9	− 0·8	09 01·0	−48 27	8×8	b	G 25
41	270·3	+ 0·8	238·0	+ 1·3	09 14·8	−47 45	8×4	m	
42	274·1	− 1·3	241·8	− 0·9	09 22·4	−51 54	9×7	b	G 26
45	282·2	− 0·1	249·9	+ 0·1	10 10·0	−56 09	16×16	f	
46	282·4	− 1·3	250·0	− 1·1	10 06·0	−57 15	15×15	f	
47	283·0	− 2·7	250·6	− 2·5	10 03·5	−58 42	25×20	m	
48	283·5	− 1·0	251·1	− 0·8	10 14·0	−57 36	15×10	b	NGC 3199; G 28
49	284·3	− 0·3	252·0	− 0·2	10 22	−57 27	90×35	b	(NGC 3247); G 29
50	284·3	+ 0·4	252·0	+ 0·5	10 24·5	−56 54	12×12	m	
51	286·0	+ 0·5	253·7	+ 0·5	10 36·1	−57 42	12×12	b	
52	287·2	+ 0·4	254·9	+ 0·5	10 43·5	−58 18	15×15	b	BBW 25500; G 32
53	287·4	− 0·9	255·0	− 0·8	10 40	−59 30	210×210	vb	NGC 3293, 3324, 3372; IC 2599; BBW 25500; G 30, 31, 33
54	288·8	+ 0·7	256·5	+ 0·8	10 56	−58 42	210×60	m	(NGC 3503)? (NGC
	→289·4	→− 2·1	→257·0	→− 2·1	→10 50	→−61 30			3572)? G 34, a, b, 35,
	→291·1	→− 0·3	→258·8	→− 0·4	→11 09	→−60 36			36, 37
55	290·4	− 3·0	258·0	− 3·0	10 54·2	−62 45	8×8	m	
57	291·6	− 0·5	259·3	− 0·5	11 12·5	−60 56	170×40	m	NGC 3603; G 38, a, b

TABLE II—*continued*

No.	l^{II}	b^{II}	l	b^{I}	α_{1950}	δ_{1950}	Dimensions	Brightness	Comparison
					h m	° ′	(min of arc)		
58	292·4	− 4·9	260·0	− 5·0	11 04·3	−65 18	7×7	m	
59	293·0	+ 4·5	260·8	+ 4·4	11 35	−56 40	180×150	m	
60	293·7	− 1·4	261·4	− 1·5	11 26·5	−62 30	50×50	b	IC 2872; BBW 26201; G 39, 40
61	294·2	− 2·3	261·8	− 2·4	11 28·3	−63 30	15×15	b	G 41
62	294·8	− 1·5	262·4	− 1·6	11 35	−62 54	80×80	b	IC 2944, 8; BBW 26201; G 42
63	296·7	+ 7·1	264·6	+ 6·9	12 05	−55 00	250×40	f	
	→299·5	→+13·5	→267·6	→+13·2	→12 28	→−49 00			
65	301·0	+ 1·2	268·7	+ 0·9	12 31·5	−61 18	11×6	m	G 43
68	301·7	+ 1·0	269·4	+ 0·7	12 37·3	−61 36	15×15	f	
69	302·2	+ 0·3	269·9	0·0	12 41·5	−62 18	5×3	m	G 45
74	305·2	0·0	272·9	− 0·4	13 07·8	−62 33	15×12	f	
75	306·3	+ 0·2	273·9	− 0·2	13 16·5	−62 15	18×13	m	BBW 27300; G 48a
78	307·9	+ 0·2	275·6	− 0·3	13 30·5	−62 00	45×30	f	BBW 27500; G 48b
79	308·7	+ 0·6	276·4	+ 0·1	13 36·5	−61 30	9×5	m	BBW 27600; G 48c
80	309·3	− 0·5	277·0	− 1·0	13 43·5	−62 24	21×10	m	BBW 27700; G 48d
82	311·0	+ 0·4	278·7	− 0·2	13 55·7	−61 12	5×4	b	
83	311·9	− 0·5	279·6	− 1·1	14 05·0	−61 50	60×50	f	BBW 27901
85	313·5	− 0·4	281·1	− 1·0	14 17·0	−61 10	25×20	f	BBW 28100
91	321·2	− 0·5	288·8	− 1·3	15 12·5	−58 01	11×10	f	BBW 28801
92	322·2	+ 0·6	289·9	− 0·2	15 14·5	−56 30	8×5	f	BBW 28900
94	326·2	+ 0·9	293·9	0·0	15 37·0	−54 00	20×20	f	BBW 29400a
97	327·1	− 0·5	294·8	− 1·4	15 47·7	−54 36	6×5	m	BBW 29401
98	327·6	− 0·8	295·3	− 1·7	15 51·5	−54 30	6×5	b	BBW 29501; G 49
102	331·9	− 1·0	299·6	− 2·0	16 14·0	−51 48	12×8	b	BBW 29902
103	332·4	− 0·4	300·1	− 1·4	16 13·3	−51 00	5×3	b	
104	332·9	− 1·4	300·5	− 2·4	16 20·2	−51 24	20×20	m	
105	332·9	+ 1·8	300·6	+ 0·8	16 06·3	−49 00	45×35	b	BBW 30000; G 51
106	332·9	− 0·6	300·6	− 1·7	16 17·0	−50 48	35×20	m	
107	336·4	− 0·2	304·0	− 1·3	16 29·8	−48 03	8×4	b	NGC 6164, 5; G 52
108	336·5	− 1·3	304·1	− 2·3	16 35·0	−48 40	210×120	f	(NGC 6193); BBW 30402; G 53
110	340·9	− 0·8	308·6	− 1·9	16 50·0	−45 00	7×3	b	G 54
111	341·1	− 1·0	308·8	− 2·2	16 51·5	−45 00	5×3	b	G 54
113	342·7	+ 1·8	310·4	+ 0·6	16 45	−42 00	360×300	m	(NGC 6231); BBW 31100; G 55
114	343·9	− 4·7	311·5	− 5·9	17 18	−45 00	330×330	f	
119	347·7	+ 1·9	315·4	+ 0·7	17 01·3	−38 00	180×145	m	(NGC 6281); BBW 31500; G 57, a, b; E 1
120	348·3	+ 0·5	316·0	− 0·8	17 09·0	−38 24	6×6	b	G 58; E 2
123	349·5	− 0·8	317·2	− 2·1	17 17·8	−38 09	75×75	f	NGC 6337; G 59; E 6?
125	350·0	+ 0·2	317·7	− 1·0	17 15·0	−37 09	8×8	f	
126	350·6	+ 1·0	318·2	− 0·3	17 13·5	−36 18	16×4	m	BBW 31800a
127	351·4	+ 0·7	319·1	− 0·6	17 17·0	−35 48	50×25	b	NGC 6334; BBW 31800b; E 7; HS 119; G 61, 62, 63, 64a, b, c
128	351·4	− 0·1	319·1	− 1·4	17 20·4	−36 15	10×10	f	
129	351·9	+12·7	319·7	+11·4	16 34·0	−28 00	180×180	m	
130	352·4	+ 2·1	320·1	+ 0·8	17 14·2	−34 06	30×20	m	E 4
131	353·2	+ 0·7	320·9	− 0·6	17 22	−34 18	170×55	b	(NGC 6357); BBW 32100; HS 120; E 8; G 66
132	355·4	+ 0·2	323·1	− 1·1	17 30	−32 42	110×80	m	(NGC 6383); BBW 32301; HS 121; E 11; G 67
133	355·9	+ 1·5	323·6	+ 0·2	17 26·0	−31 36	45×40	m	BBW 32300; E 10; G 68
134	358·5	− 1·9	326·2	− 3·3	17 46·1	−31 14	60×50	m	BBW 32603; E 17; G 69
137	359·8	− 0·2	327·4	− 1·6	17 42·6	−29 18	18×18	b	BBW 32801; E 13
138	000·1	+ 0·2	327·7	− 1·2	17 41·7	−28 49	8×4	m	E 12
140	000·2	− 0·4	327·8	− 1·8	17 44·2	−29 02	12×12	f	BBW 32701; E 16
141	000·4	− 0·2	328·0	− 1·6	17 44·0	−28 46	6×4	f	E 15
143	003·5	+ 2·1	331·2	+ 0·7	17 42·5	−24 54	7×6	m	Near NGC 6432

TABLE II—*continued*

No.	l^{II}	b^{II}	l^{I}	b^{I}	α_{1950}	δ_{1950}	Dimensions	Brightness	Comparison
					h m	° ′	(min of arc)		
144	004·4	+ 0·5	332·1	− 1·0	17 50·7	−25 00	85×65	f	BBW 33201; HS 123; E 19; G 71
145	006·6	+ 0·1	334·3	− 1·3	17 57	−23 15	90×35	f	HS 124; E 20; G 74a, b
146	006·6	− 1·5	334·3	− 2·9	18 03	−24 00	120×90	b	NGC 6523(M8), 6559; BBW 33402; HS 126; E 23, 27, 29, 30; G 72, 75
147	007·2	− 0·2	334·9	− 1·7	17 59·5	−22 54	16×16	b	NGC 6514 (M 20); HS 125; E 22; G 76
149	008·7	− 0·6	336·4	− 2·0	18 04·0	−21 45	120×30	m	HS 129; E 24; G 77a
151	011·0	− 1·8	338·6	− 3·3	18 13·5	−20 25	100×35	f	NGC 6526; HS 134; E 32, 33; G 77b
153	012·2	− 1·8	339·9	− 3·3	18 16·0	−19 20	60×20	f	(IC 1283, 4); BBW 33903; HS 140; E 39; G 78
154	012·7	+ 2·0	340·4	+ 0·5	18 03·0	−17 00	40×30	f	
155	012·9	+ 0·3	340·6	− 1·1	18 09·3	−17 41	10×10	m	HS 133; E 31
156	013·7	− 0·8	341·4	− 2·2	18 15·0	−17 30	50×50	f	HS 136; E 34
157	014·3	+ 0·1	342·0	− 1·4	18 13·2	−16 36	60×60	b	(IC 4701); BBW 34101; HS 137; E 35; G 79
158	015·2	+ 3·3	342·9	+ 1·8	18 03·5	−14 12	23×23	m	BBW 34201; HS 128; E 25; G 80
159	015·3	− 1·8	343·0	− 3·3	18 22·0	−16 36	15×15	m	
160	015·4	− 0·8	343·1	− 2·3	18 18·5	−16 00	70×60	b	NGC 6618; (IC 4706, 7); BBW 34202; HS 144, 145; E 43; G 81a, b
161	016·1	− 0·3	343·8	− 1·7	18 18·0	−15 09	80×40	m	HS 143
162	016·7	− 0·5	344·4	− 1·9	18 20·0	−14 40	22×10	b	BBW 34401; HS 146; E 44; G 82
163	016·9	− 2·3	344·6	− 3·8	18 27·1	−15 24	10×9	m	
164	016·9	− 1·2	344·6	− 2·7	18 23·0	−14 51	8×6	b	HS 148; E 46
165	017·0	+ 0·8	344·6	− 0·7	18 16	−13 54	90×66	b	NGC 6611; BBW 34400; HS 142; E 42; G 83
166	018·4	− 0·3	346·1	− 1·8	18 22·6	−13 09	15×15	f	HS 147; E 45
167	019·0	+ 1·3	346·6	− 0·2	18 18	−11 54	180×90	m	(NGC 6604); BBW 34600; E 41; G 84, 85
169	022·0	+ 0·1	349·7	− 1·4	18 28·2	−09 48	7×7	m	HS 150; E 48
170	022·6	+ 0·3	350·3	− 1·2	18 28·5	−09 09	7×5	f	
171	023·2	+ 0·6	350·9	− 0·9	18 28·6	−08 27	5×5	m	HS 151; E 49
172	024·6	− 0·1	352·3	− 1·6	18 33·8	−07 32	7×7	f	HS 155?; E 53
173	025·4	+ 0·2	353·1	− 1·2	18 34·0	−06 41	17×17	m	BBW 35201; HS 154; E 52
174	028·8	+ 3·4	356·5	+ 1·9	18 29·2	−02 13	5×4	f	HS 152
175	029·1	− 0·7	356·8	− 2·1	18 44·2	−03 48	7×5	m	HS 159; E 57
176	030·5	+ 0·4	358·2	− 1·0	18 42·7	−02 04	8×8	m	HS 158; E 56
177	031·9	+ 1·4	359·6	0·0	18 41·8	−00 24	12×12	m	HS 156; E 55
179	036·4	− 1·7	004·1	− 3·1	19 01·2	+02 09	20×15	f	
181	038·8	+ 2·0	006·5	+ 0·6	18 52·3	+06 00	5×5	f	

TABLE III

List of possible regions less than 4′ diam.

No.	l^{II}	b^{II}	l^{I}	b^{I}	α_{1950}	δ_{1950}	Dimensions	Brightness	Comparison
					h m	° ′	(min of arc)		
3	224·2	+1·2	191·9	+2·5	07 14·0	−09 18	4×4	b	HS 115
8	233·9	−0·1	201·6	+1·1	07 28·3	−18 27	3×2	b	
17	243·5	−1·0	211·1	0·0	07 45·4	−27 13	2×2	b	
18	250·3	−2·2	218·0	−1·3	07 57·2	−33 42	1×1	b	
21	257·6	+0·6	225·3	+1·4	08 28·8	−38 10	1×1	b	

TABLE III—*continued*

No.	l_{II}	b_{II}	l_I	b_I	α_{1950}	δ_{1950}	Dimensions	Brightness	Comparison
					h m	° ′	(min of arc)		
23	258·5	+1·4	226·2	+2·2	08 35·0	−38 21	2×1	b	
24	258·7	−1·4	226·3	−0·7	08 23·6	−40 12	3×2	f	
25	259·2	+1·3	227·0	+2·1	08 36·9	−39 02	2×1	b	
26	259·7	+2·9	227·5	+3·6	08 44·6	−38 27	3×3	m	
28	260·1	−3·4	227·8	−2·7	08 19·6	−42 33	2×1	b	
29	260·2	−3·3	227·8	−2·6	08 20·0	−42 32	2×2	b	G 13
30	260·2	−3·1	227·9	−2·4	08 21·1	−42 29	2×2	b	
31	260·7	−3·2	228·4	−2·5	08 22·3	−42 55	3×2	b	
34	264·4	+1·4	232·1	+2·0	08 54·4	−42 56	2×2	b	G 19
39	269·2	−1·1	236·8	−0·6	09 01·9	−48 12	2×2	b	
43	277·2	−3·8	244·8	−3·5	09 25·5	−55 54	2×2	b	NGC 2899; G 27
44	277·8	−3·6	245·4	−3·3	09 29·6	−56·05	2×2	f	
56	291·1	−2·1	258·7	−2·1	11 03·3	−62 12	2×1	m	
64	299·4	−0·3	267·0	−0·6	12 16·7	−62 41	3×2	b	
66	301·1	+0·9	268·8	+0·6	12 32·6	−61 39	2×1	m	G 44
67	301·2	+0·8	268·9	+0·5	12 33·0	−61 45	4×4	m	
70	302·7	−1·0	270·3	−1·3	12 45·6	−63 34	1×1	b	
71	302·9	+1·3	270·6	+1·0	12 47·3	−61 18	4×3	b	G 46
72	303·2	+1·6	270·9	+1·3	12 50·3	−61 00	2×2	f	
73	303·4	+1·4	271·1	+1·0	12 52·0	−61 12	2×2	m	
76	307·2	−3·5	274·8	−3·9	13 29·8	−65 45	3×2	b	NGC 5189; G 47
77	307·6	−5·0	275·1	−5·4	13 35·4	−67 10	1×1	b	
81	310·6	+0·6	278·3	+0·1	13 51·9	−61 06	1×1	m	
84	312·6	−2·7	280·2	−3·3	14 16·4	−63 40	1×1	m	
86	315·0	−2·3	282·7	−3·0	14 35·5	−62 27	3×3	m	
87	320·2	+0·8	287·9	+0·1	15 01·0	−57 19	2×2	b	
88	320·2	+0·5	287·9	−0·3	15 02·7	−57 36	3×2	b	
89	320·4	−1·0	288·1	−1·7	15 09·5	−58 46	4×4	f	
90	321·0	+2·2	288·7	+1·4	15 01·5	−55 46	0·5×0·5	m	
93	322·6	−2·5	290·2	−3·3	15 29·7	−58 54	2×2	m	
95	326·7	+0·8	294·4	−0·1	15 39·7	−53 47	3×2	b	BBW 29400 c
96	326·9	−1·0	294·6	−1·9	15 48·9	−55 06	2×2	f	
99	328·7	−0·5	296·3	−1·4	15 55·8	−53 35	4×2	b	G 50
100	329·1	+2·0	296·8	+1·0	15 47·7	−51 22	1×1	m	
101	331·7	−1·0	299·3	−1·9	16 12·6	−51 54	2×2	b	
109	339·7	−0·3	307·3	−1·4	16 43·0	−45 39	2×2	b	
112	341·7	+5·6	309·5	+4·4	16 27·0	−40 12	2×2	b	
115	344·4	+7·3	312·1	+6·1	16 29·6	−37 06	4×2	m	
117	345·5	−1·0	313·1	−2·2	17 06·2	−41 33	2×2	b	
118	347·3	−0·5	315·0	−1·8	17 10·0	−39 48	2×2	m	
121	348·4	−1·1	316·0	−2·3	17 15·5	−39 15	3×2	m	E 5
122	348·9	−1·1	316·5	−2·4	17 17·1	−38 54	2×2	m	
124	349·6	+1·1	317·3	−0·2	17 10·4	−37 00	3×2	m	NGC 6302; E 3; G 60
135	359·0	−0·7	326·6	−2·0	17 42·4	−30 12	2×2	m	
136	359·0	−3·6	326·7	−5·0	17 54·4	−31 40	1×1	m	
139	000·1	−0·3	327·8	−1·7	17 43·8	−29 02	2×2	m	E 14
142	000·6	−0·7	328·3	−2·1	17 46·5	−28 50	2×2	b	E 18
148	008·2	+0·6	335·9	−0·8	17 58·5	−21 35	2×2	b	
150	009·3	+0·3	337·0	−1·2	18 02·1	−20 48	2×2	b	
152	012·2	+4·3	339·9	+2·9	17 53·3	−16 19	2×2	m	
168	021·3	+2·5	349·0	+1·0	18 18·0	−09 16	1×1	b	
178	036·3	−1·2	004·0	−2·6	18 59·2	+02 19	2×2	m	
180	038·4	+3·5	006·0	+2·1	18 46·3	+06 19	1×1	b	
182	040·0	−1·3	007·7	−2·7	19 06·3	+05 32	3×3	m	E 61

Notes to Tables II and III

1 Horseshoe-shaped bright region 2° in diameter, with 8′×5′ concentration at $07^h\ 03^m.0$, −12° 12′. Fainter region 150′ diameter, centred on $07^h\ 08^m$, −09° 30′.
2 Circular, connected to 1 by faint emission.
5 Circular region
6 Contains diffuse outer region.
7 Circular region.
9 Part of the Vela-Puppis Nebula ?
11 Part of Vela-Puppis ?
13 Circular region.

Notes to Tables II and III—continued

14 Possibly connected with Vela-Puppis. Possible concentration in 15.
15 Loop, possibly connected with Vela-Puppis.
16 Circular region.
19 Large area with one bright edge.
20 Surrounded by diffuse emission; could be associated with 19.
22 Part of Vela-Puppis ?
27 Region showing structure.
30 Two small regions 1′ × 1′.
31 Connected with Vela-Puppis ?
32 Circular region.
33 Almost circular, with more intense area " comma "-shaped.
36 Group of 3 bright regions—" S "-shaped.
37 Filamentary.
38 Emission region containing four concentrations at: $08^h\,57^m{\cdot}5$, −47° 16′ (6′ × 4′); $08^h\,57^m{\cdot}7$, −47° 22′ (3′ × 2′); $08^h\,58^m{\cdot}0$, −47° 08′ (9′ × 7′); and $08^h\,58^m{\cdot}4$, −47° 20′ (12′ × 9′).
40 Bright region possibly associated with diffuse surrounding background emission.
42 Circular.
43 Stellar-like.
48 Bright crescent shape.
49 Emission region outlying η Carina nebula.
50 Possibly associated with 49.
51 Bright knot possibly separated from main η Carina nebula by obscuration.
52 Bright knot in η Carina nebula separated from main region by absorption.
53 Main irregular η Carina nebula. Boundaries at $10^h\,28^m$, −58°; $10^h\,55^m$, −58° 18′; $10^h\,27^m$, −60° 48′.
54 Outlying η Carina, with concentrations at: $10^h\,57^m{\cdot}5$, −61° 00 (40′ × 20′); $10^h\,58^m{\cdot}0$, −59° 20′ (70′ × 40′) (filamentary); $11^h\,08^m{\cdot}0$, −59° 54′ (25′ × 25′); $11^h\,10^m{\cdot}5$, −58° 30′ (25′ × 10′).
55 Circular region, appears to have central star; not part of η Carina.
57 Appears obscuration-bounded and contains bright crescent-shaped region 50′ × 20′.
59 3° diameter loop.
60 Outlying part of λ Cen nebula. Contains bright regions centred at: $11^h\,26^m{\cdot}5$, −62° 21′ (21′ × 18′); $11^h\,26^m{\cdot}5$, −62° 42′ (15′ × 10′).
61 Circular region near λ Cen nebula.
62 Main λ Cen nebula, uneven intensity.
63 Large band of emission.
65 Region has diffuse edges.
74 Crescent-shaped.
75 Diffuse edges.
76 Planetary ?
78 Brighter central region (10′ × 6′).
82 Circular.
85 Possibly obscuration bound.
86 Crescent-shaped.
91 Possibly obscuration bound.
93 Like a planetary in appearance.
94 Circular and filamentary.
96 Appears to be surrounding a star.
98 Appears to be distributed about a faint central star.
100 Stellar-like.
101 Stellar-like.
106 Contains two bright areas: $16^h\,15^m{\cdot}5$, −50° 51′ (20′ × 7′); $16^h\,17^m{\cdot}0$, −50° 42′ (12′ × 12′).
107 Bright region near 108.
108 Irregular intensity variation with bright region at $16^h\,36^m$, −48° 30′ (60′ × 60′).
109 Stellar-like.
110 Could be connected to 113 by faint emission.
111 Near 110, possibly connected.
113 Large loop of ionization in region of fainter emission. Boundaries: ($16^h\,37^m$, −41°50′) to ($16^h\,58^m$, −41° 30′); and ($16^h\,50^m$, −43° 30′) to ($16^h\,45^m$, −39° 40′).
114 Ring of emission 50′ wide.
116 Concentration inside 113.
119 Filamentary, with bright concentration at $16^h\,57^m{\cdot}4$, −38° 13′ (15′ × 15′).
120 Contains dark central rift.
123 Loop.
127 Faint extensions to $17^h\,10^m$, −35° 30′. Composed mainly of four bright concentrations.
129 Region contains the star τ Sco.
130 Appears to be a more centrated region of a large area of diffuse emission.
131 Concentrations at: $17^h\,21^m{\cdot}0$, −33° 58′ (30′ × 30′); $17^h\,21^m{\cdot}8$, −34° 10′ (9′ × 9′); $17^h\,23^m{\cdot}1$, −34° 27′ (6′ × 6′); $17^h\,23^m{\cdot}9$, −34° 03′ (5′ × 5′).
132 Crescent-shaped bright region with faint extensions to $17^h\,35^m$, −34°.
133 Almost circular.

Notes to Tables II and III—continued

134 Circular.
136 Stellar in appearance.
137 Near galactic centre.
138 Diffuse edges.
140 Perhaps connected to 141.
144 Circular.
146 Main bright area divided in three, probably by obscuration, with centres: $18^h\ 01^m.8$, $-24°\ 12'$ ($100' \times 45'$); $18^h\ 03^m.0$, $-23°\ 30'$ ($45' \times 45'$); $18^h\ 06^m.5$, $-23°\ 50'$ ($60' \times 50'$).
147 Almost circular.
150 Stellar in appearance.
151 Band of emission, one side bounded by heavy obscuration.
152 Stellar in appearance.
153 Faint region with bright area [$18^h\ 14^m.7$, $-19°\ 40'$ ($19' \times 19'$)] at one end.
155 Two concentrations: $18^h\ 08^m.9$, $-17°\ 36'$ ($7' \times 7'$); $18^h\ 09^m.3$, $-17°\ 40'$ ($8' \times 5'$).
156 Possibly local concentration of general diffuse emission present. Brighter region at $18^h\ 14^m.0$, $-17°\ 18'$ ($40' \times 20'$).
157 Faint extensions to $18^h\ 01^m$, $-14°\ 00$ (E 25); and $18^h\ 14^m$, $-17°\ 00$.
159 Surrounded by diffuse emission.
160 Surrounded by diffuse emission 40′ wide.
162 Oval-shaped, possible concentration of general diffuse emission present.
165 Appears connected with adjacent regions by diffuse emission.
166 Surrounded by diffuse emission.
169 Circular region.
175 Crescent-shaped.
180 Stellar-like.

The majority of the nebulae listed in Tables II and III show complex structure over large areas. In part this complexity is due to overlying absorption. Thus in many cases the identification of individual exciting stars from existing spectral data is impossible; an example of this is the extremely faint nebulosity against which the Southern Coalsack is silhouetted. The dimensions of this nebulosity approximately 7 degrees in diameter, are similar to those of the whole concentration of B stars forming the I Crucis association, and it is probable that all the earlier stars of the association contribute to the excitation of the nebula.

Acknowledgments.—We wish to thank Professor B. J. Bok and Dr H. M. Johnson for their interest and stimulating advice during the course of this survey.

Mount Stromlo Observatory,
Australian National University,
Canberra, A.C.T.:

1959 *November* 30.

References

(1) C. S. Gum, *Mem. R.A.S.*, **67**, 155, 1955.
(2) S. Sharpless, *Ap. J.*, **118**, 362, 1953.
(3) J. L. E. Dreyer, New General Catalogue 1953.
(4) V. F. Hase and G. A. Shajn; *Bull. Crimea. Ast. Obs.*, **15**, 11, 1955.
(5) B. J. Bok, M. J. Bester and C. M. Wade, *Daedalus*, **86**, 9, 1955, Harvard Reprint No. 416.
(6) B. V. Kukarkin, P. P. Parengo, Yu. I. Efremov and P. N. Kholopov, *General Catalogue of Variable Stars*, 2nd edition, 1958.
(7) C. S. Gum, *Observatory*, **72**, 151, 1952.
(8) H. A. Abt, W. W. Morgan and B. Strömgren, *Ap. J.*, **126**, 322, 1957.
(9) C. S. Gum, *Observatory*, **76**, 150, 1956.

THE SPECTRUM OF THE CYGNUS (19N4A) AND CASSIOPEIA (23N5A) RADIO SOURCES BELOW 30 MC/S

A. C. B. Lovell and H. W. Wells

(Received 1960 January 30)

Summary

The 250 ft steerable radio telescope and the 220 ft transit radio telescope at Jodrell Bank have been used as an interferometer to measure the ratio of the intensities of the Cygnus and Cassiopeia radio sources from 16·0 to 26·0 Mc/s. The ratio remains constant at 0·53. The results are compared with previous measurements. The amount of absorption to be expected in H II regions is calculated and it is shown that the difference in H II content along the lines of sight to Cassiopeia and Cygnus cannot be greater than that contained in a cloud of extent 4 parsecs and electron density less than 3 electrons per c.c.; which is well below the value normally assumed for an average H II cloud.

---

1. *Introduction.*—A recent survey by Whitfield (**1**) has focused attention on the existing discrepancies and difficulties in the determination of the spectra of the radio sources. At low frequencies in the 10 to 30 Mc/s region experimental difficulties are increased because of the interference from long distance ionospheric scatter signals, and the possible existence of differential ionospheric absorption introduces another uncertainty into the evaluation of the measurements. These uncertainties are manifest in the discrepancies which exist in the published spectral information below 30 Mc/s for the Cygnus (19N4A) and Cassiopeia (23N5A) radio sources as given by Hey and Hughes (**2**), Lamden and Lovell (**3**) and Wells (**4**). Some of these results indicate that absorption in H II regions might be responsible for the introduction of a sharp and differential fall in intensity of the two sources below 22 Mc/s. The work described in the present paper does not aspire to present new determinations of the absolute intensities of the sources in this frequency region. The aim was specifically limited to a measurement of the ratio of the intensities of the two sources over the frequency range below 26 Mc/s.

2. *Apparatus.*—The aerial systems consisted of the 220 ft transit telescope and the 250 ft steerable radio telescope at Jodrell Bank. In each case the primary feeds were broad-band cage type dipoles and reflectors. These were combined in a phase switched interferometer, and since the E–W separation of the instruments is about 305 metres the lobe interval varied between about 2 and 4 degrees over the frequency range used. The receiver consisted of two commercial Eddystone Type 680X receivers with a common local oscillator. The separate intermediate frequency outputs were fed into an interferometer unit which performed the phase switching, detection, amplification and other necessary functions. By switching at the I.F. and using broad-band preamplifiers coupled to the aerials through broad-band transformers, it was possible to change the recording frequency by simply adjusting the two receivers and balancing to compensate for gain changes. Normally the receivers were used at maximum selectivity with crystal filters giving a band width of about 1 Kc/s.

3. *Results.*—The apparatus was used in various forms from February to July 1959. The successive transits of the Cygnus and Cassiopeia sources through the aerial beams required at least four hours and the long distance scatter interference made such measurements impossible until around midsummer when the sources were in transit during the early morning hours. Even so, very few records were sufficiently free from interference or other effects to facilitate the determination of the ratio. The successful measurements are summarized in Table I. The lowest frequency at which a complete interferometer record of both sources was obtained was 16 Mc/s on 1959 July 18–19. This record is reproduced in Fig. 1.

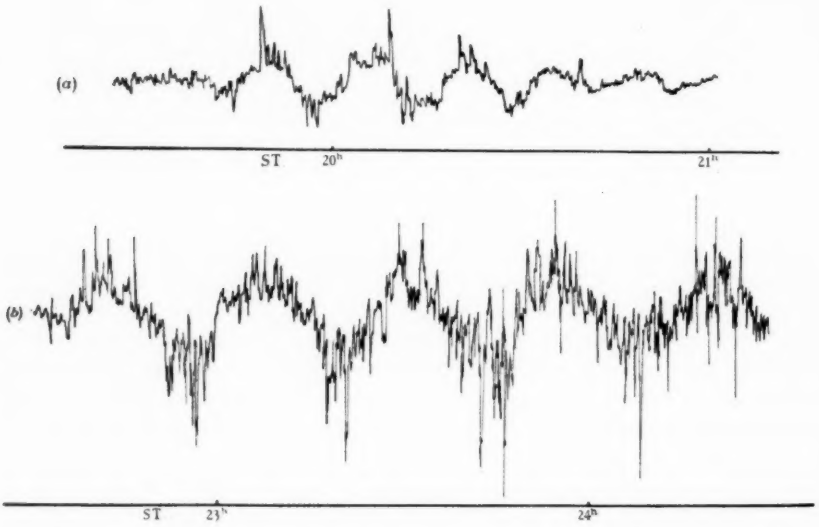

FIG. 1. *The interferometer record (a) of Cygnus and (b) of Cassiopeia obtained on 1959 July 18–19 on a frequency of 16·0 Mc/s. The abscissae are in sidereal time and the ordinates are intensity of signal in arbitrary units. Scintillations are prominent on the Cassiopeia record.*

TABLE I

The ratio of intensities of the Cygnus and Cassiopeia radio sources from 16 to 26 Mc/s

Date		Frequency Mc/s	Ratio Cygnus/Cassiopeia
1959 May	17	26·00	0·56
	20	26·15	0·58
	22	26·15	0·54
	24	26·15	0·52
	25	26·15	0·52
	31	26·15	0·51
June	4	22·20	0·52
	18	22·60	0·51
July	4	22·20	0·54
	5	22·20	0·53
June	21	16·80	0·52
July	18–19	16·00	0·55

Apart from the interference problems, periods of selective absorption invalidated several of the records. For example, during some 16·7 Mc/s measurements on 1959 June 28 the fringes associated with Cygnus failed to appear although the Cassiopeia source gave a normal record three hours later. On June 29 the Cygnus source was obscured for the first half of the transit but then appeared normal, whereas the Cassiopeia source was again unaffected.

4. *Discussion.*—The new results for the ratio of Cygnus to Cassiopeia given in Table I are plotted in Fig. 2, together with the already published data on this ratio for frequencies below 40 Mc/s. In addition the ratio assessed by Whitfield (**1**) for the range 30 to 350 Mc/s is shown. Although there is no evidence for the marked

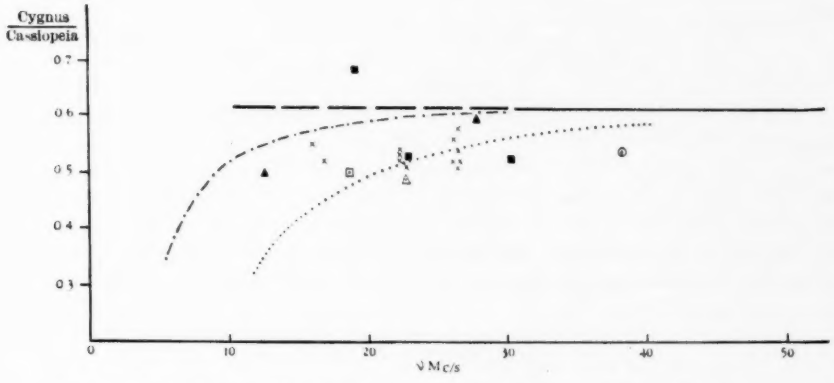

FIG. 2. *The ratio of intensities of the Cygnus and Cassiopeia sources as a function of frequency.*

——— *Mean ratio assessed by Whitfield* (**1**) *for the range 30 to 350 Mc/s.*

△ *Hey and Hughes* (**2**) ○ *Adgie and Smith* (**6**)

■ *Lamden and Lovell* (**3**) ⊡ *Wells* (**4**)

▲ *Wells* (**12**) × *Lovell and Wells* (*this paper*).

..... *Theoretical curve for* $\int N^2\,ds = 5 \times 10^{20}\ cm^{-5}$

– · – · – *Theoretical curve for* $\int N^2\,ds = 10^{20}\ cm^{-5}$.

differential absorption below 20 Mc/s which appeared to be indicated by the earlier results (**3**), the bias of the collected results is well below the ratio of 0·62 given by Whitfield in the 30 to 350 Mc/s range. According to Whitfield, whereas the spectral index of Cassiopeia remains constant at −0·80, that of Cygnus changes from −0·66 in this range to −1·02 above 350 Mc/s, and a further change in this low frequency region below 30 Mc/s cannot be excluded by the present results.

Since Cassiopeia lies at 2 degrees from the galactic plane and Cygnus at 5 degrees, this result must be compared with the existing evidence for the presence of substantial H II absorption (Shain (**5**), Adgie and Smith (**6**)). The result is not necessarily inconsistent, particularly since Shain (**7**) has shown that even near the galactic centre, there can be very little H II absorption at 4 degrees from the plane. An upper limit for the differential absorption by H II regions in the line of sight of Cygnus and Cassiopeia can be calculated from these results. Based on earlier work of Smerd and Westfold (**8**) and of Ryle and Scheuer (**9**), Lamden

and Lovell (**3**) calculated the ratio of intensities before and after absorption in an H II region at frequency ν as

$$I = I_0 \exp\left\{ -0{\cdot}177 \times 10^{-6} \nu^{-2} \int_0^\infty N_e^2 \, ds \right\}$$

where N_e is the number of electrons per cm^3 in the region. Thus

$$\frac{I_{\text{Cyg}}}{I_{\text{Cass}}} = \frac{\kappa_1 \nu^{-x_1} \exp\left\{ \nu^{-2} \int_0^\infty N_e^2 \, ds \right\}_{\text{Cyg}}}{\kappa_2 \nu^{-x_2} \exp\left\{ \nu^{-2} \int_0^\infty N_e^2 \, ds \right\}_{\text{Cass}}}$$

or if we assume that the spectral indices x_1, x_2 over this frequency range are the same

$$\frac{I_{\text{Cyg}}}{I_{\text{Cass}}} = \kappa \exp \nu^{-2} \left\{ \int_{\text{Cyg}} N_e^2 \, ds - \int_{\text{Cass}} N_e^2 \, ds \right\}.$$

The effect of such differential absorption on the ratios is plotted in Fig. 2 for values of $\int N_e^2 \, ds = 5 \times 10^{20}$ cm^{-5} and 10^{20} cm^{-5} respectively together with the experimental points. This indicates that the difference in H II content along the two lines of sight is such that $\int N_e^2 \, ds$ is about 10^{20} cm^{-5}. For an H II region with an extent of 4 parsecs in the line of sight this implies that the electron density must be less than 3 cm^{-3}. This is well below the figure for an average H II cloud of 20 cm^{-3} and dimensions 5 parsecs given by Oort (**10**) which would imply a value of

$$\int N_e^2 \, ds = 6 \times 10^{21} \text{ cm}^{-5}.$$

This result is consistent with some unpublished measurements of Davies (**11**) in which the 250 ft radio telescope was used to measure the continuous emission on frequencies of 400 Mc/s and 1390 Mc/s in the neighbourhood of Cygnus and Cassiopeia. The comparison of the brightness temperatures on the two frequencies implied that any H II region in the line of sight of Cassiopeia gave a value of $\int N_e^2 \, ds < 10 \times 10^{20}$ cm^{-5} and of $< 6 \times 10^{20}$ cm^{-5} for Cygnus.

University of Manchester,
Jodrell Bank Experimental Station:
1960 *January* 29.

References

(**1**) Whitfield, G. R., *M.N.*, **117**, 680, 1957.
(**2**) Hey, J. S., and Hughes, V. A., *Nature*, **173**, 819, 1954.
(**3**) Lamden, R. J., and Lovell, A. C. B., *Phil. Mag. Ser.* 8, **1**, 725, 1956.
(**4**) Wells, H. W., *Proc. I.R.E.*, **46**, 205, 1958.
(**5**) Shain, C. A., *Austr. J. Phys.*, **10**, 195, 1957.
(**6**) Adgie, R., and Smith, F. G., *Observatory*, **76**, 181, 1956.
(**7**) Shain, C. A., *I.A.U. Symposium on Radio Astronomy*, Stanford 1959, p. 451.
(**8**) Smerd, S. F., and Westfold, K. C., *Phil. Mag.*, **40**, 831, 1949.
(**9**) Scheuer, P. A. G., and Ryle, M., *M.N.*, **113**, 3, 1953.
(**10**) Oort, J. H., *A.J.*, **116**, 233, 1952.
(**11**) Davies, R. D., Jodrell Bank (unpublished).
(**12**) Wells, H. W., *J. Geophys. Res.*, **61**, 541, 1956.

INFORMATIONAL CONSIDERATIONS IN THE DESIGN OF ASTRONOMICAL SPECTROGRAPHS

E. H. Linfoot

(Received 1960 February 15)

Summary

The problem of designing spectrographs so as to maximize their information rate on random low-contrast spectral distributions is considered. In Section 2 it is shown how spectrographs can be discussed within the general framework of Fourier optics. In Section 3 the effects of optical aberrations, of photographic spread and granularity, and of variation of slit width are briefly considered and the implications of the band-limitedness of optical images in the problem of allowing for instrumental bandwidth are pointed out. An approximate expression for the information rate is obtained in the special case of an aberration-free spectrograph.

---

1. *Introduction.*—The basic problem which confronts the astronomical spectroscopist is to make the most efficient use of his time. This includes both observing time, during which spectra are recorded photographically, and time spent on extracting information from the photographic plates.

The advent of very large and expensive telescopes and the increasing use of rockets for astronomical spectroscopy have made it of great importance to use the *observing time* as efficiently as possible, even if this should involve the introduction of more elaborate reduction techniques. For example, a 10 per cent increase in the efficiency with which information is recorded on the photographic emulsion carried by a large rocket spectrograph would justify the purchase of many hours of machine time on a microsecond computer to extract this information and recode it into assimilable form.

In the provisional and incomplete discussion which follows, it will be indicated how the problem of making the best use of observing time can be approached in a more systematic way than has been customary among astronomers in the past. We restrict the discussion to the case in which the cost of observing time is so large compared with the cost of reduction that the latter can be neglected. This limiting case is a specially favourable one for analytical discussion because it can be treated in a fairly simple way by an application of Shannon's information theory. Before making the application, we first consider how spectrographs fit into the general framework of Fourier optics. This will be examined in the next section.

2. *Notation and preliminaries*

Let S be the plane of an incoherently lit optical object, (x, y) Cartesian coordinates in S. An optical system images a small region F (the working field) near the origin in S on to a plane S'. (x', y') are rectangular coordinates in S', but we keep the *scale* of these coordinates at our disposal. In the later discussion (Section 3) S will be the plane of the spectrograph slit, S' that of the photographic receiving surface.

2.01 *Point-response functions.*—A point source situated at (x, y) in S, emitting quasi-monochromatic light of wavelength λ, is imaged on to S' by the optical system. We can describe the energy distribution in the image by a *point-image function* $w(x', y';\ x, y;\ \lambda)$, normalized so that for all x, y, λ

$$\int\int_{-\infty}^{\infty} w\,dx'\,dy' = 1. \tag{2.1}$$

We regard x', y' as the argument-variables of the function w and x, y, λ as parameters. The Fourier transform

$$\tilde{\tau}(u, v;\ x, y;\ \lambda) = F[w] = \int\int_{\infty}^{-\infty} e^{-2\pi i(ux' + vy')} w\,dx'\,dy' \tag{2.2}$$

will be called the *local frequency response* of the optical system. It is, of course, closely related to the well known *ct*-function $\tau(u, v;\lambda)$ of an isoplanatic system, but here the system is not restricted to be isoplanatic. The formal relationship between $\tilde{\tau}$ and τ will become clear later (Sections 2.2, 2.3). We regard the spatial frequencies u, v relative to the (x', y')-coordinate system as the argument-variables of the function $\tilde{\tau}$, and we regard x, y, λ as parameters.

By (2.1) and (2.2)

$$\tilde{\tau}(0,\ 0;\ x,\ y;\ \lambda) = 1 \tag{2.3}$$

for all x, y, λ.

Each of the functions w, $\tilde{\tau}$ suffices to describe the imaging by the system of incoherently illuminated objects lying in the working field F. By Fourier's inversion theorem, applied to (2.2),

$$w = \int\int_{-\infty}^{\infty} e^{2\pi i(ux' + vy')}\,\tilde{\tau}\,du\,dv. \tag{2.4}$$

Thus any property of the optical imaging which can be expressed in terms of w can be expressed with equal completeness in terms of $\tilde{\tau}$.

Evidently $\tilde{\tau}$, like w, depends on the choice of coordinates in S and S' as well as on the imaging process. In particular, we easily see from (2.2) that a shift of (x', y')-origin to the point $x' = \xi, y' = \eta$ multiplies $\tilde{\tau}$ by $e^{2\pi i(u\xi + v\eta)}$.

2.1 *Gauss optics of a centred system in terms of* $\tilde{\tau}$.—In this case we take the (x, y)-origin and the (x', y')-origin on the optic axis of the system and the coordinate axes Ox', Oy' parallel to Ox, Oy respectively. On the Gauss approximation, the image of a luminous object point situated at (x, y) in S is a sharply defined point at (x', y') in S', where

$$x' = Mx,\ y' = My. \tag{2.5}$$

If the scale of the rectangular coordinates x', y' is the same as that of the coordinates (x, y), $M = M(\lambda)$ is the *magnification at wave-length* λ. In any case, we have

$$w(x', y';\ x, y;\ \lambda) = \delta(x' - Mx, y' - My), \tag{2.6}$$

where δ denotes the Dirac δ-function, and

$$\tilde{\tau}(u,\ v;\ x,\ y;\ \lambda) = e^{-2\pi i(ux + vy)M(\lambda)}. \tag{2.7}$$

In discussing monochromats, it is often worth while to choose the scale of the (x', y')-coordinates so that $M = 1$. Then, in the Gauss approximation, the image of a bright object point at (x, y) in S is situated at the point $x' = x$, $y' = y$ in S'.

This gives

$$w(x', y'; x, y; \lambda) = \delta(x' - x, y' - y) \tag{2.8}$$

$$\tilde{\tau}(u, v; x, y; \lambda) = e^{-2\pi i(ux+vy)}. \tag{2.9}$$

We can describe these (x', y')-coordinates as *paraxially matched* to the (x, y)-coordinates.

2.2 *Diffraction optics of a centred isoplanat; relation between $\tilde{\tau}$ and τ.*—In a centred isoplanat the image of a bright point (x, y) is a light-distribution centred on the point (2.5) and radially symmetrical about that point. In other words, the point-image function $w(x', y'; x, y; \lambda)$ has the special form $w(x''^2 + y''^2; \lambda)$, where

$$x'' = x' - Mx,\ y'' = y' - My \tag{2.10}$$

are so-called *local coordinates* relative to the point (Mx, My) in S'. The factor $M = M(\lambda)$ represents the magnification at wave-length λ when (x', y') are ordinary Cartesian coordinates. In a system of this kind the *ct*-function at wavelength λ, represented by the function $\tau(u, v; \lambda)$, satisfies the equation

$$\tau(u, v; \lambda) = \int\int_{-\infty}^{\infty} e^{-2\pi i(ux''+vy'')} w(x''^2 + y''^2; \lambda)\, dx''\, dy''$$

$$= e^{2\pi i(ux+vy)M(\lambda)} \int\int_{-\infty}^{\infty} e^{-2\pi i(ux'+vy')} w(x', y'; x, y; \lambda)\, dx'\, dy',$$

by (2.10),

$$= e^{2\pi i(ux+vy)M(\lambda)}\, \tilde{\tau}(u, v; x, y; \lambda). \tag{2.11}$$

From the remark at the end of Section 2.01 we see that $\tau(u, v; \lambda)$ is the value which $\tilde{\tau}(u, v; x, y; \lambda)$ would assume if the (x', y')-origin were shifted to the point which is the 'ideal image' of (x, y), namely the point $x' = Mx$, $y' = My$. From (2.7) and (2.11) we see that in the approximation represented by Gauss optics

$$\tau(u, v; \lambda) = 1$$

for all u, v, λ.

2.3 *Extension to more general systems.*—The last result can be immediately extended to the more general case of a system, not necessarily centred, working in an isoplanatism patch A throughout which the optical distortion can be regarded as negligibly small.

The familiar concept of optical distortion presupposes that some procedure has been laid down for specifying which point (x', y') in S' corresponds optically to a given point (x, y) in S. In Section 2.2 the symmetry of the spread function w provided a basis for such a procedure; we took the centre of the diffraction image of (x, y) to be the point of S' corresponding 'ideally' to (x, y) or, to put it simply, matched against (x, y). This procedure is easily seen to be equivalent, in the case of symmetrical point-images, with the classical one based on ray tracing.

In the general case it seems better to depart from the classical procedure and to take the mean centre (ξ, η) of the ray-theoretic image as the point of S' matched against (x, y). Then (2.11) is replaced by the equation

$$\tau_A(u, v; \lambda) = e^{2\pi i(u\xi+v\eta)}\, \tilde{\tau}(u, v; x, y; \lambda)$$

$$= e^{2\pi i(u\xi+v\eta)}\, F[w], \tag{2.12}$$

where $F[w]$ is the Fourier transform (2.2), and where the quantities $\xi = \xi(x, y; \lambda)$, $\eta = \eta(x, y; \lambda)$ depend on x, y and λ.

A theoretical advantage of the present choice of matching is that with this matching the limiting rate of change, near the (u, v)-origin, of the ct-function $\tau_A(u, v; \lambda)$ depends only on the aperture of the system and on the wavelength λ. An inconvenience (which it shares with the classical matching procedure by principal rays) is that in general the matching is slightly different in different wave lengths λ.

Let $\tau_0(u, v; \lambda)$ denote the ct-function of a system with the same aperture as the given system, but free from aberrations or defocusing. Then it can be shown that

$$\left.\begin{aligned}\left[\frac{\partial\tilde{\tau}}{\partial u}\right]_{+0} &= -2\pi i\xi + \left[\frac{\partial\tau_0}{\partial u}\right]_{+0}\\ \left[\frac{\partial\tilde{\tau}}{\partial v}\right]_{+0} &= -2\pi i\eta + \left[\frac{\partial\tau_0}{\partial v}\right]_{+0}.\end{aligned}\right\} \tag{2.13}$$

Here $[\partial\tilde{\tau}/\partial u]_{+0}$ stands for

$$\lim_{u\to 0}\frac{\partial}{\partial u}\,\tilde{\tau}(u, 0; x, y; \lambda),$$

and similarly for the others. If the stop is circular,

$$\left[\frac{\partial\tau_0}{\partial u}\right]_{+0} = \left[\frac{\partial\tau_0}{\partial v}\right]_{+0} = -\frac{2\lambda}{\pi\sin\alpha}, \tag{2.14}$$

where $\sin\alpha$ is the numerical aperture of the system*.

A distortion-free system in the usual sense is one in which, at the so-called principal wavelength $\lambda = \lambda_0$, $\tilde{\tau}$ satisfies the condition

$$\frac{1}{2\pi i}\left[\left(\frac{\partial}{\partial u} + i\frac{\partial}{\partial v}\right)(\tilde{\tau} - \tau_0)\right]_{+0} = -Me^{i\psi}(x + iy) - p - iq, \tag{2.15}$$

where the real numbers p, q, the positive factor M, and the real azimuth ψ remain constant as (x, y) varies in F. For, by (2.13) this property of $\tilde{\tau}$ ensures that

$$\left.\begin{aligned}\xi &= M.(x\cos\psi - y\sin\psi) + p\\ \eta &= M.(x\sin\psi + y\cos\psi) + q\end{aligned}\right\} \tag{2.16}$$

and a change of axes in S' converts (2.16) into the form

$$\xi = Mx,\ \eta = My. \tag{2.17}$$

In general, colour aberrations of the system may be present, and may show themselves in a small, slow variation of M, ψ, p, q with λ. In practical cases it is often a permissible approximation to assume that (2.15) remains valid for suitably chosen M, ψ, p, q; that is, that the system is distortion-free in each λ separately. When this is the case, it follows from the definition of isoplanatism that in any isoplanatism patch A the values of M and ψ can be regarded as independent of λ to a sufficient approximation. This facilitates the use of a single (x', y')-coordinate system for the different values of λ.

The usual arguments can now be applied to prove the basic theorem that, in quasi-monochromatic light of wavelength λ, the intensity distribution in the image of an incoherently lit, extended object occupying an isoplanatism patch A can be represented, with acceptably small error, as the convolution of the 'ideal' image of this object with the spread function $w_A(x'', y''; \lambda)$. The proof can be

* The last result is due to H. H. Hopkins (1956).

extended to systems with the usual small amounts of distortion, but we shall not go into further detail here.

2.4 *Spectrographs.*—In a spectrograph we choose the (x', y')-coordinates so that the x'-axis is parallel to the dispersion. Then $\tilde{\tau}$ still satisfies a condition of the form (2.15), but now the variation of p with λ is no longer small and slow; it is smooth and monotonic, and its λ-derivative is a measure of the dispersion. Conversely, an optical system of which the local frequency response $\tilde{\tau}$ both falls off relatively slowly in size as $\sqrt{u^2+v^2}$ increases from zero and satisfies a condition (2.15) with the properties just described can be used as a spectrograph; it is sufficient to take as object a suitably oriented, incoherently illuminated slit.

In astronomical spectrographs the illumination of the slit is partially coherent, but in some cases we can make the simplifying assumption that the slit may, without serious error, be replaced by an incoherent object of the same size and shape. This is generally true in prime focus spectroscopy and in wide-slit spectroscopy using high dispersion and fast Schmidt cameras. In the case of prime focus spectroscopy with an $F/4$ paraboloid, for example, the radius of the first Airy dark ring is about 5λ, or about 10^{-4} inch. Thus the effects of coherence on the intensity distribution in the image of a slit 0·001 inch wide may be expected to be small. The same could not safely be said of coudé spectrographs working, with narrow slits, at focal ratios in the neighbourhood of $F/30$ and we therefore exclude them from the present discussion.

3. *Information in photographic spectra.*—In an astronomical spectrograph, we try to use a slit wide enough to receive nearly all the "wanted" light, a high-resolution grating to reduce the overlap of slit images in different wavelengths, a fast camera, and an emulsion of suitable speed.

Even if optical aberrations are left out of the discussion, the choice of camera speed requires some thought. Of course, an increase in camera speed reduces the time needed to obtain a suitably dense photographic image, but what really matters in present circumstances is whether the increase in information rate implied by this reduction in exposure time outweighs the reduction in information rate which results from the greater relative effect of photographic spread and noise (granularity) in the smaller picture. Actually, the use of a faster camera of the same aperture implies larger optical aberrations, and this means a greater reduction in the information content of the photographic spectra due to the interaction between aberrations and photographic noise. (See Fellgett and Linfoot 1955, p. 371; Black and Linfoot 1958, Fig. 12. In Section 5 of the latter paper, $F/2$ should read $F/4$ throughout; on p. 583 line 3 the values 20 and 5 megabits/cm^2 should read 3·5 and 1 respectively; and on p. 539, bottom line, $\pm 10\mu$ should read $\pm 32\mu$.) We need a means of estimating quantitatively the relative importance of these two effects on the information rate, in order to be able to make the best choice of camera speed for a given slit-width, a given grating and a given emulsion. The best choice obviously changes as progress in optical design makes new types of system available; for example, the invention of the Schmidt camera made the 'best' speed much faster than before because it improved the relationship between speed and aberrations in available optical systems. The result was an increase in the information rate obtainable with a given slit-width, a given grating, and a given emulsion.

The choice of the photographic emulsion involves similar considerations. A faster emulsion means in practice one with larger silver halide grains, similar or larger spread, and more granularity. An increase in spread or granularity lowers, in a calculable manner, the information content of the photographic image. Thus both exposure time and information gained are less with a faster emulsion. It is their ratio which we wish to optimize. If the spread of the 'aerial' image of the slit in each separate wavelength λ is small in comparison with the photographic spread, this ratio (the information rate) is only weakly dependent on the speed in a range of emulsions of the same equivalent quantum efficiency; that is, the same signal-to-noise ratio. But if the emulsion spread is small compared with the spread of the aerial image, then the gain in speed obtained by using a coarser emulsion outweighs the loss in information due to the larger spread and granularity; the information-rate increases with the emulsion speed if the signal-to-noise ratio in the developed emulsion remains constant.

Quantitative discussion of photographic image quality depends essentially on being able to treat the effects of spread and of granularity quantitatively within a single analytical framework. Spread can be handled by the use of Fourier transforms; the discussion of granularity requires the use of probability theory. The particular branch of probability theory needed for this purpose is entropy theory or, what amounts to the same thing, information theory.

The discussion of the best choice of slit width is complicated by the question of image decoding. From measurements of the photographic density along the spectrum we should like to be able to infer the energy density along the 'ideal' spectrum which the system would give in the absence of diffraction, optical aberrations, non-linearity of photographic response, and photographic noise. Because an optical system has a finite spatial-frequency pass band, this cannot be done. What we can infer is the probability distributions of those coefficients in the Fourier transform of the 'ideal' spectrum which belong to spatial frequencies lying in the pass-band. This is the logically correct method of 'allowing for instrumental band-width'. It requires the use of a fast computer to carry it through, however. To test a theory (about line profiles, for example) the logically correct procedure is to calculate what values a predicted line profile should give to the above-mentioned Fourier coefficients when observed with the system, and to compare the calculated values with those obtained by carrying out a Fourier transformation on the 'observed' intensity distribution obtained by measuring the photographic densities along the spectrum and allowing for photographic response, which of course varies with λ as well as being non-linear.

Widening the slit leaves the mean values of the above-mentioned inferred probability-distributions unaltered, but increases their probability-spreads. Thus it decreases the information content. At the same time, it reduces the exposure time. Again, we need a means of deciding when their ratio, the information rate, is maximized.

In the remainder of this section we try to indicate briefly the lines on which it seems that a useful attempt to deal with these problems could be made. We base the attempt on the assumption that the *discrimination rate* of a spectrograph, here defined as the effective number of distinguishable spectra which it can record per hour when used to observe a normalized random low-contrast set of spectral distributions, is a reasonable indicator of its potential usefulness. The normalization just referred to consists in prescribing for the working wavelength range (λ_1, λ_2)

(1) the statistical mean total surface brightness in the slit aperture, (2) the statistical r.m.s. deviation of the spectral 'shape function' $\rho(\lambda)$ from its mean value in (λ_1, λ_2). The effective number of distinguishable spectra per hour has for its logarithm (to base 2) the statistical mean information rate in bits per hour (compare Fellgett and Linfoot 1955).

We consider a spectrograph with negligible optical aberrations, working over a short wavelength range (λ_1, λ_2) which, however, is large compared with the resolution limit*. The rectangular grating acts as an aperture stop. The slit is taken as an incoherently lit object; as already noted, this necessitates excluding some cases of practical importance. A simplified 1-dimensional treatment is possible in the aberration-free case.

The geometrical image x' of an object point x emitting λ-light can be taken as given by the equation

$$\lambda - \lambda_0 = \alpha(x' - Mx) = \alpha x'', \tag{3.1}$$

where $\lambda_0 = (\lambda_1 + \lambda_2)/2$ and $x' = Mx$ in λ_0-light. Evidently α is the linear dispersion, M the geometrical magnification for fixed λ. We can assume photographic sensitivity constant over the short λ-range, and photographic spread function $w_1(x'; x; \lambda) = w_1(x'')$ for all x in the slit, λ in the short λ-range. In dealing with low-contrast images, the photographic process can be treated as linear.

Then the photographic image is a convolution $(\sigma * w * w_1 * h)(x)$, where $\sigma = \sigma(x'')$ is equal to 1 in the geometrical image of the slit, to 0 outside it; $h = h(x'')$ describes the spectral density function of the object geometrically mapped on to the photographic surface S' in accordance with (3.1); $w = w(x''; \lambda)$ is the point-image function of the camera with the edge of the grating as aperture stop. Evidently

$$h(x'') = \rho(\lambda), \tag{3.2}$$

where x'' and λ are connected by (3.1). If $I(x')$ denotes the intensity function of the image freed from emulsion noise (that is, the statistical mean image-intensity function over a large number of repetitions of the photographic observation of a single object), we have by the Fourier product theorem

$$F[I] = F[\sigma]F[w]F[w_1]F[h]. \tag{3.3}$$

Because the wavelength range (λ_1, λ_2) is short, the *ct*-function $F[w]$ is approximately given by the equation

$$F[w] \begin{cases} = 1 - F\lambda_0 |u| & \left(|u| < \frac{1}{F\lambda_0}\right) \\ = 0 & \left(|u| \geqq \frac{1}{F\lambda_0}\right), \end{cases} \tag{3.4}$$

where F on the right of (3.4) is the focal ratio of the converging pencils and u the spatial frequency in S'. For a slit $-a < x < a$ of width $2a$,

$$F[\sigma] = \frac{1}{2a'} \int_{-a'}^{a'} e^{-2\pi i u x''} \, dx'' = \frac{\sin 2\pi a' u}{2\pi a' u}, \tag{3.5}$$

where $a' = Ma$.

* A longer wavelength range can be treated by dividing it up into short ranges and considering these separately.

By arguments similar to those of Fellgett and Linfoot (1955) it now follows that the information rate per unit λ in the short section (λ_1, λ_2) of the spectrum is, to a fairly good approximation, proportional to

$$l\int_{-1/F\lambda_0}^{1/F\lambda_0} \log\left\{1+(1-F\lambda_0|u|)^2\left(\frac{\sin 2\pi Mau}{2\pi Mau}\right)^2|\tau_1(u)|^2\frac{P}{N}\right\}du, \qquad (3.6)$$

where l denotes the emulsion speed (measured in some arbitrarily fixed unit), M the geometrical magnification of the slit image on the emulsion, $\tau_1 = F[w_1]$ the acceptance factor of the emulsion near the wavelength λ_0, N the emulsion noise power level, P the statistical mean structure power in the low-contrast spectral shape-function $\rho(\lambda)$. The constant of proportionality is independent of the slit width $2a$, of the linear dispersion α, of the slit image magnification M, of the camera focal ratio F, of the emulsion, and of the mean spectral contrast in the object set, provided it is small. (But P/N need not be small.)

The conclusion that when the object set is spectrally random the information rate per unit λ is independent of the dispersion is not really paradoxical. It corresponds to the fact that, with a spectrally random object set, the information density per unit x' at a given mean density level is independent of the linear dispersion, because a linear magnification of a random set does not change its statistical structure. Doubling the linear dispersion therefore doubles the information content per unit λ and doubles the exposure time needed to obtain this information.

The expression (3.6) does not, of course, purport to give a numerical measure of the practical usefulness of the system under ordinary observatory conditions. But it provides an indication of the changes which should be made in the slit-width, the camera speed, and the emulsion type in order to convert an orthodox spectrograph with very small aberrations into one designed to work in the special conditions where as much information as possible has to be recorded in a limited time, and where a fast electronic computer is available to extract this information. The slit-width, camera speed, and emulsion type should be varied within their disposable ranges so as to maximize the value of the expression (3.6) for a value of P near to that expected for the set of objects to be examined.

An extension of the analysis to spectrographs in which appreciable aberrations are present can be based on the formalism in Section 2. In this more general case the expression $(l-F\lambda_0|u|)^2$ in the integrand of (3.6) is replaced by $|\tau(u)|^2$, where $\tau(u)$ is the local optical contrast transfer function of the system at the wavelength λ_0, evaluated for spatial frequencies along the length of the spectrum.

The Observatories,
Madingley Road,
Cambridge:
1960 *February*.

References

G. Black and E. H. Linfoot, 1958, *Proc. Roy. Soc.* A, **239**, 582.
P. B. Fellgett and E. H. Linfoot, 1955, *Phil. Trans. Roy. Soc.* A, **248**, 269.
H. H. Hopkins, 1956, *Proc. Phys. Soc.*, **69**, 562.
E. H. Linfoot, 1958, *Physica*, **24**, 476.